SYNTHESIS AND LUMINESCENCE OF ZINC OXIDE NANORODS-BLENDED THIOPHENO-ORGANOSILICON POLYMERS

UNIVERSITY *of the* **WESTERN CAPE**

By

Nolukholo Tyombo

(BSc Honours)

A mini-thesis submitted in partial fulfilment of the requirements for the degree of

Magister Scientiae in Nanoscience

Faculty of Science

University of the Western Cape

Bellville, Cape Town, South Africa

Supervisor: Prof Emmanuel Iwuoha

December, 2017

Abstract

The increasing cost of fossil fuel energy production and its implication in environmental pollution and climate change created high demand for alternative and renewable sources of energy. This has led to great interest in research in the field of photovoltaic or solar cells Due to the abundance of sunlight, the technology is sustainable, non-polluting and can be implemented at places where power demand is needed, for example in rural areas. Solar cell devices that have been commercialized are currently based on silicon technology, involving the use of monocrystalline, polycrystalline and amorphous silicon. Although they produce highly efficient solar cells, the cost of Si solar cells is too high. Second generation solar cell materials such as cadmium telluride and third generation materials such as perovskites and organic polymers have been receiving much attention recently. However, they lack the efficiency of Si solar cells. This research proposes the development of high energy conservation photovoltaic cells from novel low-cost organosilicon polymers. The aim was to develop novel highly branched organosilane polymers such as poly(3-hexythiophene), polydi(thien-2-yl)dimethylsilane, poly(3-hexyl-[2,2'] bithiophenyl-5-yl)-dimethyl-thiophen-2yl-silane) as electron donors along with zinc oxide nanorod as the electron acceptor which were able to bring the efficiency of the resultant photovoltaic cell close to that of current Si solar cell. The zinc oxide nanorods were prepared by wet chemistry methodology involving the use of zinc acetate and sodium hydroxide and absolute ethanol and were annealed at different temperatures. Organosilane polymers were prepared through a reaction route that involved the use of ferric chloride as catalyst, where safety measures were used. The structural characterisations of the materials were performed by proton nuclear magnetic resonance spectroscopy (HNMR), Fourier transform infrared spectroscopy

2

(FTIR) and energy dispersive x-ray spectroscopy (EDX) Morphological analysis were done by high-resolution scanning electron microscopy (HR-SEM), high-resolution tunneling electron microscopy (HR-TEM) and x-ray diffraction (XRD), while optical properties of the materials were studied by ultraviolet-visible (UV-vis), photoluminescence (PL) and electrochemistry. Based on the cyclic voltammetry and UV-Vis results, we were able to calculate the HOMO, LUMO and band gap energy (Eg) values of the donor and acceptor as well as their blend. The obtained optical band gap of polymers blended with zinc oxide nanorods was calculated, for P3HT, PDDS and P3HDS were all found to be 2.291 eV, 2.42 eV and 1.96 eV respectively. The electrochemical bandgaps for donor polymers obtained were lesser than the optical bandgaps and this could be due to the electrochemical reactions that are faster and might have an effect on the shifting of peaks to less potentials.

3
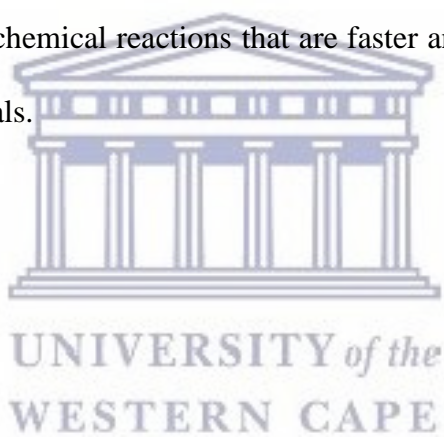
Declaration

I, hereby declare that "Synthesis and Luminescence of Zinc Oxide nanorods-blended Thiopheno-Organosilicon polymers" is the result of my own work that was done by me under the supervision of Prof Emmanuel Iwuoha, and that it has not been previously submitted for any degree or examination in any other university or higher education; and that all the sources and quotations have been indicated and acknowledged by complete references.

Nolukholo Tyombo   March, 2018

Signed: …………………….   Date: 02-03-2018……………….

UNIVERSITY *of the*
WESTERN CAPE

4

Dedication

This work is dedicated to my family; Nokuthozama Buyiswa Tyombo (mother), Bonani Tyombo (father), Nolukhanyiso Tyombo & Sinovuyo Tyombo (sisters), Thanduxolo Tyombo & Luthando Tyombo (brothers), Nokwandisa Lulama Bangisi (Aunt) as well as Mihlali Bangisi, Yolanda Cleo Bangisi & Lihle Bangisi (cousins) for their moral support, love, prayers and all they have provided for me throughout.

UNIVERSITY *of the*
WESTERN CAPE

5

Acknowledgements

First of all, I will like to give all the glory to the Almighty God, who showed me love, and gave me the courage, strength and wisdom that enabled me to complete the research work and to write this thesis. (Isaiah 40:31 "but those who hope in the Lord will renew their strength. They will soar on wings like eagles; they will run and not grow weary'; they will walk and not be faint.")

I will like to express my special thanks and gratitude to my supervisor, Prof Emmanuel Iwuoha, for his great guidance, support, encouragement and giving me the opportunity to pursue my life goals and make my dreams come true, as well as, giving me the opportunity to be part of the SensorLab research group.

I will like to thank the father God gave me, my mentor Dr Miliua Masikini for his support, guidance and encouragement. Thank you for grooming me to be the researcher I am today. May the Lord bless you for being the father you are to others as well.

A special thanks to my colleagues from the 2016 Nanoscience class, as well as, the SensorLab family. It has been fun working with you guys. You were with me through frustrations, and you wiped my tears when things were not going fine. Thanks to everyone who was ever willing to help me.

To my pillars, my support system, my lovely family; more especially my mother. Thank you very much for your support, prayers, encouragement and care. You were always there when I needed you the most and you showed me love: (Mark 10:9 "Therefore what God has joined together, let no one separate.")

Lastly, I will like to acknowledge the National Nanoscience Postgraduate Teaching and Training Platform (NNPTTP) for the award of MSc Nanoscience Scholarship, and the Chemistry Department and the University of Western Cape (UWC), for providing me the opportunity to study for this postgraduate degree.

6

Key Words

Energy

Photovoltaics

Conductive polymers

Organosilicon

Thiophene

Optical bandgap

Electrochemical bandgap

Ultra-violet visible spectroscopy

Photoluminescence spectroscopy

Cyclic voltammetry

7

Acronyms and Abbreviations

HRSEM: High resolution Scanning Electron Microscopy

HRTEM: High resolution Transmission Electron Microscopy

EDX: Energy Dispersive Spectroscopy

FTIR: Fourier Transform Infra-Red Spectroscopy

H'NMR: Proton Nuclear Magnetic Resonance Spectroscopy

XRD: X-ray Diffraction

UV-Vis: Ultraviolet-Visible

PL: Photoluminescence

TGA: Thermogravimetric Analysis

GPC: Gel Permeation Chromatography

SAXS: Small-Angle X-ray Scattering

CV: Cyclic Voltammetry

OPV: Organic Photovoltaic

P3HT: Poly(3-hexylthiophene)

PDDS: Polydi(thien-2-yl)dimethylsilane

P3HDS: poly(3-hexyl-[2,2'] bithiophenyl-5-yl)-dimethyl-thiophen-2yl-silane)

8

ZnO: Zinc Oxide

Epa: Anodic peak potential

Ipa: Anodic Peak current

Epc: Cathodic peak potential

Ipc: Cathodic peak current

Eox: oxidation potential

Ep: peak potential

Ered: reduction potential

E^o: Formal potential

ΔEp: change in potential

PCE: Power Conversion Efficiencies

HOMO: Highest Occupied Molecular Orbital
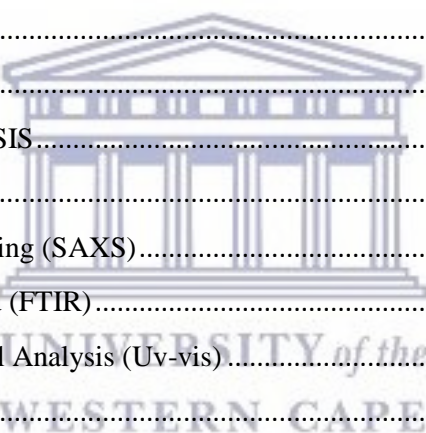
LUMO: lowest Unoccupied Molecular Orbital

Eg: Band gap

9

Table of Contents

11

List of figures

12

13

Figure 6.1.3: The UV-vis spectrum of P3HDS/ZnO nanorods in different ratios.

Figure 6.2: The PL spectra of (A) P3HT, (B) PDDS, (C) P3HDS polymers blended with ZnO nanorods in different ratio in a solution.

14

List of Schemes and Tables

Scheme 2.2.1: The reactions of aryl- and alkenylsilanols with organic halides using Ag_2O $Pd(PPh_3)_4$ as catalysts.

Table 1: CV data, HOMO, LUMO and band gap of P3HT.

Table 2: CV data, HOMO, LUMO and Band gap of PDDS.

Table 3: CV data, HOMO, LUMO and Band gap of P3HDS.

Table 4: The UV-Vis table of absorption band and optical band gap.

Table 5: The UV-vis table of absorption band and optical band gap

Table 6: The UV-vis table of absorption band and optical band gap

UNIVERSITY *of the*
WESTERN CAPE

15

Chapter 1

Introduction

1.1 Background

Energy is a need, such that it is one of the central global issues affecting world social, economic and environmental. The South African Department of energy reported that the primary energy supply in South Africa is dominated by coal, as shown in figure 1.1 [1]. The energy crisis in the country is expected soon because there is high demand of electricity while the coal is limited. Hence South Africa is in need of an alternative unlimited energy resource. Generally there are two types of energy resources which are renewable and non-renewable resources. The non-renewable resources are mostly the energy that is formed or found in nature that can be used up such as fossil fuels, while the renewable comes from natural processes such as sunlight and they cannot be used up. Figure 1.1 shows that only 1% of energy comes from renewable sources used even though it is clean and also unlimited [1]. Solar energy is one of the renewable and promising alternative sources of energy; solar energy received by the earth per year is more than thousand times than the energy we are currently using.

16
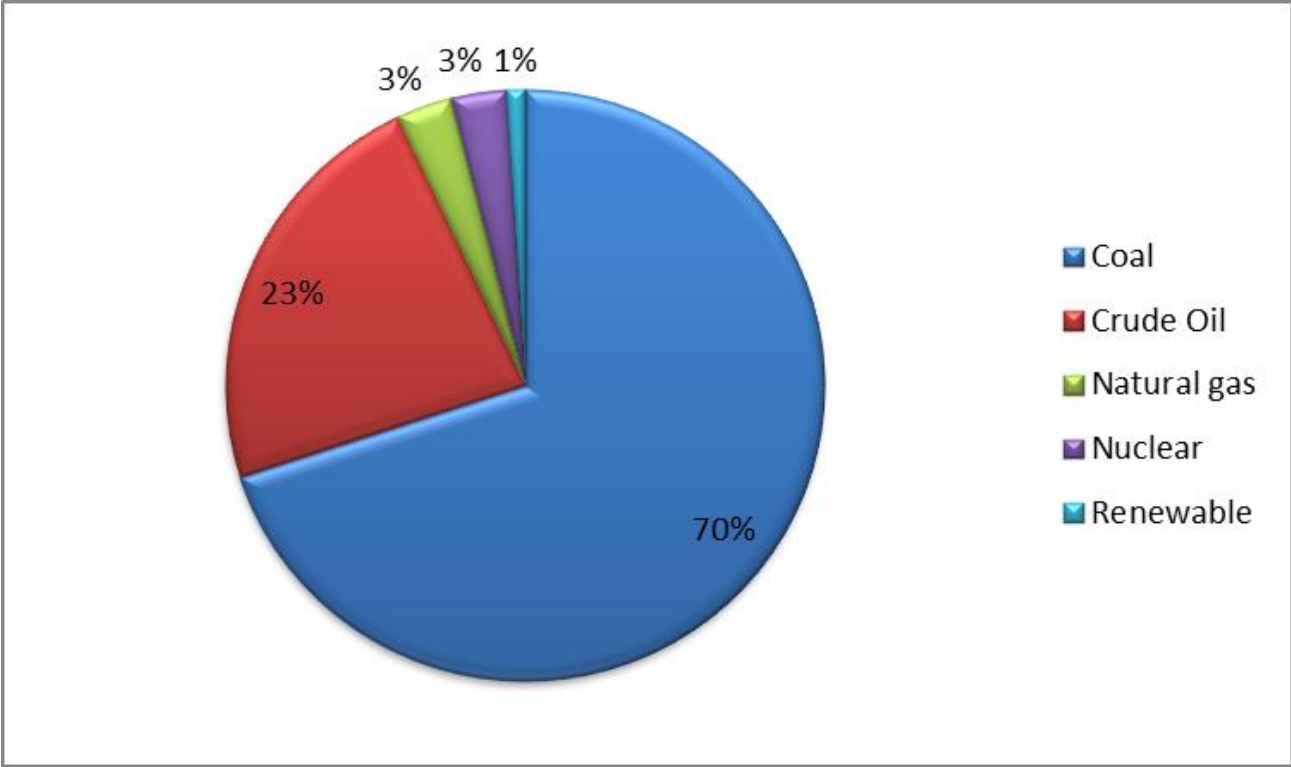
Figure 1.1: The amount of energy source used in South Africa by 2014. "Redrawn from Ref [1]"
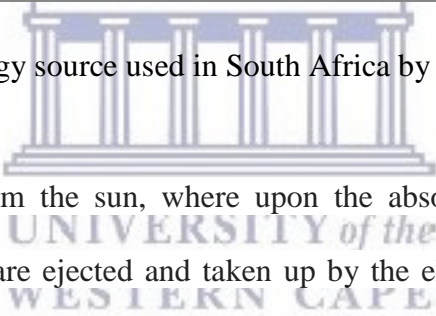
Solar energy is the energy from the sun, where upon the absorption of photons by a semi conducting material; electrons are ejected and taken up by the electric field to produce charge where electricity can be, generated [2]. Solar energy can be converted into electricity through Photovoltaic (PV) devices or solar cells. However due to the cost of production of these devices not everyone can have access to them because they are expensive. These PV devices have attracted much attention; because there is a continuous availability of sunlight throughout the year and they contribute to the decrease of the use of fossil fuels.

Silicon based solar cells, are the most used and commercial available solar cells found in the industries due to their advantages such as high power conversion efficiencies, excellent electron charge and environmental stability. These silicon devices are found to have high cost and thick

17

layer that prevents them from being flexible. This led to researchers probing organic solar cells as viable alternative option, which have both conducting and semiconducting properties. These devices are cheap, high absorption coefficient and flexible but the issue is that they have low efficiency compare to others. Hence the discovery of hybrid solar cells that combine organic and inorganic material, aimed to improve the available solar cells by combining their advantages in one solar cell.

1.2 Problem Statement and Research Motivation

The commercially available solar cells are silicon based solar materials such as monocrystalline, polycrystalline and amorphous silicon, which were discovered as good conducting materials for photovoltaic devices that produce highly efficient cells. The main problem with these inorganic materials based photovoltaic devices is high material cost, which brings about the cost of the solar cells to be too high as well. Since silicon needs to be pure for the monocrystalline, the high cost of material purification and manufacturing wafer causes the solar cells to be more expensive such that only affording people have access to them while others are only relying in non-renewable energy. Second generation solar cell materials such as cadmium telluride and third generation materials such as perovskites and organic polymers have been receiving much attention recently. These materials are light in weight, low cost and flexible, but the issue with them is the efficiency that is still lower than that of silicon solar cells.

Hybrid solar cells are found to be the best option to overcome these challenges that are faced from both organic and inorganic solar cells. Hybrid solar cells have been the cheap alternatives for conventional silicon solar cells; they are semiconductors that contain both organic and inorganic materials. In the hybrid photovoltaic cell there is a conjugated organic material found,

18

that is able to absorb light as a provider there is also inorganic material found that works as acceptor and carry electrons in the structure. The desirable features found in both organic and inorganic material shall combine in making hybrid solar cells. The target of making hybrid solar cells is to use the desirable feature of organic photovoltaics (OPV) such as low cost production of a cell and others as well, from inorganic such as tuneable absorption spectra. Hybrid solar cells have the capacity to obtain high power conversion efficiencies (PCE) because so far the currently achieved efficiencies are quite low.

Hence this work seeks to develop thiopheno-organosilicon polymer as electron donor material along with zinc oxide nanorods as acceptor for hybrid solar cells.

1.3 Aims and Objectives

1.3.1 Aim

The aim was to develop novel highly branched organosilane polymers such as poly(3-hexythiophene), polydi(thien-2-yl)dimethylsilane, and poly(3-hexyl-[2,2'] bithiophenyl-5-yl)-dimethyl-thiophen-2yl-silane) as electron donors (zinc oxide nanorod as acceptors) to improve both the efficiency and band gap quality of the photovoltaic cell close to that of current Si solar cells.

19

1.3.2 Objectives

The objectives of the study are:

(i) To synthesise polymeric material and characterise the compounds using vibrational and electronic spectroscopy, photoluminescence, electron microscopy.

(ii) To synthesise zinc oxide and characterise them using electronic and photoluminescence spectroscopy, electron microscopy.

(iii) To study the electrochemical behavior of the polymers.

(iv) To determine the bandgap of the polymer with ZnO as an acceptor in photovoltaic cells.

1.4 Brief overview of Chapters

This thesis is divided into six chapters

- Chapter **one**: this chapter presents the background, problem statement, motivation and objectives of this research.

- Chapter **two**: this chapter introduces solar cells general and covers a detailed review on semiconducting materials used in solar cells.

- Chapter **three:** presents the research design, describes the various characterization techniques used and the general experimental procedure.

- Chapter **four to six:** discusses the experimental results achieved in the research.

- Chapter **seven**: gives conclusion, challenged and recommendation for future work.

20

Chapter 2

Literature review

2.1 Introduction

In this Chapter we dwell more on the literature forming the results. The main focus of this review is on organosilicon and polymers that combine together to form a hybrid material.

2.2 Organosilicon

Organosilicon compound which are also known as organic silicon, are organic compound containing carbon bonded with silicon inside the molecule structure. Over 90% of the Earth's crust is composed of silicate minerals, making silicon the second most abundant element in the Earth's crust (about 28% by mass) after oxygen [3]. Silicon is most widely found on things like dusts, sands, and sometimes it can be found in some rocks as various forms of silicon dioxide (silica) which is can be known as silicates. Silicon is known as a comparably environmentally benign element, since organosilicon compounds are oxidized ultimately to biologically inactive silica gel. Various organosilicon reagents are now available owing to the growth of silicon industry [4]. These reagents have advantages compared to other transition metal used such as palladium. The organosilicon reagents can be used as nucleophilic partners in cross-coupling with pseudo halides and organic halide because of their good feature such as low molecular weight, high chemical stability and also they are lacking toxicity. Towards palladium-catalyzed cross coupling the silicon-based reagent were always considered to be insufficiently active, but the research done by Hiyama *et al.* showed that the nucleophilic promoter is able to activate organosilanes [4, 5].

21

2.2.1 Silanols

Silanols are organisilicon compounds that are containing the Si-OH bond in the molecule and are mostly referred to as alcohols. However, the two compounds (silanol and alcohol) are containing close apparent similarities. The only difference between the two is their preparation, unlike alcohol silanols such as silanediols $[R_2Si(OH)_2]$ and silanetriols $[RSi(OH)_3]$ it is easy to prepare them than their carbon analogues [6]. Silanol containing species are essential industrial intermediates, for example, in the silicone industry polycondensation of silanols leads to the formation of silicones, and the hydrolysis of alkoxysilanes leads to silanols as intermediates in sol-gel processes and in surface functionalisation using silane coupling agents. In addition, the silanols group is found low concentration in water as $Si(OH)_4$ and it has a great significant value on the reactive site of the surface of silicate rock as well as minerals [6]. Silica is mostly studied in details in researches based to water. Number of silica technological applications are depending on its specific surface properties, for example the surface silanol groups can serve as hydrogen-bonding sites for a variety of chemical species, their reactivity can make them convenient for chemical modifications which makes silica surfaces strategic for instance in biosensing applications [7, 8].

Marialore Sulpizi and his colleagues did the research based on the molecular behavior of the silica-water interface [9]. In their research, density functional theory based molecular dynamics (DFTMD) simulations was employed, where the solvent and surface treatment of the electronic structure was provided. During their research they have only managed to find two types of solanol groups at the quartz surface, out-of-plane forming a strong and short hydrogen bond at the interface of water molecules because of the strong acidic character found in silanol and in-

22

plane weak hydrogen bond was found at the interfacial water molecules [9]. Silanols was not only studied by the above mentioned researchers but also others, where they were interested on the synthetic utilization of silanols [10]. The researchers' interest was basically focused on the transformation carbon-silicon (C-Si) bond to carbon-carbon (C-C) bond which was reported as a weak bond compared to (C-Si). The reaction that was used during the study was a cross-coupling reaction that in silver (I) oxide as the reagent that is shown in the scheme below [10].
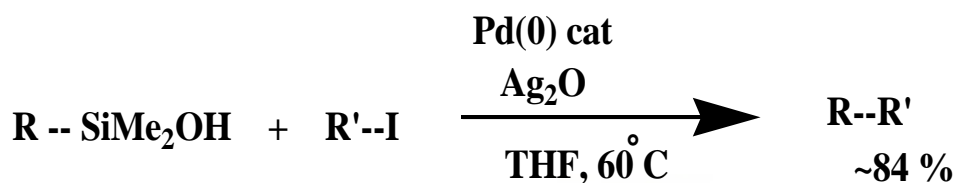
$$R\text{ -- }SiMe_2OH \quad + \quad R'\text{--}I \quad \xrightarrow[\textbf{THF, 60}^{\circ}\textbf{C}]{\substack{\textbf{Pd(0) cat}\\ \textbf{Ag}_2\textbf{O}}} \quad R\text{--}R' \quad \text{~84 \%}$$

Scheme 2.2.1: The reactions of aryl- and alkenylsilanols with organic halides using Ag_2O $Pd(PPh_3)_4$ as catalysts.

Silanols are mostly used in the synthesis of silicon based polymeric materials where they are employed as nucleophilic partners in transition-metal catalyzed reaction mentioned above. They are not only employed for such reaction but for organocatalysts for activating carbonyl compounds, intramolecular guiding groups for C−H bond activation reactions, inhibitors of enzymes, and isosteres of bioactive compounds [11].

2.2.2 Silenes

Silenes are organometallic molecules such as silaethylenes and silaethene, these molecules are consists of silicon and carbon (Si=C) double bond. The first evidence for the existence of silenes was established in 1967 when Gusel'Nikov and Flowers reported silene generation as an intermediate during the pyrolysis of dimethylsilacyclobutane [12]. Silenes are highly air and

moisture sensitive and this hampers the facile application of reactions involving these compounds in target directed synthesis.

2.3 Conductive Polymers

A polymer is a chemical compound where molecules are bonded together in long repeating chains, nowadays it is known as plastics especially in the industries [13]. Polymers can be man-made or be naturally occurring or both, for example rubber is a natural polymeric material that is extremely useful and has been used for years. Polymers make up many of the materials in living organisms such as proteins, and nucleic acids. Depending on the desired use, polymers can be finely tuned to leverage the advantageous property. Conductive polymers are polymers with highly π conjugated polymeric chain; there are two general types of conducting polymers that exist. Those are the polymers that are composite materials that use polymers to hold together conducting filler such as metal flakes or carbon black and polymers whose backbone intrinsically propagates charge, making the polymer itself conducting [14].

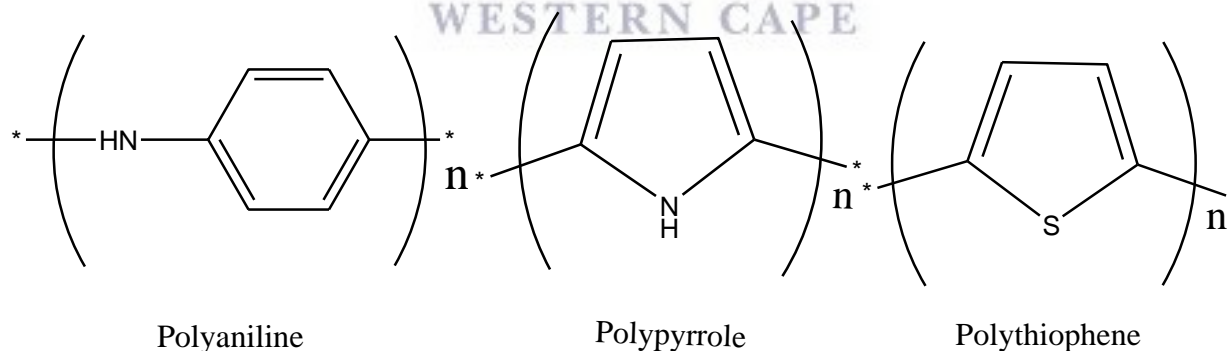Polyaniline   Polypyrrole   Polythiophene

Figure 2.1: Different types of conductive polymers.

In order for conducting polymers to be used in applications, they needs to have an excellent electronic and mechanical properties, greater solubility as well as high environmental stability,

24

for an example polyacetylene (PA), polyaniline (PANI), polypyrrrole (PPy), polythiophene (PTh) and polyfuran (PF) are the good examples of polymers as shown in figure 2.1 above [15]. Conductive polymers can be synthesized via chemical polymerization or electrochemical polymerization. These polymers can be used for various applications especially in microelectronics industry because of their properties.

2.4 Polythiophene

Polythiophene (PT) has been considered one of the most promising conjugated polymers due to its advantages compared to other polymers. Polythiophene and its derivatives have an advantage of high stability, ease of structural modification and controllable optical and electrochemical properties. When polythiophenes did not have the alkyl substitution they were very limited because of its insolubility in many common organic solvents, due to its extended conjugated structure [16]. The alkyl substituted polythiophenes are the most studied and important classes of conjugated polymers with a lot of applications such as electrochromic and transistors as well as conducting films. These polymers can be synthesized through electropolymerisation, metal-catalyzed coupling reaction and chemical oxidative polymerization [17].

The electropolymerisation of thiophene has advantages such as producing free-standing polythiophene films directly on the electrodes and the ease of controlling the thickness of the films. The factors affecting this synthetic route are indicated, including solvents, temperatures, concentration of the monomer and electrolytes [18]. The electro-deposition or eletropolymerisation of polythiophene was performed by cyclic voltammetry or galvanostatic methods in which thiophene (monomer) was deposited on a working electron such as platinum electrode as shown by figure 2.2. The research done by Li and Li, 2003 [18] was based on the

25

study of concentration as a factor affecting the electron polymerization of thiophene. They discovered that the onset potential of the oxidation process decreases with an increase in concentration, while the conductivity increases with increase in concentration.
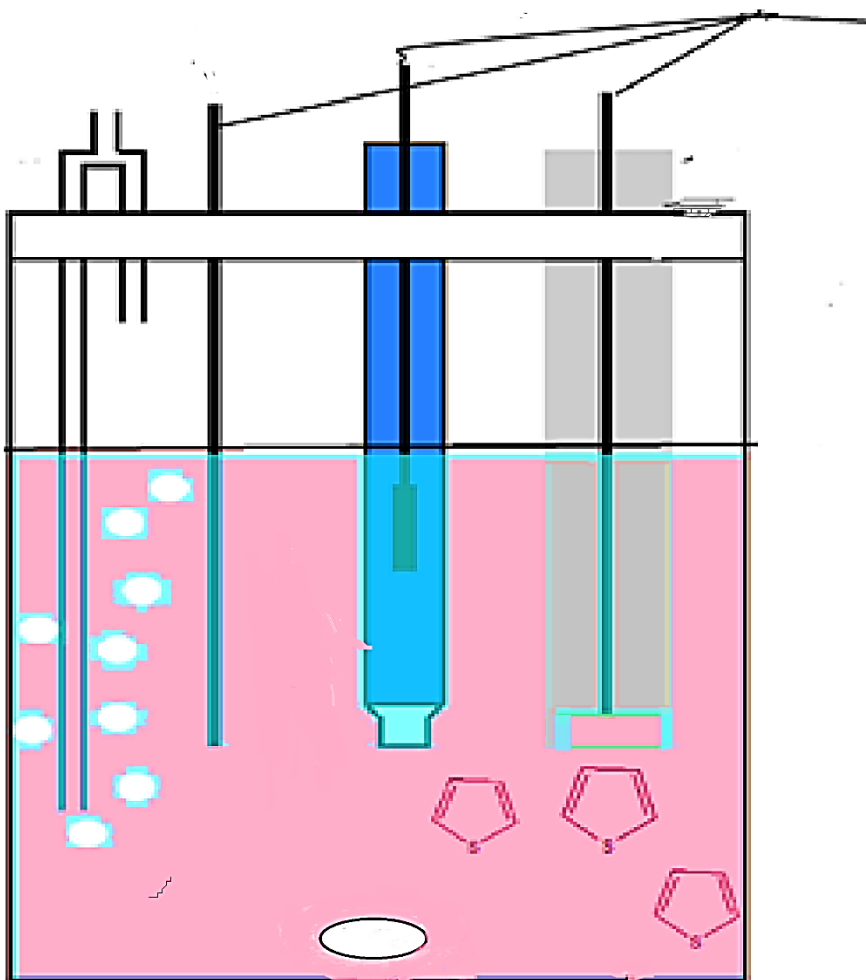
Figure 2.2: The electro-deposition of thiophene monomer through electrolytic cell.

The metal catalyzed coupling reaction was discovered in the past few decades, where they managed to develop new and useful chemical transformations. There are different types of metal catalyzed coupled reactions studied, such as palladium, nickel, ruthenium, iron and so on. The metal catalyzed coupling reactions are found to have advantages such as their compatibility with

26

many types of functional groups and the ease in preparing various monomers into polymers even if it's a complex polymer [19]. These reactions have some unresolved problems such as low reactivity of aryl chloride and some catalysts such as palladium for example are expensive. Many studies are done based on these reactions and some researchers are finding ways of replacing the expensive catalysts.

The chemical oxidative polymerization of polythiophene is the removal of hydrogen atoms from thiophene (monomer) to give polythiophene (polymer) and it can be classified as polycondensation. Wadatkar and co-worker [20] reported the polymerization of thiophene via chemical oxidation in the present of ferric chloride ($FeCl_3$), where hydrogen peroxide was used as a catalyst. The sample was analysed by Fourier transform infrared spectroscopy (FTIR) and the material was confirmed [20].

2.5 Zinc Oxide nanoparticle (ZnO)

Nanotechnology is one of the most active analyses in the area of material science; it produces and improves better material properties such as strength, electrical and chemical properties. Researchers have realized that environmentally friendly materials are in demand. Hence they have decided to chemically synthesize metal oxide nanoparticles such as zinc oxide. ZnO nanoparticles are found on the earth crust while other metal oxides have been commercially synthesized [21]. The ZnO nanoparticle is used as semiconducting material for sensors, catalysts and photo electron. Its band gap is reported to be ~3.37 eV with an excitation energy of 60 eV at room temperature [22, 23] as well as high mechanical and thermal stability [21]. Zinc oxide is optical active, which make ZnO a very interesting material for various applications such that, due to its UV absorption it is now used as sunscreen [24].

27

Zinc oxide has been studied or synthesized through various number of methods such as physical or chemical vapour deposition, pulse laser deposition, electro-spinning and sputtering etc. Out of so many synthetic procedures wet chemistry is found to be the promising, ease handled, low cost and able the scaling up synthesis method [23]. Samanta and colleagues [24] reported the synthesis of hexagonal ZnO nanorods through wet chemical method that was reported to be the controllable experiment. During the preparation the zinc nitrate hexahydrate and sodium hydroxide were employed and the product was annealed at different temperature. Different characterization techniques such high-resolution tunneling electron microscopy (HR-TEM), x-ray diffraction (XRD), while optical properties of the materials were studied by ultraviolet-visible (UV-vis), and photoluminescence (PL) were used to confirm the hexagonal structure and emission [24].

2.6 Polythiophenes with Zinc Oxides

Polythiophene and its derivatives have attracted lot of researchers but their conductivity is found to be very low due to the wide energy gap and the fact that the antibonding orbital lack electrons [25]. To improve these properties of polythiophene and reveal new performance the researchers decided to dope the polymers or make a composite with inorganic nanoparticles such as ZnO, SnO_2 and TiO_2, etc. These hybrid materials of polymers and inorganic-nanoparticle bulk heterojunctions can take advantage of the beneficial properties of both types of materials, such as solution processing of polymer semiconductors and high electron mobility of inorganic semiconductor [26]. In most hybrid solar cells the organic or polymer semiconductor serves as the electron donor and transports the photogenerated holes while the inorganic semiconductor accepts and transports electrons [27].

28

The application of conducting polymer/metal oxide nanocomposites are used in photovoltaic devices and have been studied for the last several years by characteristics of light absorption, charge separation, and charge transportation can be achieved. The fabrication of polymer or metal oxide nanocomposite is mostly accomplished through blending and penetration method. During the blending method, the conducting polymer and metal oxide nanoparticle are mixed in solution by different ratios; while the penetration method the film of metal oxide is prepared first then the conducting polymer is drop coated on top of it [27].

The study of polythiophene with ZnO nanowire was done by Briseno *et al.,* 2009; where they were both blended together and characterized by electron microscopy and absorption to determine the probe the morphology as well as the optoelectronic properties at the organic/inorganic interface. The ideal characteristics and reproducible results were measured and observed in the p-n heterojunction device that was made [28]. The problem discovered by researcher on the device was the thickness that might affect the movement of electrons. This study is focused on the production of novel thiopheno-organosilicon polymers blended with zinc oxide nanorods to produce composite materials that have improved band gap, diffusion length and charge mobility.

29

References

1. Department of Mineral Resources (DMR)., 2015. South Africa's Mineral Industry 2013/2014. DMR, Pretoria.

   http://www.iea.org/ciab/South_Africa_Role_Coal_Energy_Security.pdf

2. Kasap, S. O., 2001. Optoelectronic and photonics: principles and practices. Prentice Hall New Jersey, pp. 199-202.

3. Nave, R., 2013. Abundances of the Elements in the Earth's Crust. *Georgia State University*.

4. Hiyama, T., 2002. How I came across the silicon-based cross-coupling reaction. Journal of organometallic chemistry, 653(1), pp.58-61.

5. Denmark, S.E. and Ober, M.H., 2003. Organosilicon reagents: Synthesis and application to palladium-catalyzed cross-coupling reactions. Aldrichim. Acta, 36, pp.75-85.

6. Baxter, I., Cother, L.D., Dupuy, C., Lickiss, P.D., White, A.J. and Williams, D.J., 1997. Hydrogen bonding to silanols. Department of Chemistry, Imperial College of Science, Technology and Medicine, London SW7 2AY, UK.

7. Gray, J.J., 2004. The interaction of proteins with solid surfaces. Current opinion in structural biology, 14(1), pp.110-115.

8. Somorjai, G.A., Frei, H. and Park, J.Y., 2009. Advancing the frontiers in nanocatalysis, biointerfaces, and renewable energy conversion by innovations of surface techniques. Journal of the American Chemical Society, 131(46), pp.16589-16605.

9.   Sulpizi, M., Gaigeot, M.P. and Sprik, M., 2012. The silica–water interface: how the silanols determine the surface acidity and modulate the water properties. Journal of chemical theory and computation, 8(3), pp.1037-1047.

10.   Hirabayashi, K., Kawashima, J., Nishihara, Y., Mori, A. and Hiyama, T., 1999. A New Transformation of Silanols. Palladium-Catalyzed Cross-Coupling with Organic Halides in the Presence of Silver (I) Oxide. Organic Letters, 1(2), pp.299-302.

11.   Jeon, M., Han, J. and Park, J., 2012. Catalytic synthesis of silanols from hydrosilanes and applications. ACS Catalysis, 2(8), pp.1539-1549.

12.   Gusel'Nikov, L.E. and Flowers, M.C., 1967. The thermal decomposition of 1, 1-dimethyl-1-silacyclobutane and some reactions of an unstable intermediate containing a silicon–carbon double bond. Chemical Communications (London), (17), pp.864-865.

13.   Skotheim, T. A., 1986. Handbook of conducting polymers. Vol. 2. 1986, New York: Marcel Dekker.

14.   Heinze, J., 1991. Electrochemistry of conducting polymers. Synthetic metals, 43(1), pp.2805-2823.

15.   Saxena, V. and Malhotra, B.D., 2003. Prospects of conducting polymers in molecular electronics. Current Applied Physics, 3(2), pp.293-305.

16.   Valderrama-García, B.X., Rodríguez-Alba, E., Morales-Espinoza, E.G., Moineau Chane-Ching, K. and Rivera, E., 2016. Synthesis and characterization of novel polythiophenes containing pyrene chromophores: Thermal, optical and electrochemical properties. Molecules, 21(2), p.172.

31

17.   McCullough, R.D., 1998. The chemistry of conducting polythiophenes. Advanced Materials, 10(2), pp.93-116.

18.   Li, X. and Li, Y., 2003. Electrochemical preparation of polythiophene in acetonitrile solution with boron fluoride–ethyl ether as the electrolyte. Journal of applied polymer science, 90(4), pp.940-946.

19.   Xu, S., Kim, E.H., Wei, A. and Negishi, E.I., 2014. Pd-and Ni-catalyzed cross-coupling reactions in the synthesis of organic electronic materials. Science and technology of advanced materials, 15(4), p.044201.

20.   Wadatkar, N.S. and Waghuley, S.A., 2012. Study of Chemically Synthesized Polythiophene. International Journal of Basic and Applied Research Special Issue, 51(2), pp.51-53.

21.   Mirzaei, H. and Darroudi, M., 2017. Zinc oxide nanoparticles: biological synthesis and biomedical applications. Ceramics International, 43(1), pp.907-914.

22.   Kumar, S.S., Venkateswarlu, P., Rao, V.R. and Rao, G.N., 2013. Synthesis, characterization and optical properties of zinc oxide nanoparticles. International Nano Letters, 3(1), p.30.

23.   Ramachandran, D., Brijitta, J., Raj, N.N., Jayanthi, V. and Rabel, A.M., 2013, July. Synthesis and characterization of Zinc Oxide nanorods. In Advanced Nanomaterials and Emerging Engineering Technologies (ICANMEET), 2013 International Conference on (pp. 566-568). IEEE.

24.   Samanta, P.K. and Bandyopadhyay, A.K., 2012. Chemical growth of hexagonal zinc oxide nanorods and their optical properties. Applied Nanoscience, 2(2), pp.111-117.

25.   Ma, G., Liang, X., Li, L., Qiao, R., Jiang, D., Ding, Y. and Chen, H., 2014. Cu-doped zinc oxide and its polythiophene composites: Preparation and antibacterial properties. Chemosphere, 100, pp.146-151.

26.   Beek, W.J., Wienk, M.M. and Janssen, R.A., 2006. Hybrid solar cells from regioregular polythiophene and ZnO nanoparticles. Advanced Functional Materials, 16(8), pp.1112-1116.

27.   Briseno, A.L., Holcombe, T.W., Boukai, A.I., Garnett, E.C., Shelton, S.W., Fréchet, J.J. and Yang, P., 2009. Oligo-and polythiophene/ZnO hybrid nanowire solar cells. Nano letters, 10(1), pp.334-340.

28.   Sakthivel, S. and Boopathi, A., 2015. Synthesis and Fabrication of Polythiophene/Zinc Oxide Nanocomposites Thin film and Characterizations. Nano Vision, 5(4), pp.77-82.
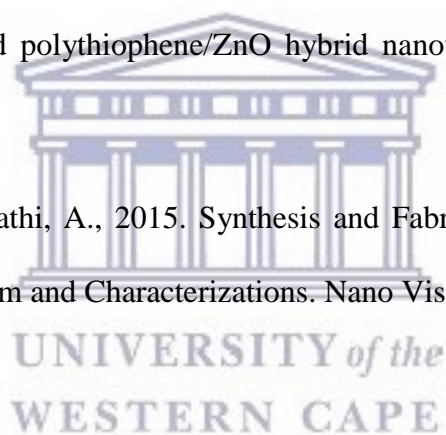
CHAPTER 3

Experimental methodology

3.1 Introduction

This chapter gives a detailed description of the materials used, research design, the characterization techniques that are used and method on which the main purpose or aim of the research was achieved. The chemical properties were studied by nuclear magnetic resonance (NMR) and Fourier-transform infra-red (FTIR), while morphological studies were carried out by transmission electron microscopy (TEM), scanning electron microscopy (SEM) and energy dispersive X-ray spectroscopy (EDS) as well as electrochemistry.

3.2 Materials

All the reagents were of analytical grade such as 3-hexylthiophene (Sigma-Aldrich), ferric chloride (Merck), anhydrous and deuterated chloroform (Sigma-Aldrich), anhydrous methanol (Sigma-aldrich), polytetrafluoroethylene (PTFE) membrane 1 μm (MilliporeSigma), acetone (Sigma-Aldrich), zinc nitrate hexahydrate (Merck) and sodium hydroxide (Sigma-Aldrich). Deionized water was prepared with Millipore filtration system (MilliporeSigma).

3.3 Methodology

3.3.1 Preparation of Poly(3-hexylthiophene)

Synthesis of poly(3-hexylthiophene) (P3HT) was achieved by a route, using $FeCl_3$ as catalyst. $FeCl_3$ (2 g, 12.3 mmol) was added to dry $CHCl_3$ (12 mL) and stirred for 15 min at room temperature. The monomer 3-hexylthiophene (3HT) (534 μL, 3 mmol) in dry $CHCl_3$ (12 mL)

34

was then added drop-wise to the $FeCl_3$ solution and the reaction mixture was stirred overnight under Ar at room temperature. The polymerization reaction was then terminated by pouring the reaction mixture into excess methanol MeOH (50 mL). The crude polymer precipitate was filtered using a PTFE membrane filter (1 μm, MilliporeSigma) and washed with ethanol (200 mL), a distilled water: acetone mixture (1:1 v:v, 250 mL:250 mL) and finally with acetone (250 mL). The dark brown solid product obtained was dried under vacuum for 72 h.

3.3.2 Synthesis of Poly (di(thien-2-yl)dimethylsilane)

Synthesis of poly(di(thien-2-yl)dimethylsilane) (PDDS) was achieved by a route, using $FeCl_3$ as catalyst. $FeCl_3$ (1.784 g, 12.3 mmol) was added to dry $CHCl_3$ (12 mL) and stirred for 15 min at room temperature. The monomer di(thien-2-yl)dimethylsilane (DDS) (446 μL, 3 mmol) in dry $CHCl_3$ (12 mL) was then added drop-wise to the $FeCl_3$ solution and the reaction mixture was stirred overnight under Ar at room temperature. The polymerization reaction was then terminated by pouring the reaction mixture into excess MeOH (50 mL). The crude polymer precipitate was filtered using a PTFE membrane filter (1 μm, MilliporeSigma) and washed with ethanol (200 mL), a distilled water: acetone mixture (1:1 v:v, 250 mL:250 mL) and finally with acetone (250 mL). The dark brown solid product obtained was dried under vacuum for 72 h.

3.3.3 Preparation of Poly{(3'-hexyl-[2,2']bithiophenyl-5-yl)-dimethyl-thiophen-2-yl-silane}

Synthesis of poly{(3'-hexyl-[2,2']bithiophenyl-5-yl)-dimethyl-thiophen-2-yl-silane} (P3HDS) was achieved by a route, using $FeCl_3$ as catalyst. $FeCl_3$ (2.009 g, 12.3 mmol) was added to dry $CHCl_3$ (12 mL) and stirred for 15 min at room temperature. The monomer 3-hexylthiophene and di(thien-2-yl)dimethylsilane (1:1) (237 μL : 223 μL, 3 mmol) in dry $CHCl_3$ (12 mL) was then added drop-wise to the $FeCl_3$ solution and the reaction mixture was stirred overnight under Ar at

35

room temperature. The polymerization reaction was then terminated by pouring the reaction mixture into excess MeOH (50 mL). The crude polymer precipitate was filtered using a PTFE membrane filter (1 μm, MilliporeSigma) and washed with ethanol (200 mL), a distilled water: acetone mixture (1:1 v:v, 250:250 mL: mL) and finally with acetone (250 mL). The dark brown solid product obtained was dried under vacuum for 5 d.

3.3.4 Preparation of ZnO

The fabrication of hexagonal ZnO nanorods was done via wet chemical method. In this method, 14.87 g of zinc nitrate hexahydrate ($Zn(NO_3)_2.6H_2O$) was dissolved in deionized water to prepare 100 mL of 0.5 M ($Zn(NO_3)_2$. 4 g of NaOH was dissolved in deionized water to prepare 100 mL of 1 M NaOH. The NaOH solution was stirred vigorously at room temperature in a conical flask using a magnetic stirrer (Spinot). The 0.5 M ($Zn(NO_3)_2$ was added drop-wise to the NaOH solution for 30 min. The mechanical stirring was continued for 2 h. The pH of the solution was 11. A white precipitate was deposited at the bottom of the flask. The precipitate was then filtered and washed 2 to3 times with distilled water. Then the powdered sample was dried and annealed at different temperatures (25, 100, 200, 400, 600 and 800 °C) in a furnace for further characterizations.

3.4 Material characterization techniques and instrumentation

Various techniques and instrumentations were employed to investigate the structures and electrochemical properties of the materials.

3.4.1 Proton Nuclear Magnetic Resonance spectroscopy (^{1}H NMR).

The nuclear magnetic resonance (NMR) spectroscopy within the molecule of a substance it uses ^{1}H NMR for the application to hydrogen-1 nuclei, it is mostly used to determine the molecular structure of organic compound and you can be able to get your molecular weight as well, for example to determine a structure of protein. ^{1}H NMR is used to study the physical and chemical properties that can be found within the molecules. Proton nuclear magnetic resonance (^{1}H NMR) spectra were recorded using a Bruker EMX 600 MHz NMR spectrometer. It was used to identify the structure of the polymer as well as the impurities present on the material. These polymers were identified or characterized by chemical shifts that are in the range of 0 to 14 ppm polar solvents are used for this, such as deuterated chloroform, water, DMSO and methanol. These solvents have different effects such that their intensities are found in different region during NMR analysis.

3.4.2 Fourier Transform Infrared spectroscopy (FTIR)

FTIR is a technique that can be used to measure infrared spectra for both solid and liquid materials. The technique was used to determine electronic properties such as vibrational and rotational of the materials in simple terms it was used to determine the chemical functional groups in the sample. The instrument used was Perkin Elmer spectrum 100 series attenuated total reflection (ATR) FTIR spectrometer which was used to determine the FTIR spectra. Infrared

37

spectroscopy reveals information about the vibrational states of a molecule. Intensity and spectral position of IR absorptions allow the identification of structural elements of molecules, typically functional groups. FTIR advantaged are its speed, sensitivity and the fact that it can be used in difficult and impossible areas. The signal provided by the FTIR technique, however, contains information about the complete spectrum of the probe.

3.4.3 Surface morphology by HR-SEM and HR-TEM

A high resolution scanning microscopy and high resolution transmitted microscopy were used to evaluate or to analyze a surface morphology and the internal structure of synthesized materials for the research. HR-SEM is known to be a versatile imaging technique that can be able to produce a 3-D structure of the surface of the material. HR-SEM has high magnification, large depth of focus and greater resolution. HR-SEM is an electron microscope that produces images of a sample by scanning it with a focused beam of electrons [1]. Inside the sample the beam of electrons will be able to interact with other electrons, where various signals will be produced such that they can be detected and those signals are also containing information about the material. Scanning electron microscopic (SEM) images were obtained using a ZEISS ULTRA scanning electron microscope with acceleration voltage of 5.0 kV, where the samples were supported by carbon grid and were coated using conductive material. In this case the samples were coated for 30 s using gold-palladium alloy as a conductive material.

High resolution transmitted electron microscopy is a technique that can be able to produce an image of smaller materials even in nanoscale. It is mostly used to analyze the internal structure of the material, crystallinity of the structure and the inter-planar spacing between the atoms. The microscopic technique can produce an image by transmitting the electrons through an ultra-thin

38

specimen that can be able to interact with the sample while passing through [2]. The HR-TEM images of the material were obtained by Tecnai G^2 F_2O X-TWIN MAT 200 kV field emission, where the nickel copper grid was used to coat the material for better conductivity.

3.4.4 Energy dispersive x-ray spectroscopy (EDS)

Energy dispersive X-ray spectroscopy is detection system found in both HR-SEM and HR-TEM it is used to detect and display the elements contributing to the sample composition, it is good because it can also pick up the impurities present on your sample. This analytical technique can produce the image of the elements scanning or transmitting electron beam (10-20 kV) to the surface of the conducting sample. EDS has high resolution of electron microprobes where information can be obtained on chemical composition of materials.

3.4.5 X-ray diffraction (XRD)

X-ray diffraction is an analytical technique that can be used to study the crystal structure of the material by measuring an electronic counter with intensity of the diffracted beam. XRD is consists of three components the tube, sample holder and the detector. The x-rays are produced in the tube where the heating filament produces electrons to the targeted material by bombarding them on the material. XRD data was collected with a Bruker AXS DS Advance diffractometer, with 2θ values ranging from 20-90 °, with a step size of 0.028 ° operating at 45 kV and 40 mA at Ithemba Labs Cape Town. Monochromatic copper (Cu) Kα1 radiation with a wavelength of 0.154 nm was used as the X-ray source. XRD in this research is employed to identify the phase purity and structure of crystalline materials and for most polymers it is always found to be amorphous and for zinc oxide nanorods where it also gives the size of the material.

39

3.4.6 Ultraviolet Visible Spectroscopy (UV-vis)

Ultraviolet visible spectroscopy is an analytical technique that is used by scientist to measures the absorption and transmission of ultraviolet and visible light wavelength by matter. UV-Vis spectroscopy can be used to study the electronic transitions of materials with transition energy in the range of 10^2-10^3 kJ mol^{-1} that is found within the IR through UV region of the electromagnetic spectrum. UV-Vis absorption measurements were made with a Nicolet Evolution 100 UV-visible spectrometer (Thermo Electron, UK), using a quartz cuvette. This research UV-Vis was important and it was used to study the inter-band electronic transition and optical absorption polymers and zinc oxide materials for their behavior in hybrid solar cells. During the analysis the monochromatic radiation is passed through the sample, to the photomultiplier that detect and measure the absorption wavelength that can later be used to calculate optical band gap.

3.4.7 Photoluminescence (PL) Spectroscopy

Luminescence is the emission if light by substances that has absorbed light; hence it is important to do the UV-vis of the material to check for absorption before doing the luminescence. PL spectroscopy is a contactless and non-destructive method for electronic structure of materials (site). When the material is exposed to UV light, the light is absorbed due to the molecules inside the material. Photoluminescence is used to measure the emission and absorption of the material. During the analysis of this, three light detectors were used. These light detectors are s1 which is used for emission in the range of 850 – 1200 nm, s2 in the range of 250-850 nm and R1 is for excitation of electrons. This is important in the study for measuring the purity and crystalline

40

quality of semiconductors such as polymers. It can also be used to determine the band gap of the material used in solar cells.

3.4.8 Thermogravimetric Analysis (TGA)

Thermogravimetric analysis is analytical techniques that can be used to determine the thermal stability of the compounds. The technique monitors the mass of a given sample as function of temperature and the specimen is subjected to a relatively controlled temperature program in a controlled atmosphere. During the measurements the crucible that is used to put the sample is heated to remove the moisture present. The sample will then be weighed using microbalance, where it will be recorded. The sample inside the crucible will then be heated on a furnace and temperature will be recorded. This is for this study because the donor polymers will be exposed to high temperatures to check their stability at high temperatures. A good thermally stable donor material for application in solar cells is expected to undergo decomposition at temperature that is higher than 300 °C.

3.4.9 Small-Angle X-ray Scattering (SAXS)

SAXS experiments were performed with SAXSpace spectrometer from Anton Paar. It is an analytical technique that can be used to determine the average particle size and shape. SAXS method is accurate, non-destruction and doesn't require a lengthy sample preparation procedure [3]. The SAXS instrument consists of basic components shown in figure 3.1 above, such as beam stop, x-ray source, sample holder, collimation system and detectors. The source illuminates the sample, and at a certain range of the angles the detector measures the energy transmitted by radiation from the sample. The zero angle position is defined by collimation system that makes the beam narrow. Whilst the beams stop prevent the detector from intensive incident beam [3].

41
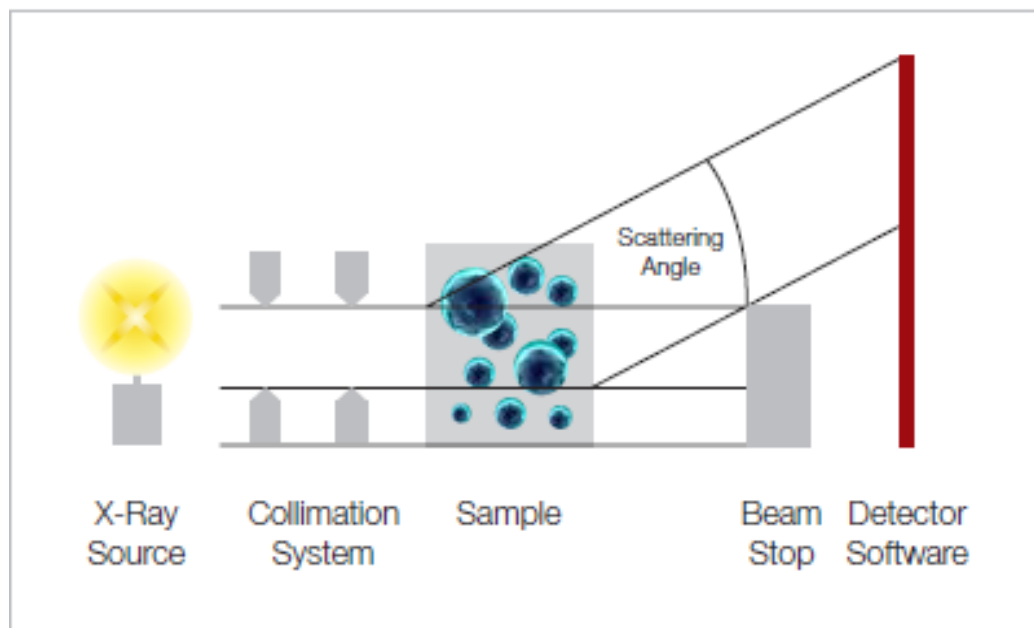
**Figure 3.1:** The components of a SAXS instrument [3].

The sample preparation of a powder was done using two sticky tapes while the liquid was measured inside a thin walled capillary. During the measurements the two sticky tape were used as blank for solid, while in liquid the solvents which is dichlorobenzene with chloroform were used as blank. The polymers and ZnO were analyzed and interpreted.

3.4.10 Electrochemistry

3.4.10.1 Cyclic Voltammetry (CV) and Square Wave Voltammetry (SWV)

Cyclic voltammetry is an electrochemical characterization technique that can be used to study electrochemical reactions such oxidation and reduction. This technique gives details about electron transfer, reaction rate and thermodynamics. Square wave voltammetry is an electrochemical technique that is more sensitive and have a lower detection limit compare to cyclic voltammetry. Both experiments were carried by the scanning of the initial and final

42

potential and the scan rate between these potential is usually what determines the rate of the reaction. CV and SWV during the experiments were carried out using a BAS 100 W integrated and automated electrochemical work station from bio analytical systems (BAS), Lafayette, USA. Where for a working electrode platinum was used for all the material while counter electrode was a platinum wire and reference was Ag/AgCl. These techniques were important in the research because we were able to find the HOMO and LUMO of the materials, which are both used for electrochemical band gap. The electronic bandgap is obtained through the analysis of data obtained by the CV measurements. CV and SWV are the most useful techniques for the characterization of organic materials and estimation of the energy band diagram [4]. These techniques are also used to determine the reversibility, reproducibility and stability of the films on the electrodes. The energy required to extract an electron from a molecule is represented by HOMO, which corresponds to oxidation process, and the amount of energy required to inject an electron into a molecule is represented by LUMO, which correspond to reduction process [5].

43
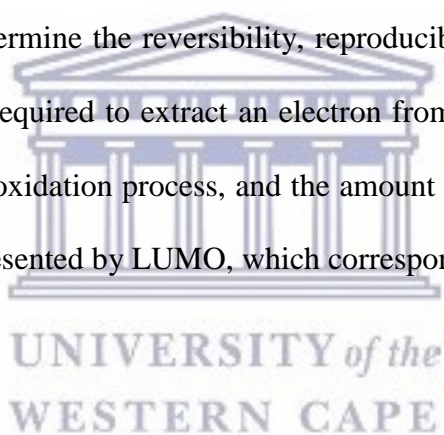
References

1. Suzuki, E., 2002. High-resolution scanning electron microscopy of immunogold-labelled cells by the use of thin plasma coating of osmium. Journal of Microscopy, 208(3), pp.153-157.

2. Skoog, D.A., West, D.M. and Holler, F.J., 1992. Fundamentals of analytical chemistry Saunders College Pub. Fort Worth.

3. Schnablegger, H. and Singh, Y., 2011. The SAXS guide: getting acquainted with the principles. Austria: Anton Paar GmbH.

4. Shafiee, A., Salleh, M.M. and Yahaya, M., 2011. Determination of HOMO and LUMO of [6, 6]-phenyl C61-butyric acid 3-ethylthiophene ester and poly (3-octyl-thiophene-2, 5-diyl) through voltametry characterization. Sains Malaysiana, 40(2), pp.173-176.

5. Freitas, A.R., Silva, M., Ramos, M.L., Justino, L.L., Fonseca, S.M., Barsan, M.M., Brett, C.M., Silva, M.R. and Burrows, H.D., 2015. Synthesis, structure, and spectral and electrochemical properties of chromium (III) tris-(8-hydroxyquinolinate). Dalton Transactions, 44(25), pp.11491-11503.

44

CHAPTER 4

Results and discussion

In this Chapter we discuss the results of P3HT, PDDS and P3HDS that are electron donor materials.

4.1 MICROSCOPIC ANALYSIS

4.1.1 High Resolution Scanning Electron Microscopy
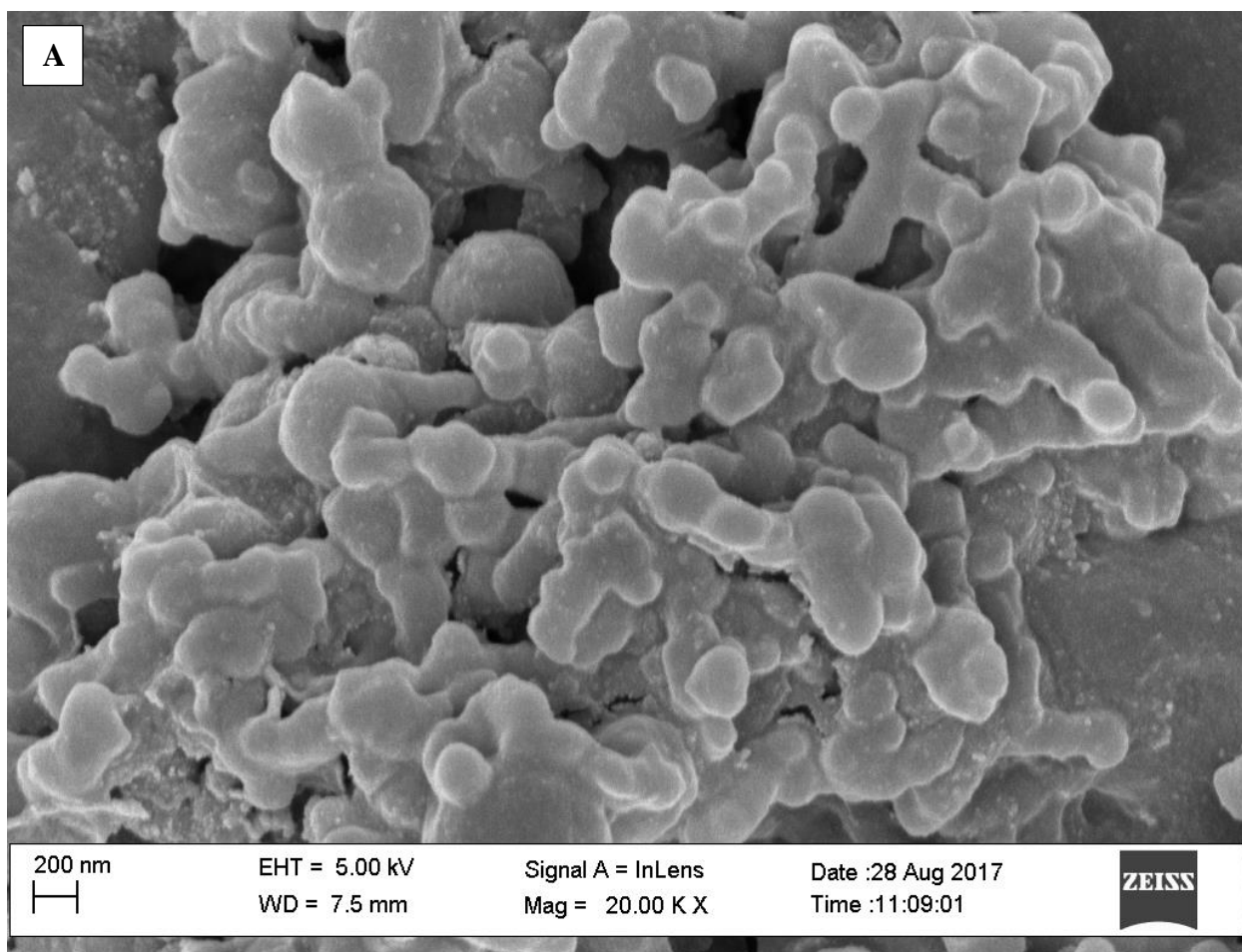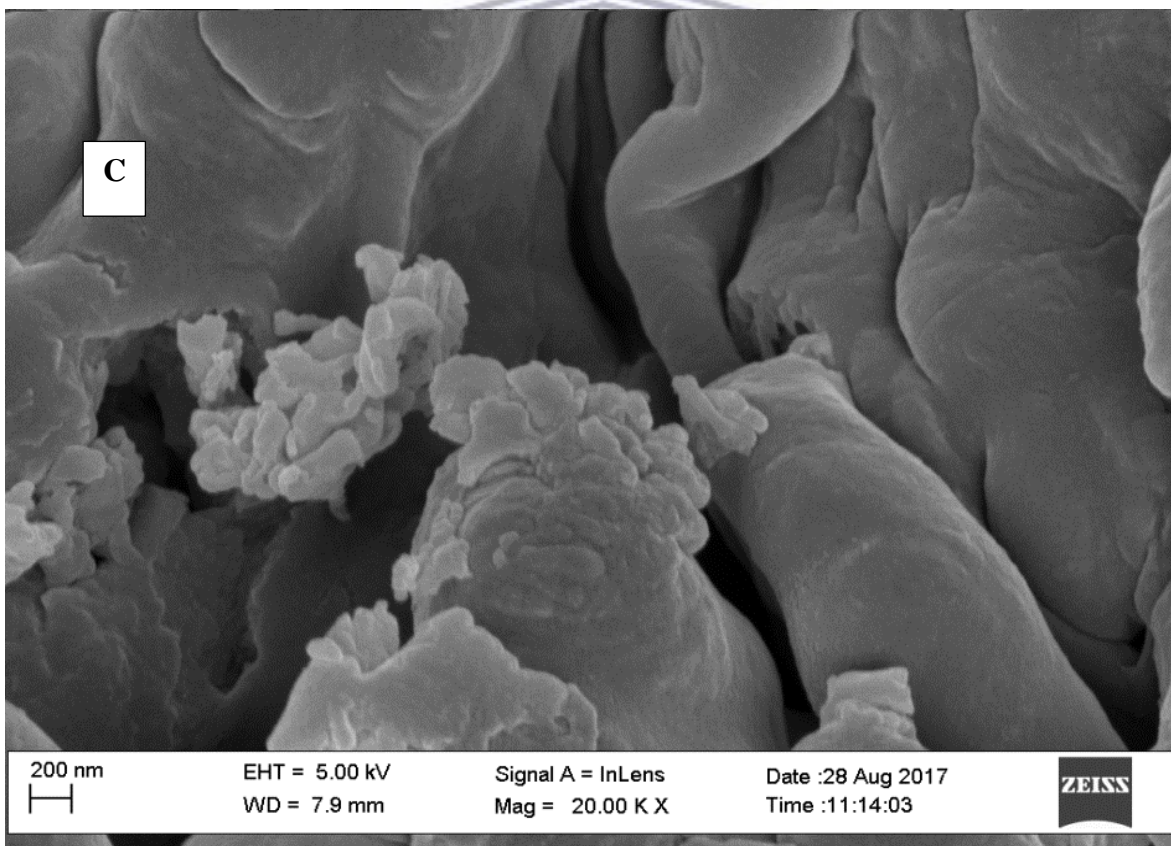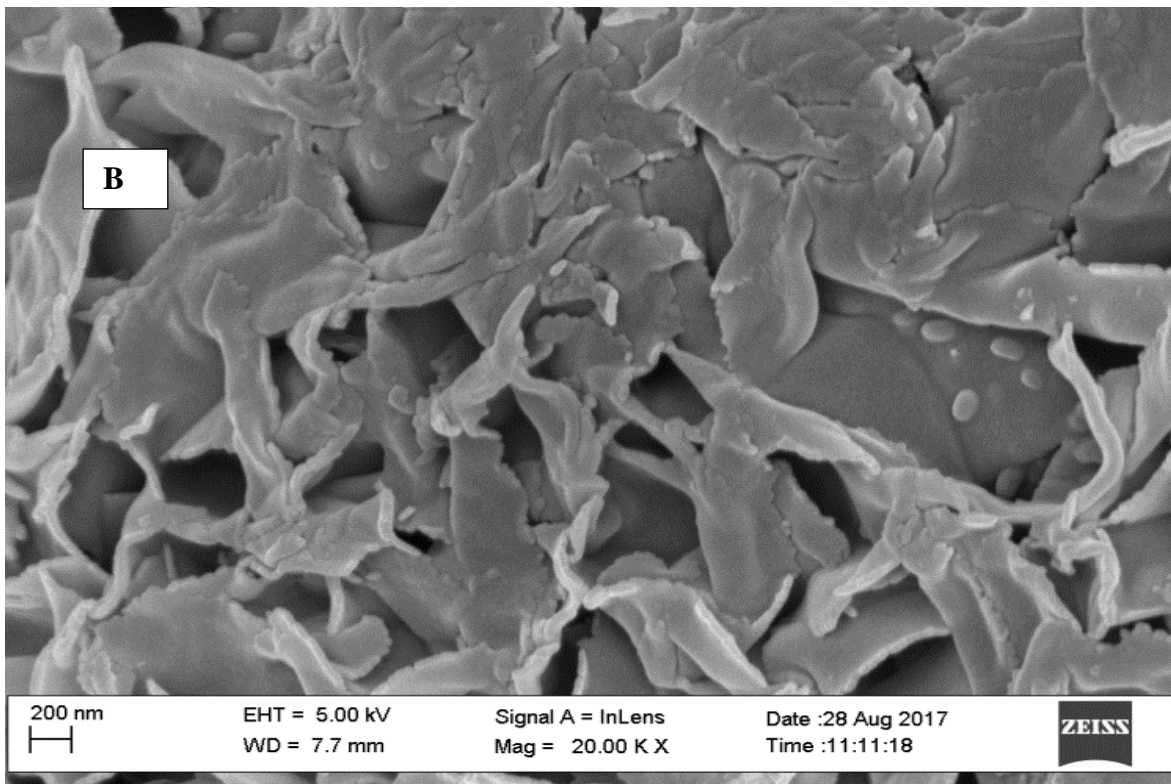
Figure 4.1.1 The SEM images for (a) P3HT, (b) PDDS and (c) P3HDS.

The surface morphology of the polymers was studied using the high resolution scanning microscopy, All the polymers represented in the data shown above are at a magnification of 100 000X. The SEM image presented in figure 4.1.1 (A) present the surface morphology of poly-3-hexybithiophene (P3HT) which is dense and round shape. It can be seen that the polydi(thien-2-yl)dimethylsilane (PDDS) has formed different sheets/layer that are not in one shape, while in the poly(3-Hexyl-[2.2'] bithiophen-5-yl)-dimethyl-bithiophen-2-yl-silane (P3HDS) image, which is the mixture of two polymers is showing two different shapes.

47

4.1.2 High Resolution Transmission Electron Microscopy
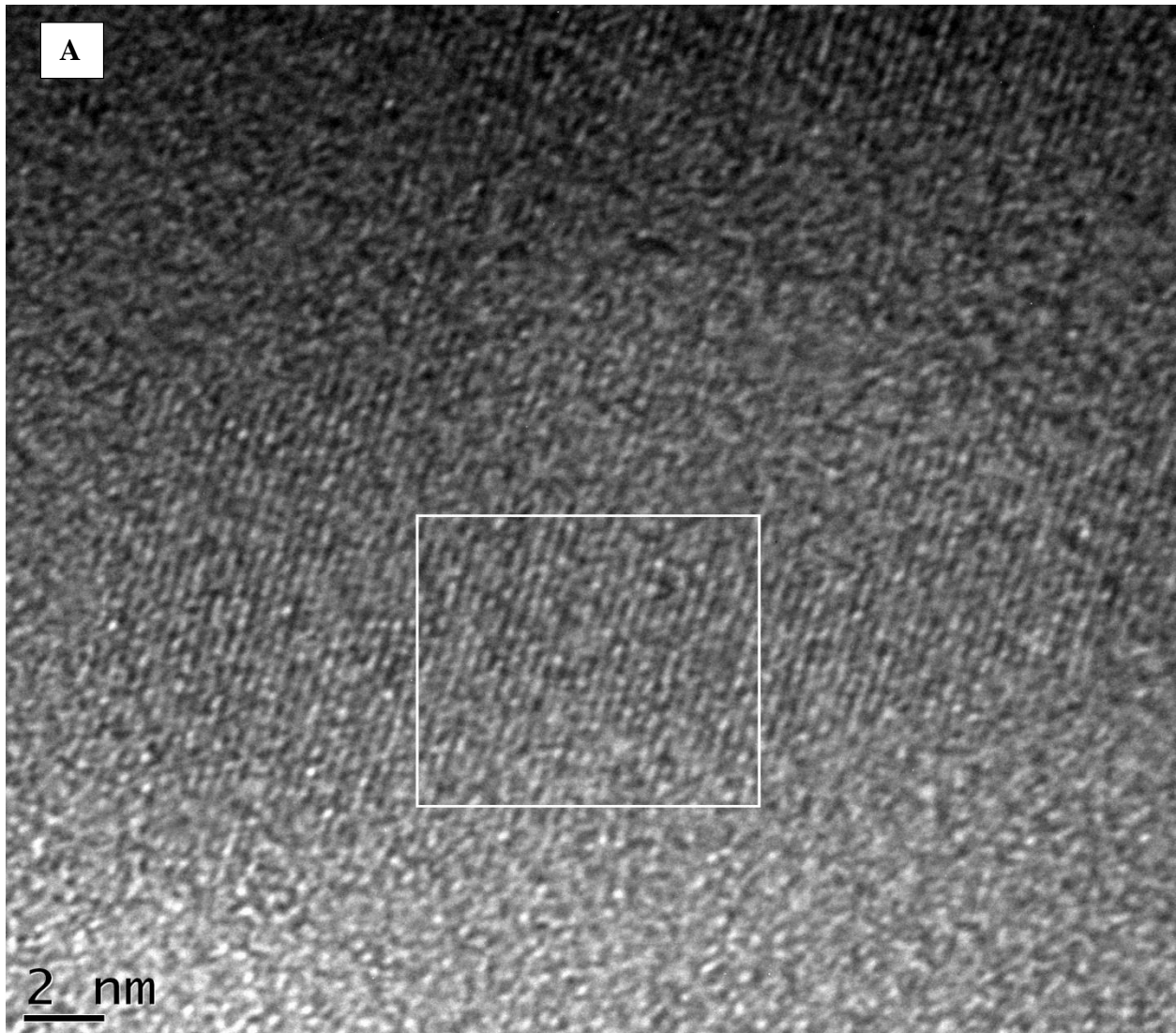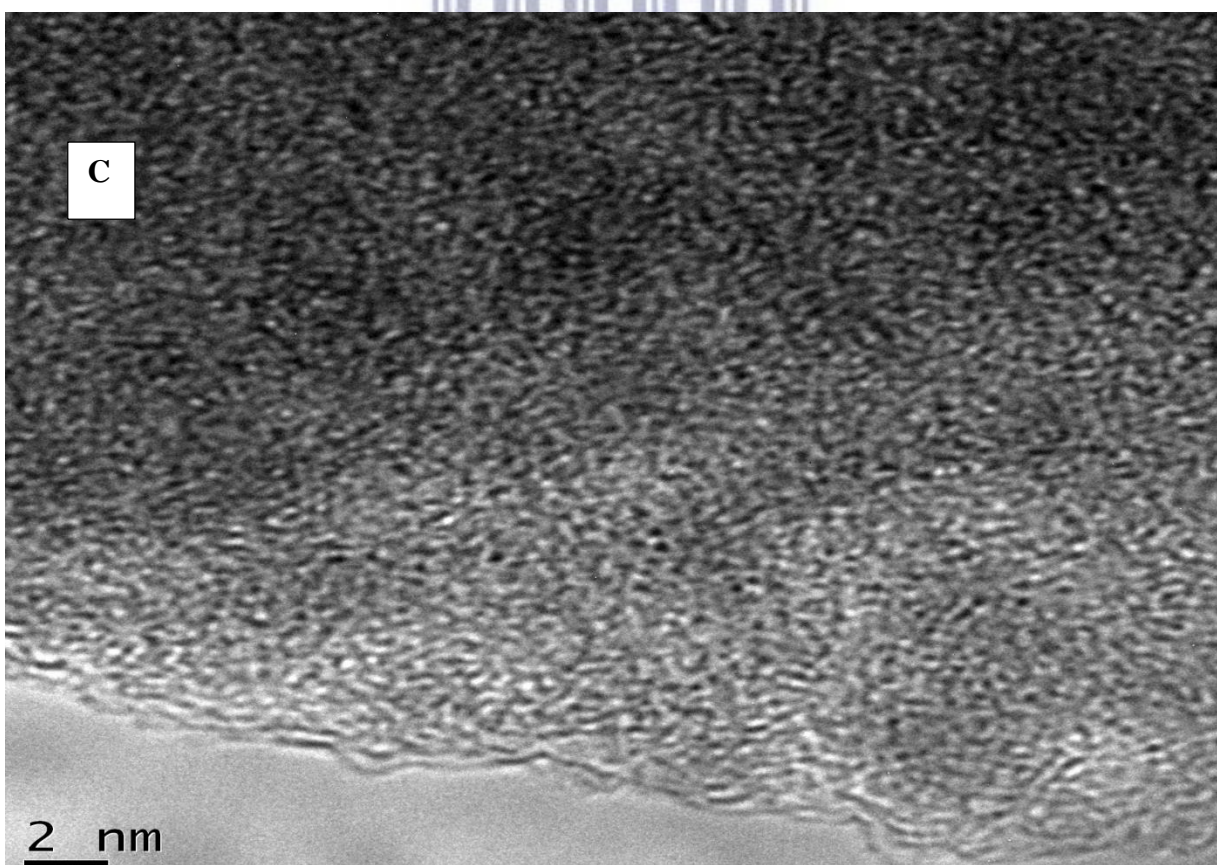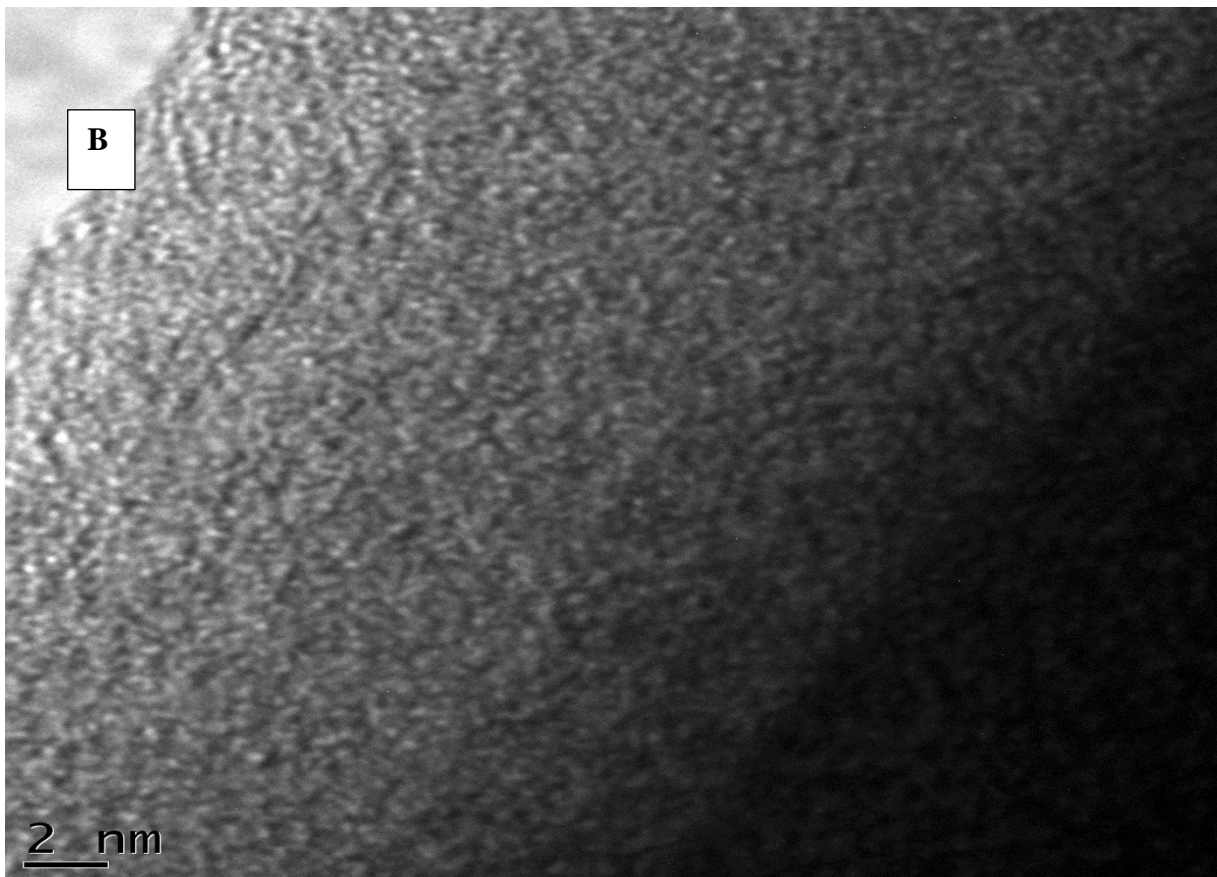
Figure 4.1.2: TEM images of (A) P3HT, (B) PDDS and (C) P3HDS.

49

The internal structures of the polymers were studied by Transmission Electron Microscopy. The images are presented in figure 4.1.2 above, where image (A) shows the morphology of P3HT with some small fringes that may indicate some crystallinity and the interplanar distance d_x was found to be 3.6 Ǎ, while image (B) PDDS and (C) P3HDS are both showing that the structures are amorphous and agglomerating which is expected on polymers.

4.1.3 Energy dispersive x-ray spectroscopy (EDS)
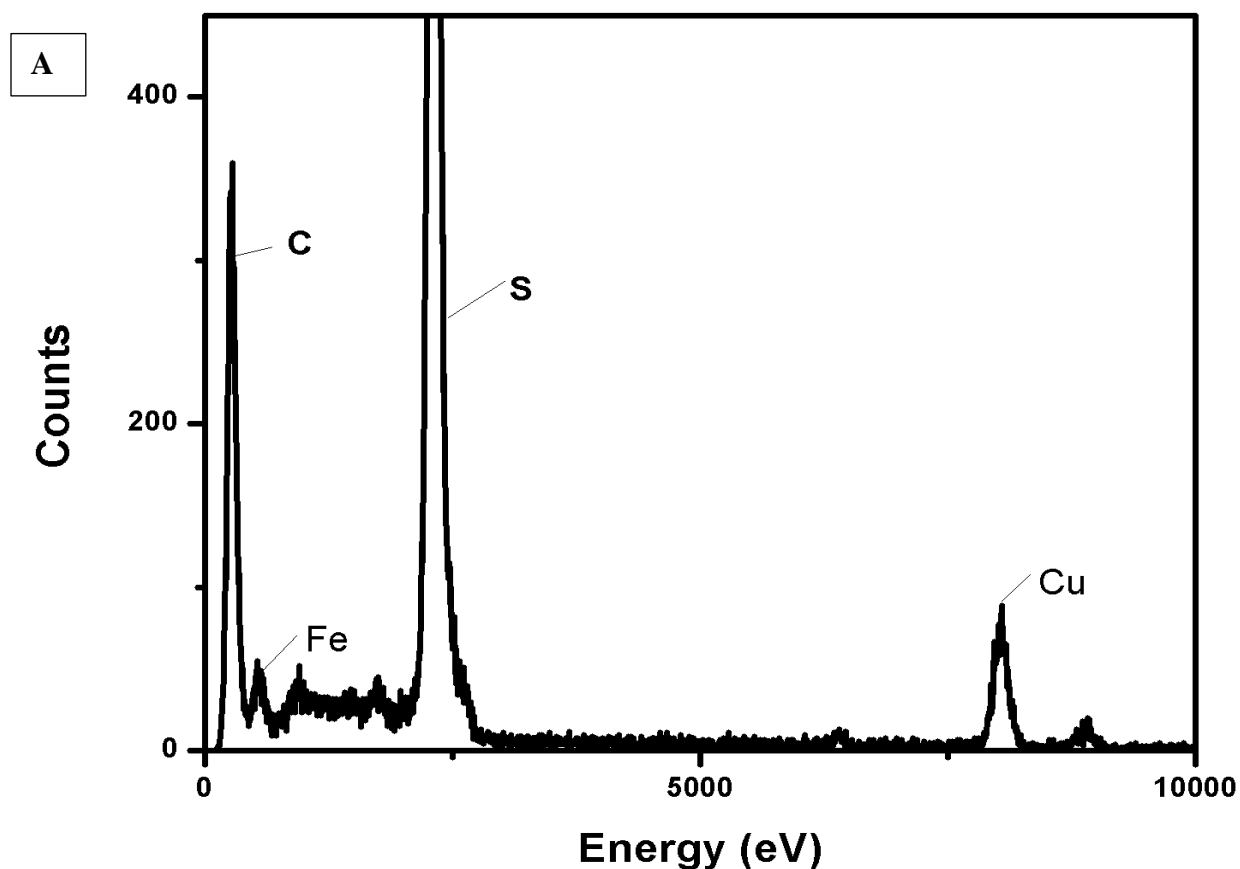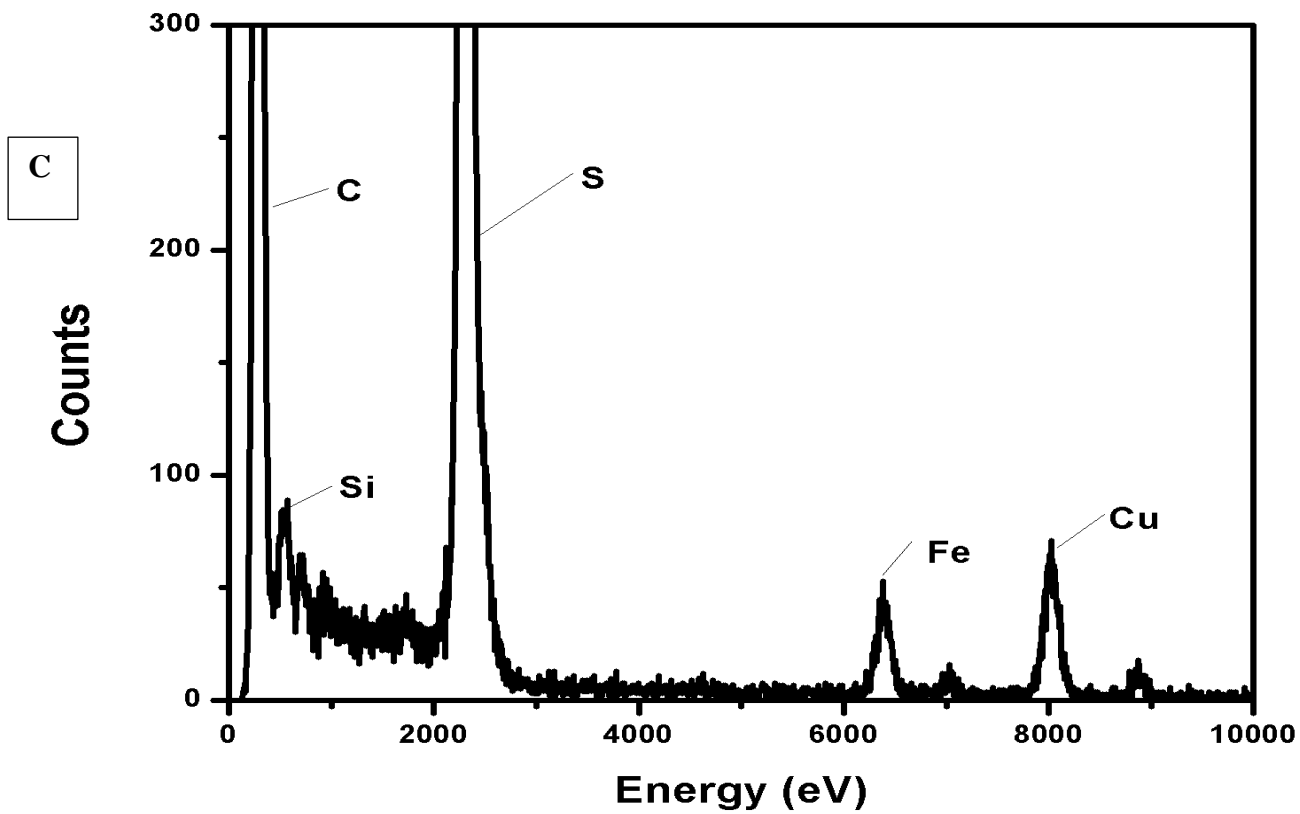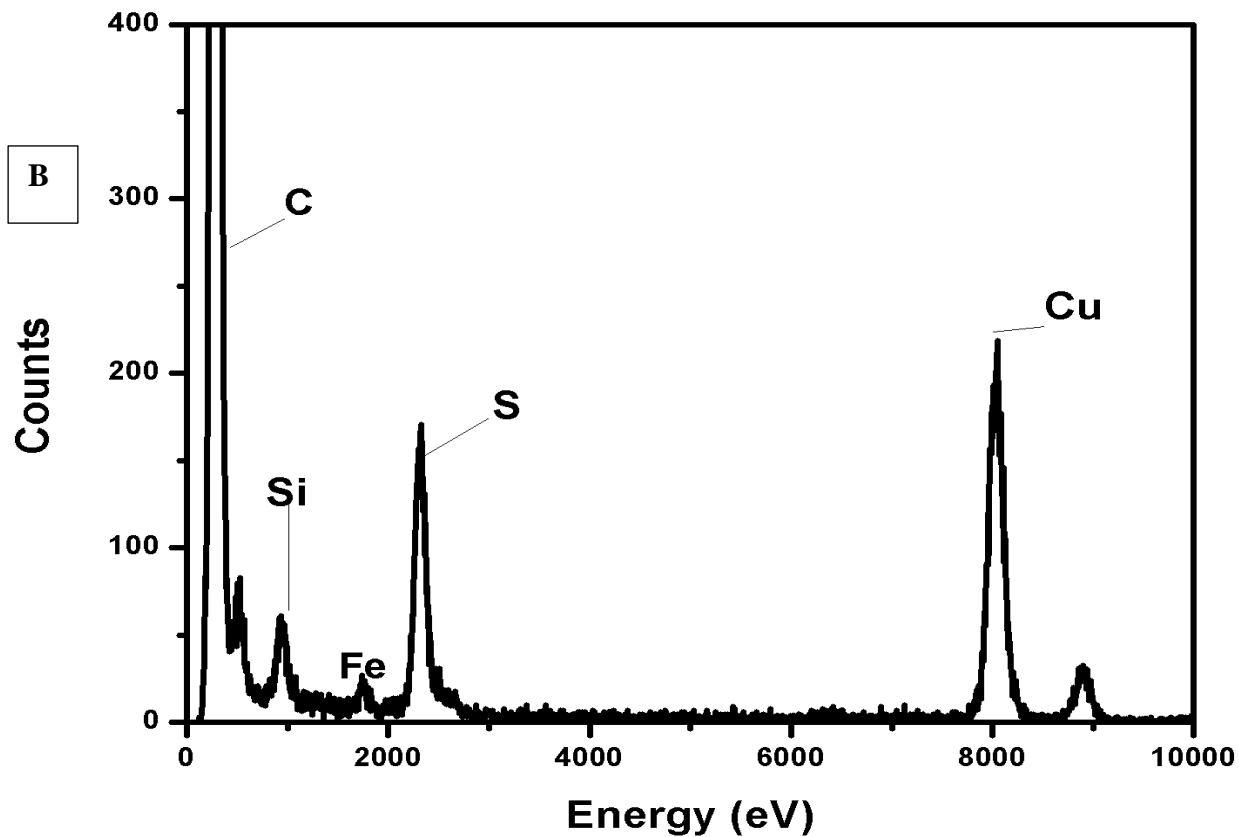
Figure 4.13: The EDS spectra of (A) P3HT, (B) PDDS and (C) P3HDS that was obtained from HR-TEM.

51

The EDX spectra of the polymers were obtained from HR-TEM where cupper grid was used. In figure 4.1.3 (A) all the element expected from P3HT are shown in the EDS spectra such as C and S, there's also Fe present which was used doing the synthesis as a catalyst. In figure 4.1.3 (B) and (C) the EDS spectra indicates that the polymers are composed of elements such as C, S and Si also there's a present of Fe that is due to the catalyst and Cu due to cupper grid.

4.2 X-ray Diffraction
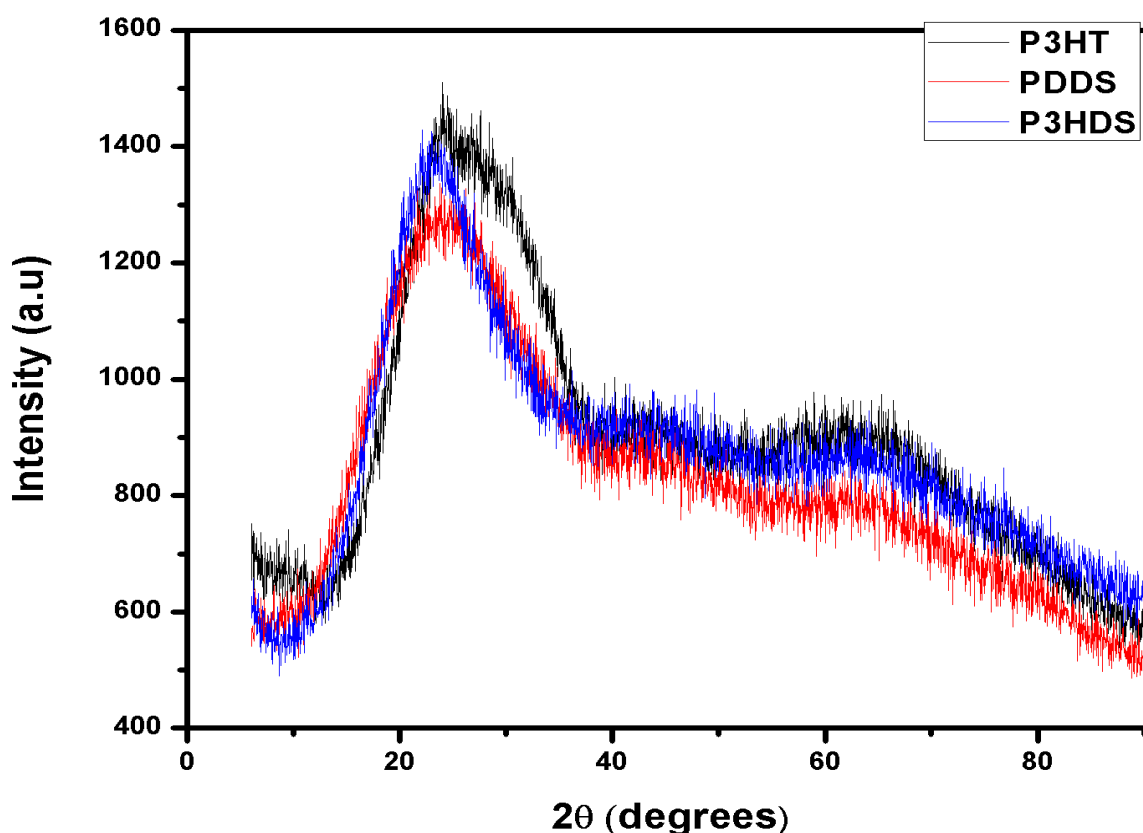
Figure 4.2: The X-ray diffraction of the three polymers.

X-ray powder diffraction (XRD) is the analytical technique that is mostly used for identification of crystalline materials where it provides information on unit cell dimension. On figure 4.2 above the XRD of the polymers is presented, they are all amorphous and P3HT is broader than others.

52

4.3 Fourier Transform Infrared (FTIR)
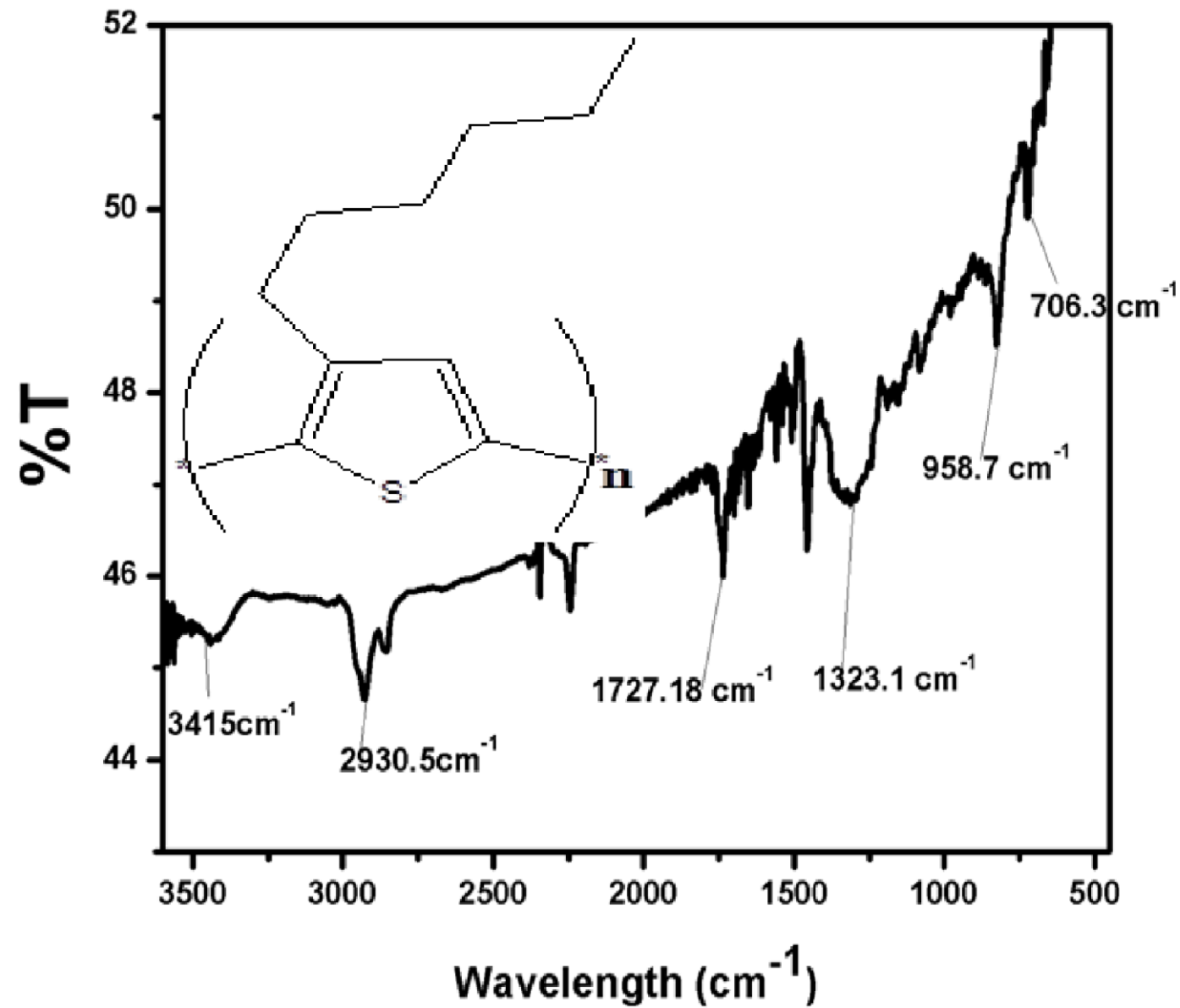
Figure 4.3.1: The FTIR spectra of P3HT in KBr.

The measured Fourier Transform Infrared (FTIR) spectrum of P3HT is shown in figure 4.3 above. In the figure 4.3 the absorption peaks are shown, the peaks at 3415, 2930.5 and 2560.5 cm^{-1} are all due to the CH$_2$ stretching for symmetric and antisymmetric from the alkyl side chains. The CH$_2$ absorption peaks in the spectrum are due to the long chain from the structure the results agreed with the results reported by Tamanai and colleagues [1]. The peak at 1727.18 and 1323.1 cm^{-1} represent C=C and C-C asymmetric stretching respectively. The peak at 958.7 cm^{-1} is due to CH$_3$ and the one at 706.3 cm^{-1} that is from C-S (S- atom) on the thiophene ring.
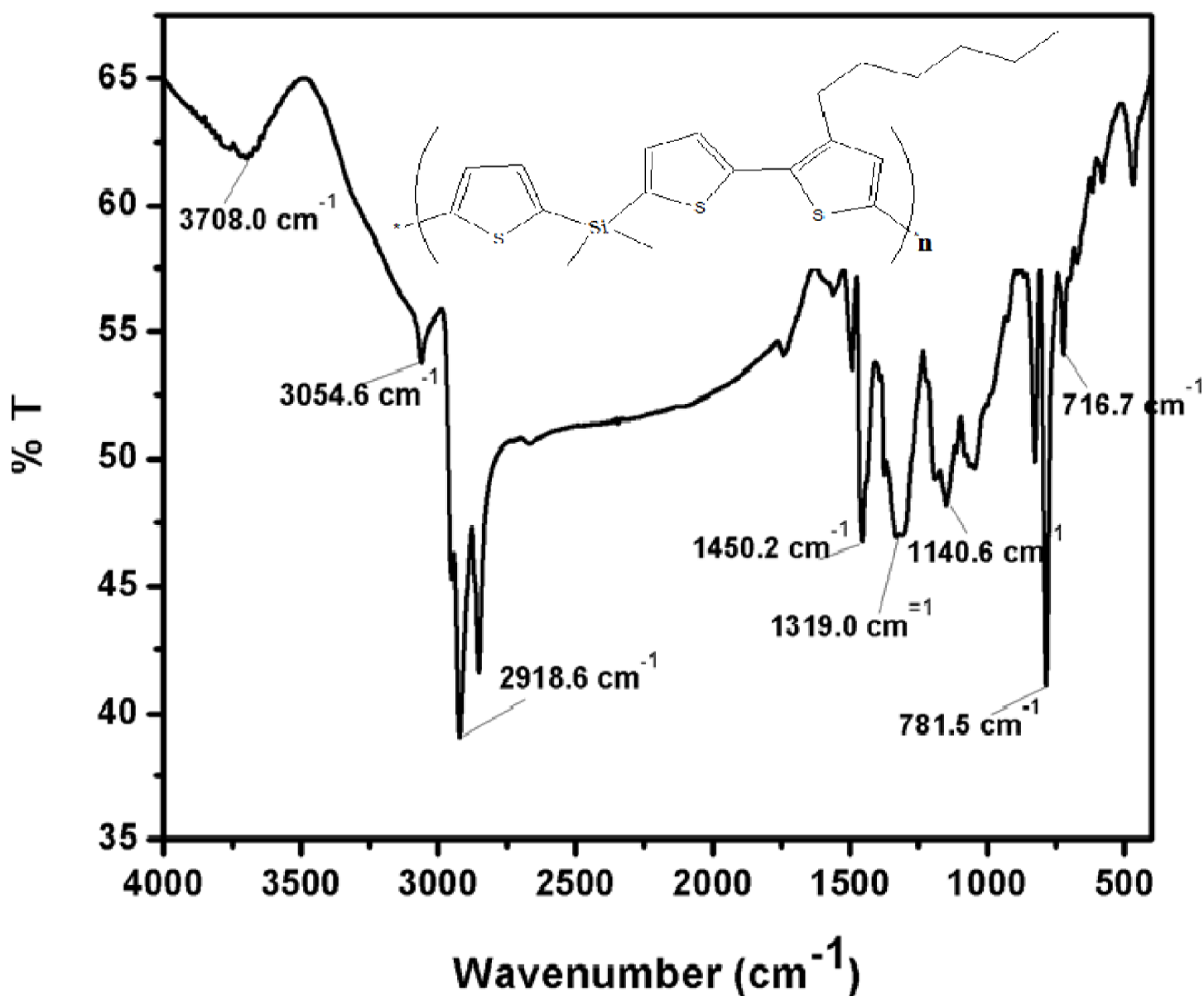
Figure 4.3.2: The FTIR absorption spectra of P3HDS in KBr

The FTIR spectrum in the figure 4.3.2 above is representing the absorption peaks of P3HDS, and it is seen at 3708.0 cm^{-1} the peak is O-H which was due to water that was used to wash the material. The absorption peaks at 3054.5 and 2918.6 cm^{-1} is due to the CH_2 of the aromatic ring and alkane chain respectively. It is shown that at 1450.2 and 1140.6 cm^{-1} there are absorption that are assigned to C=C and =CH that are from the ring. The absorption peaks at 1319.0 and 781.5 cm^{-1} are due the silicon found on the polymer and are assigned as $Si-CH_3$ and C-Si receptively reported by Andriot *et al* [2], and C-S peak that is due to sulphur in the thiophene ring is found at 716.7 cm^{-1}.

55
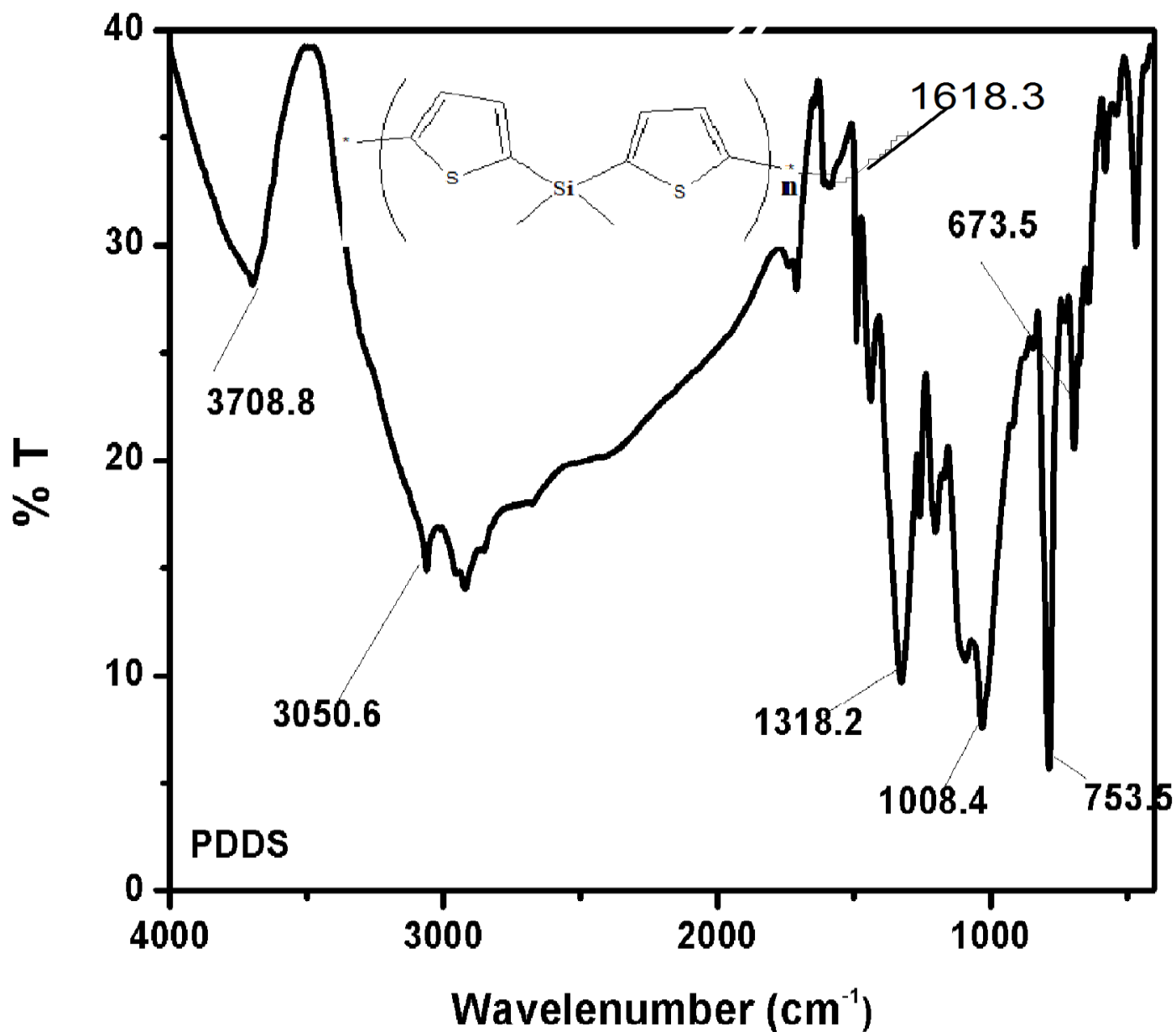
Figure 4.3.3: The FTIR absorption of PDDS in KBr.

The FTIR spectrum in the figure 4.3.3 above was used to study the absorption peaks of the polymer. The peaks presented at 3708.8 cm^{-1} was assign to water or ethanol that was used due washing of the polymer. There are peaks shown by the spectrum at 3050.6 cm^{-1} and 1613.3 cm^{-1} which are caused by CH_2 and C=C found on the methane groups attached to Si and the aromatic ring. At 1315.2 cm^{-1} and 753.5 cm^{-1} the peaks are both due to the silicon present in the structure,

56

they are assigned as Si-CH$_3$ and C-Si respectively. At 673.5 cm^{-1} the absorption peak is due to Sulphur that is due to the thiophene ring and the peak is assigned as C-S.

4.4 Gel Permeation Chromatography (GPC)
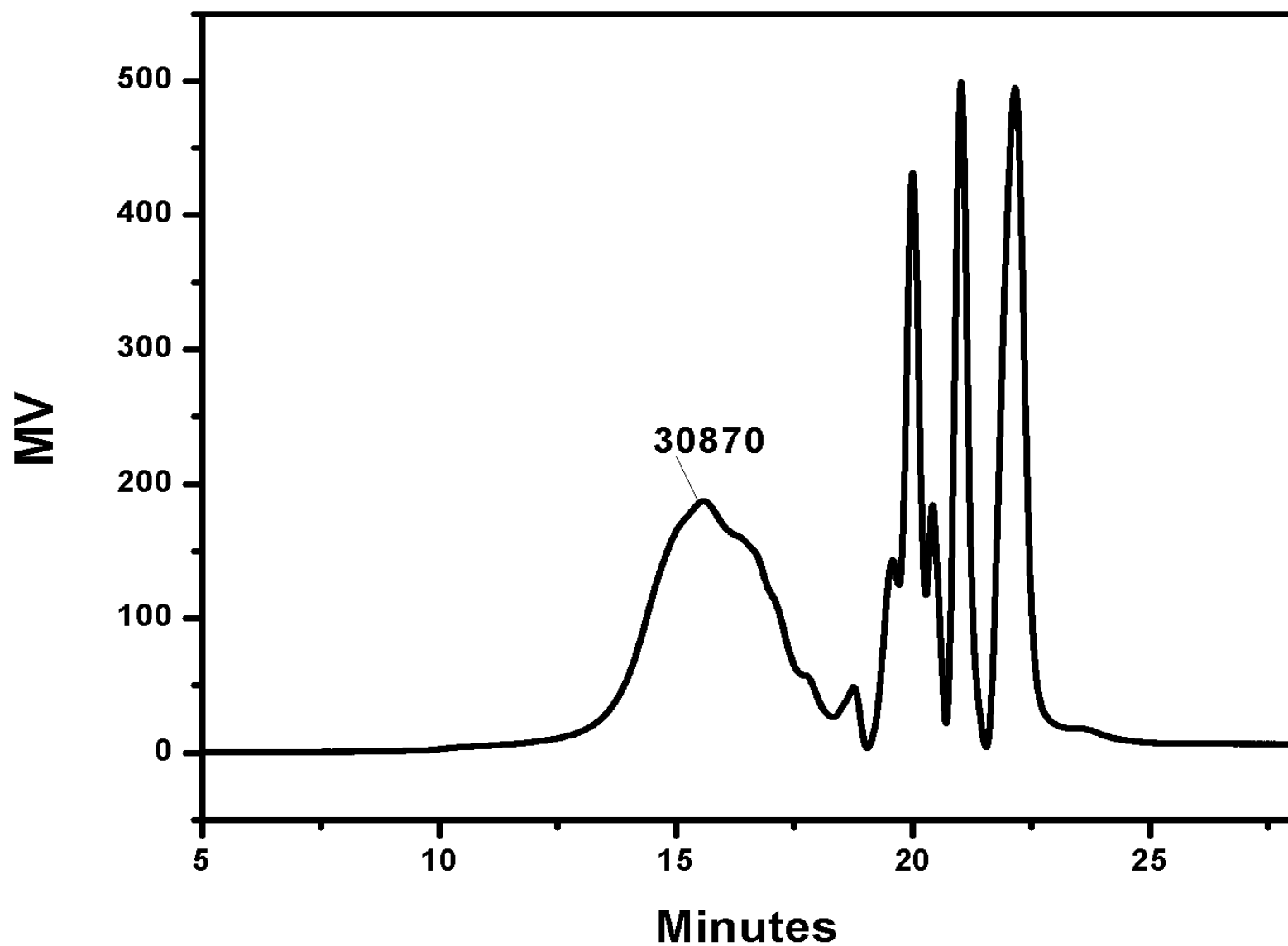
Mn (Daltons)	Mw (Daltons)	MP (Daltons)	Mz (Daltons)	Mz+1 (Daltons)	Polydispersity	Mz/Mw	Mz+1/Mw
13162	46230	30870	123569	227669	3.512432	2.672934	4.924715

Figure 4.4: The GPCfor P3HT

The use of the gel permeation chromatograph (GPC) for this study was determine the molecular weight distribution (MWD) of poly(3-hexylthiophene). In the figure 4.4 above, the chromatogram is shown on the diagrams and the different types of average molecular weights are found on the table. The Chromatogram represent the number average molecular weight (Mn) to be 13162 Daltons, where it's taken from equal numbers of molecules on each side of the polymer, at higher and lower molecular weight. The weight average molecular weight (Mw) and the Peak of the molecular weight (MP) are 46230 and 30870 Daltons respectively, the MP is used for calibration and the Mw comes from where there are equal number of masses. Size average molecular weight (Mz) and Mz+1 were found to be 123569 and 227669 Daltons respectively, this numbers can influence the viscosity of the polymer. To determine the polymer distribution, polydispersity was calculated which is the ratio of Mw to Mn, the value determined is 3.5124 this means that the polymer is broader due to different polymer chains found on the P3HT.

4.5 Thermogravimetric analysis (TGA)

The thermograms of weight loss percentage versus temperature for P3HT, PDDS and P3HDS were recorded at a heating rate of 10 °C min^{-1} in a nitrogen atmosphere. Results are shown in Figure 4.5. The weight loss observed on the graph of PDDS from 100- 190 °C may be due to the evaporation of any excess solvent and moisture that was still present in the powder as written

58

according to Baleg 2011[3], whilst the weight loss up to 310 °C could be attributed to the melting point of the PDDS, which ranges between 190-280 °C. However significant weight of the PDDS is observed from approximately 340-480 °C, this weight loss corresponds to the structural decomposition of the PDDS. While the weight loss of P3HT is observed from approximately 380-590 °C and that of P3HDS is approximately 300-470 °C.

Around 600 °C for all Polymers, some material is still present as shown in the thermogram (Figure 4.5), suggesting that the remaining material has a relatively high melting point. It has been observed that between 600-900 °C the PDDS material left is greater than that of P3HDS that is greater than P3HT which may be due to the silicon.
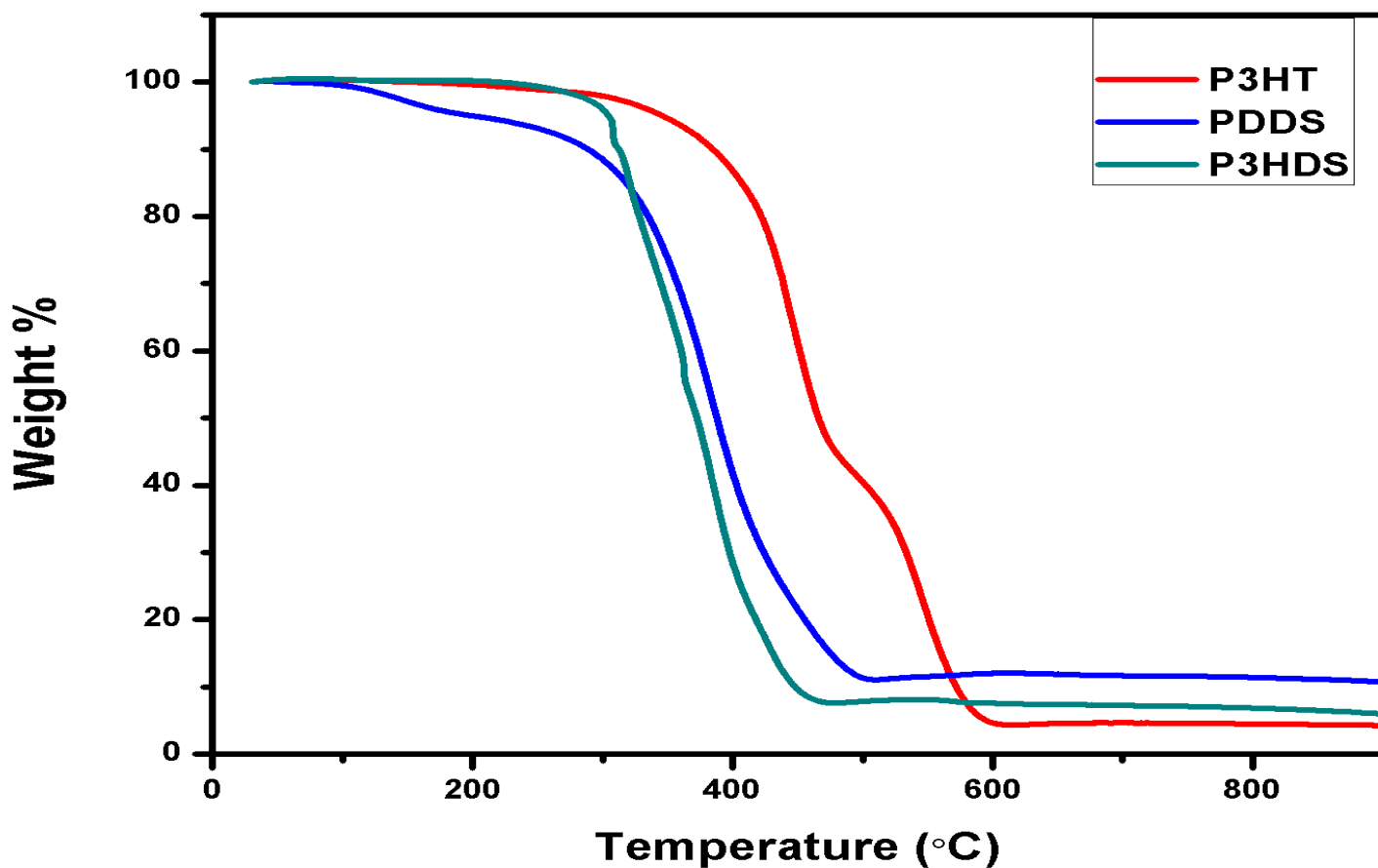
Figure 4.5: TGA thermogram of P3HT, PDDS and P3HDS showing weight decrease at different range.

59

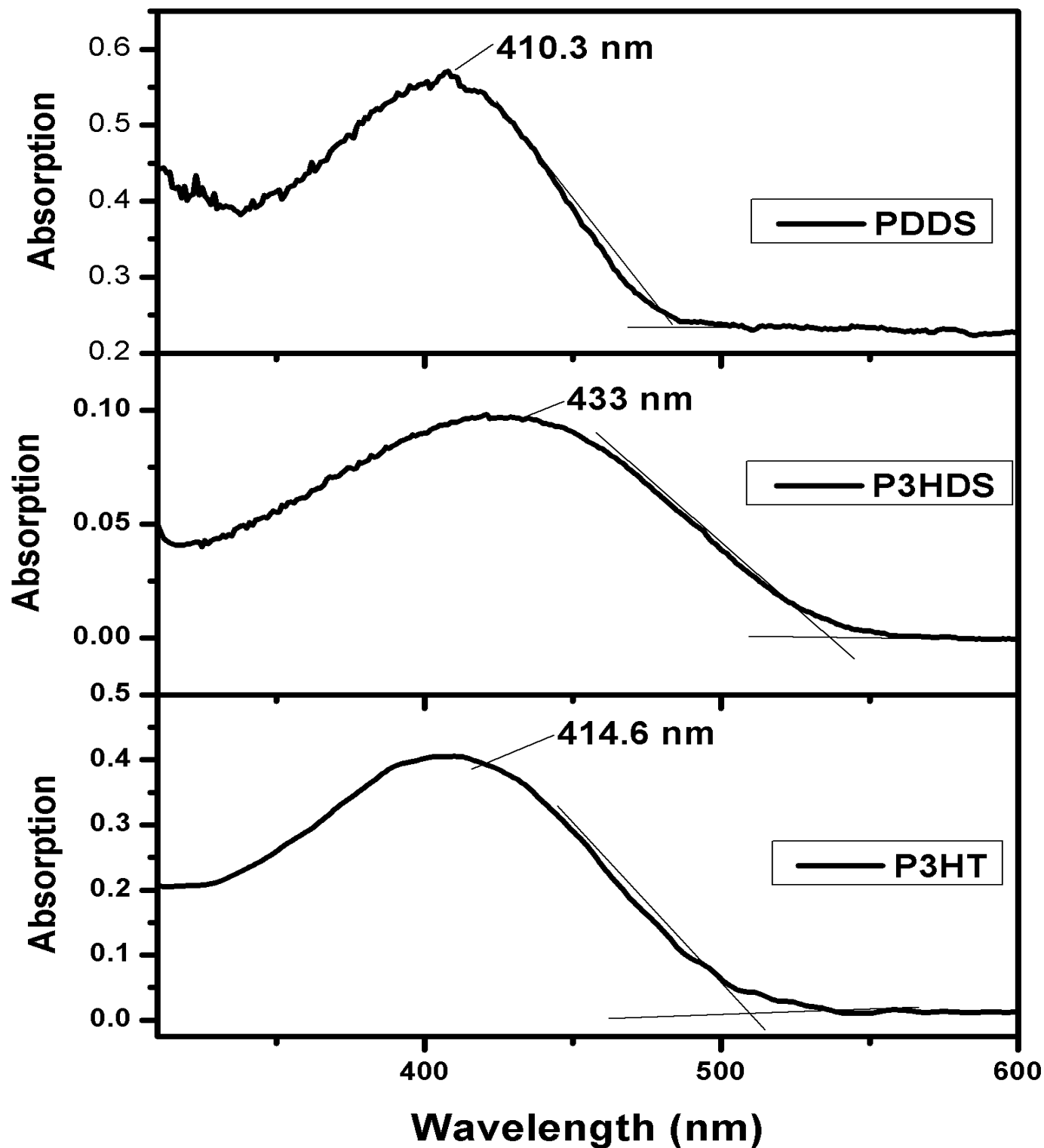**4.6 Ultraviolet Visible Spectral Analysis (Uv-vis)**

Figure 4.6: The UV-vis spectra of P3HT, PDDS and P3HDS.

Ultra-violet spectroscopy was used to determine the transition that took place during absorption of P3HT, PDDS and P3HDS and the optical band gap. The absorption spectrum in figure 4.6 shows an absorption peaks of P3HT solution at 510.45 nm while in the literature, the absorption peak was reported to be around 520 – 554 nm [4]. This blue shift that was observed might be due to the fact that the absorption was done in solution while in the literature it was done in a film. This transition bands can be attributed to the $\pi \rightarrow \pi^*$ transition due to the stacking of P3HT. The optical band gap of P3HT, estimated from the absorption band edge, amounts to ~ 1.90 eV [4] but the obtained band gap from the edge is 2.42 eV due to the blue shift. The absorption peak for PDDS solution was observed at around 487.87 nm which was less than that of P3HT and that might be due to the backbone of the molecular structure. The bandgap that was calculated from the absorption band edge was found to be 2.54 eV and the transition was $\pi \rightarrow \pi^*$ transition due to the stacking of thiophene rings. In the figure 4.6 we also observe the absorption peak of P3HDS which is the mixture of both P3HT and PDDS. In this band the red shift is observed, which was expected as the polymer was a modification of the two above. The transition band was $\pi \rightarrow \pi^*$ transition that was due to thiophene ring and the calculated band gap was 2.31 eV.
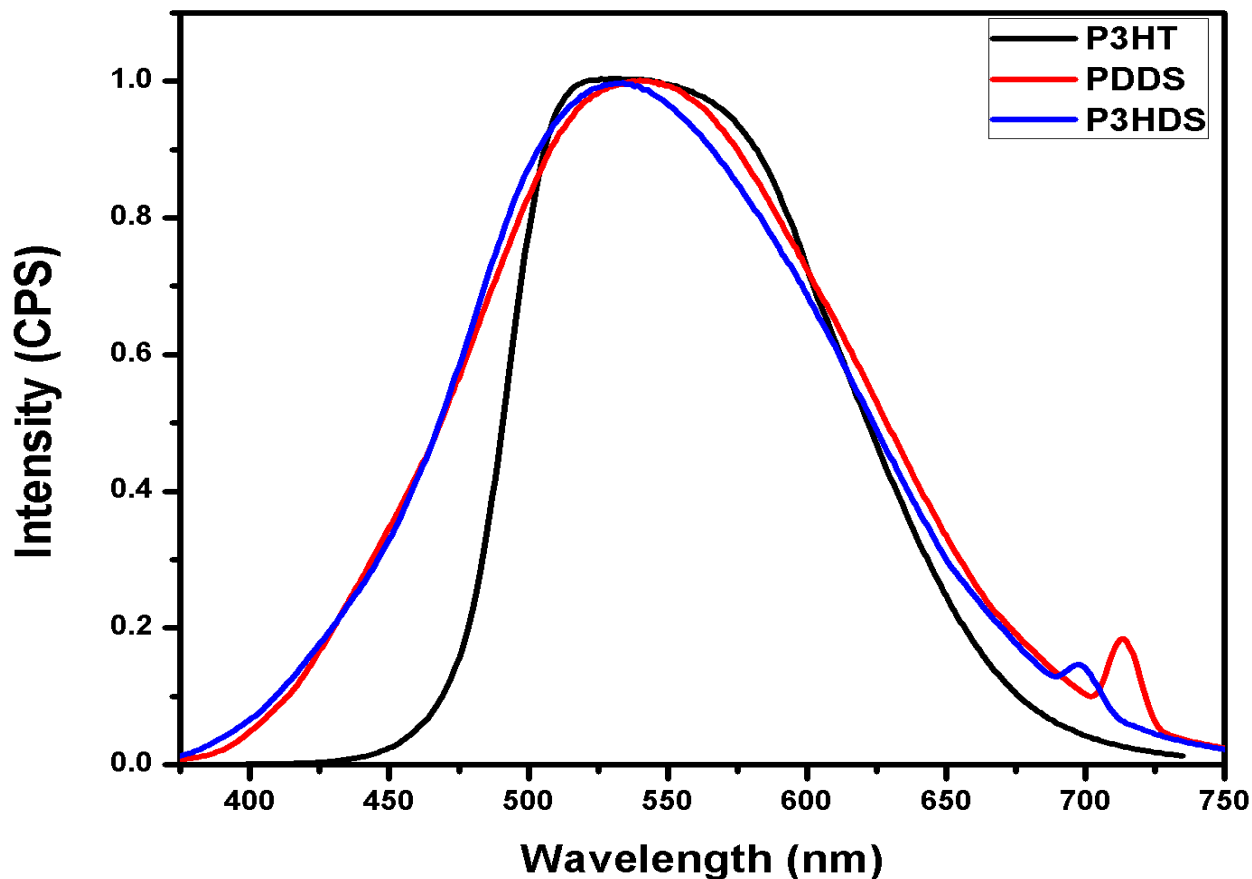
61

4.7 Photoluminescence (PL)

Figure 4.7: The PL spectra of P3HT, PDDS, P3HDS polymers in solution.

The figure 4.7 above shows the photoluminescence spectra of all three polymers under excitation wavelength of 350 nm, in the range of 350-750 nm. The photoluminescence of the compounds were studied in chloroform and 1.2-dichlorobenzene. As already illustrated in Chapter 3, photoluminescence or fluorescence is a transition that occurs when a compound in its excited state goes back to its ground state by releasing a photon. It was observed that the P3HT has a maximum peak of 546.63 nm, which might be due to the surface oxidation defects of the solution. The emission peak observed for PDDS was 542.46 nm and for P3HDS was 532.63 nm,

62

this small shift was reported that it may indicate a less distorted backbone conformation in solution for polymers [5]. On the spectrum of PDDS and P3HDS the vibronic peaks are observed around 713.175 nm and 697.76 nm respectively they might indicate that, the polymer is di-substituted polymer hence no vibronic peak observed on P3HT.
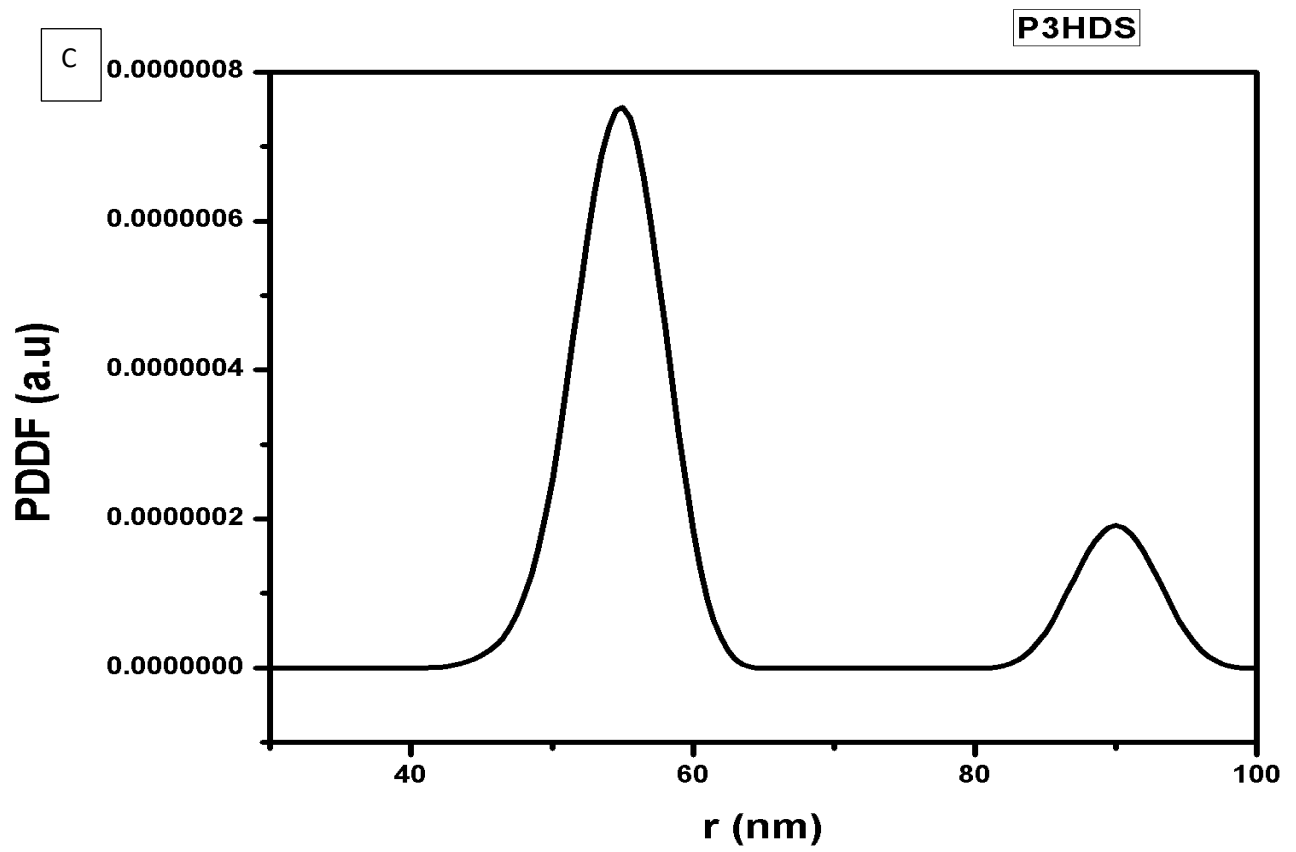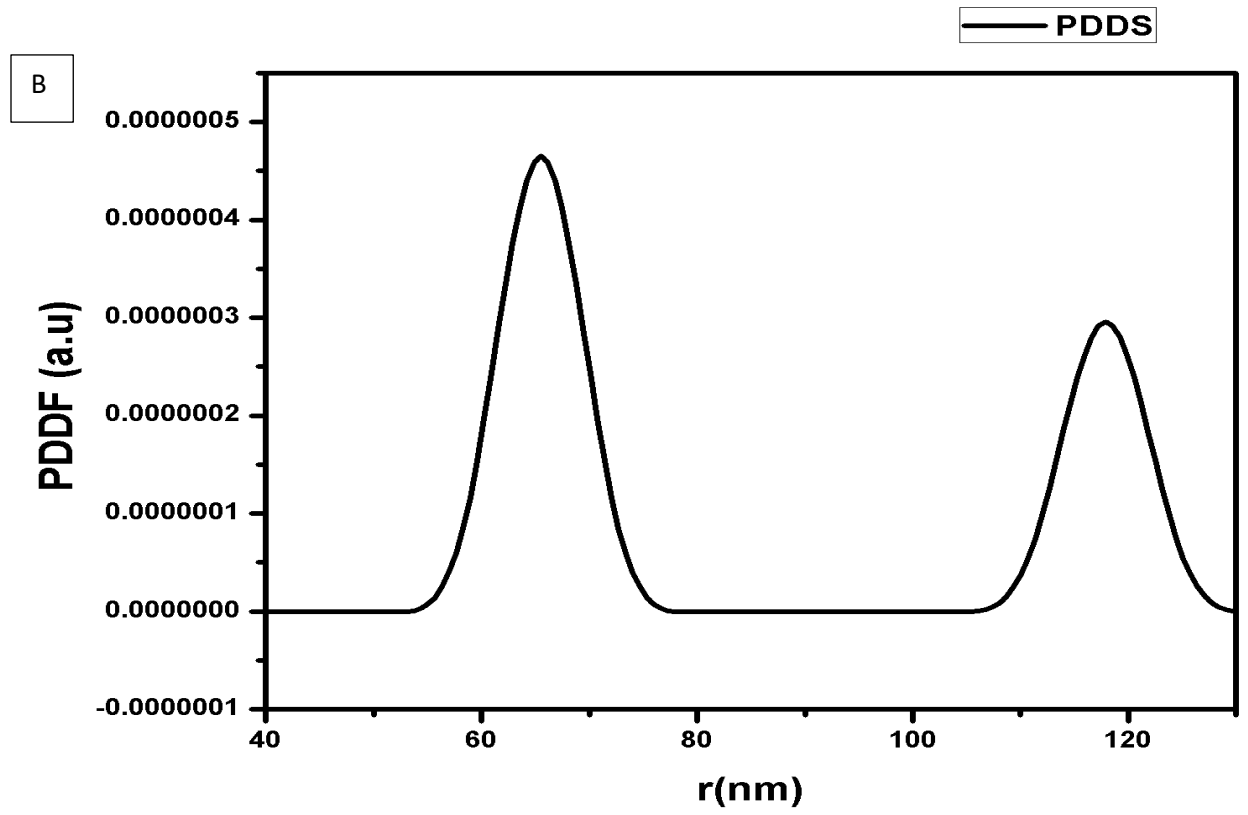
4.8 Small-Angle X-ray Scattering (SAXS)

B

PDDS

C

P3HDS

64
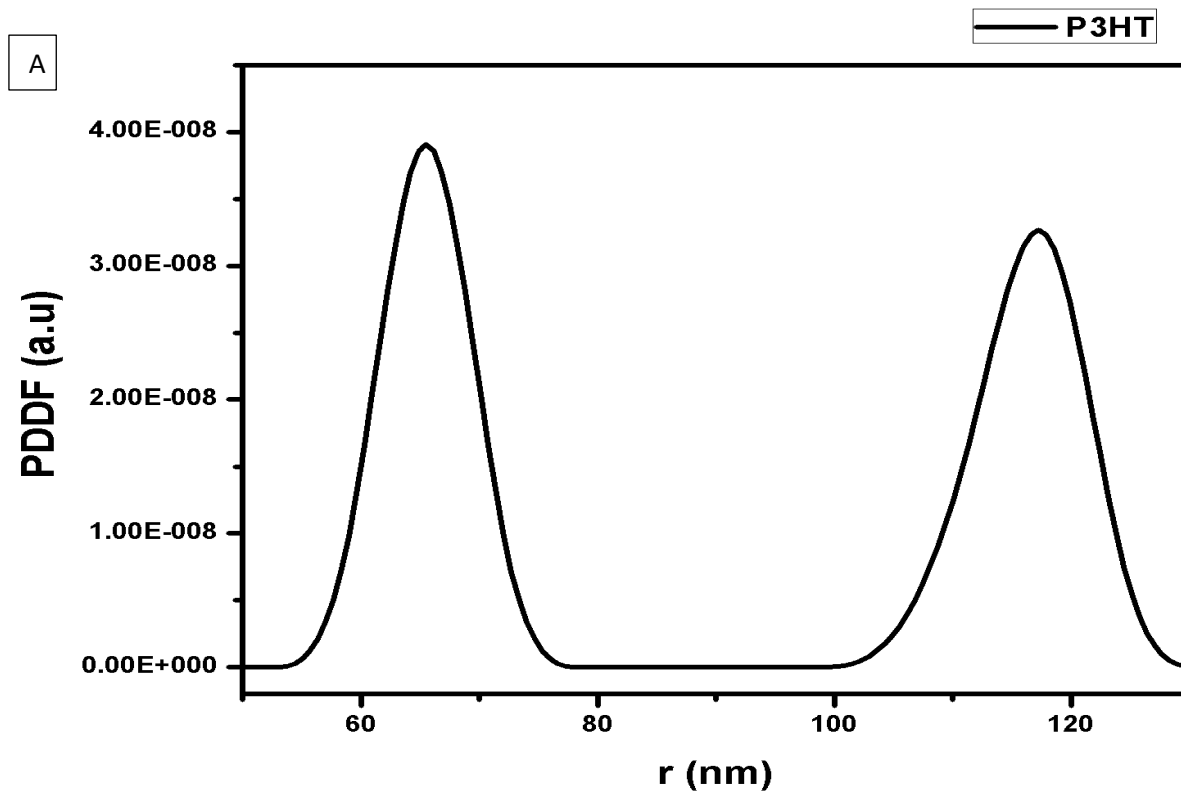
Figure 4.8: The PDDF of (a) P3HT, (b) PD DS and (c) P3HDS indicating the particle size and shape.

Every particle is known to have its own structure that can produce different characteristics [6], in the figure 4.8 above the PDDF of polymers is shown. Figure 4.8 (A) indicates the PDDF of P3HT where a spherical or globular shape was observed, same shape was observed and reported on SEM image above. P3HT was found to be inhomogeneous or having a core-shell that might be due to the Fe used during the synthesis and also the size of the particle was 65.4 nm and the core-shell was 117.36 nm. The particles found in the polymer are almost identical but there is small difference in the shape which makes them polydispersity.

The PDDF shown by figure 4.8 (B), indicates the shape of PDDS that was found to be spherical or globular. This polymer was found to have a core-shell also where the particles were the same shape but different size and that was concluded to be polydispersity. The size of the particles was found to be 65.36 nm and the core-shell was 118.14 nm. Whilst figure 4.8 (C) the PDDF of P3HDS is shown and it indicates that the shape of the polymer is spherical or globular and it has a core-shell. The size of the particle is 55 nm and the core-shell is 90.5 nm and it is polymorphous due to the fact that particles are completely different.

65

4.9 Electrochemistry

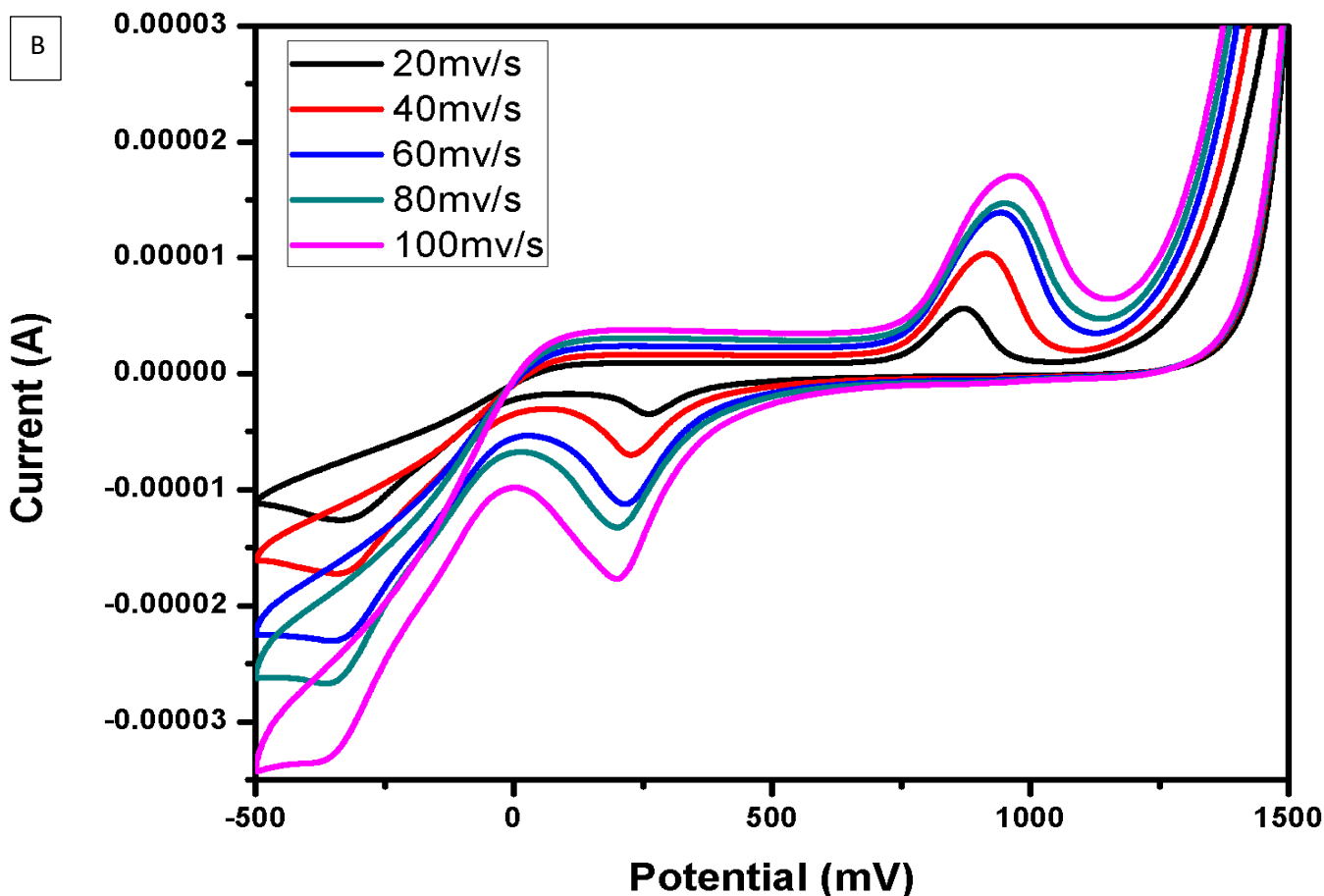**4.9.1 Cyclic Voltammetry (CV) for (poly(3-hexythiophene)**
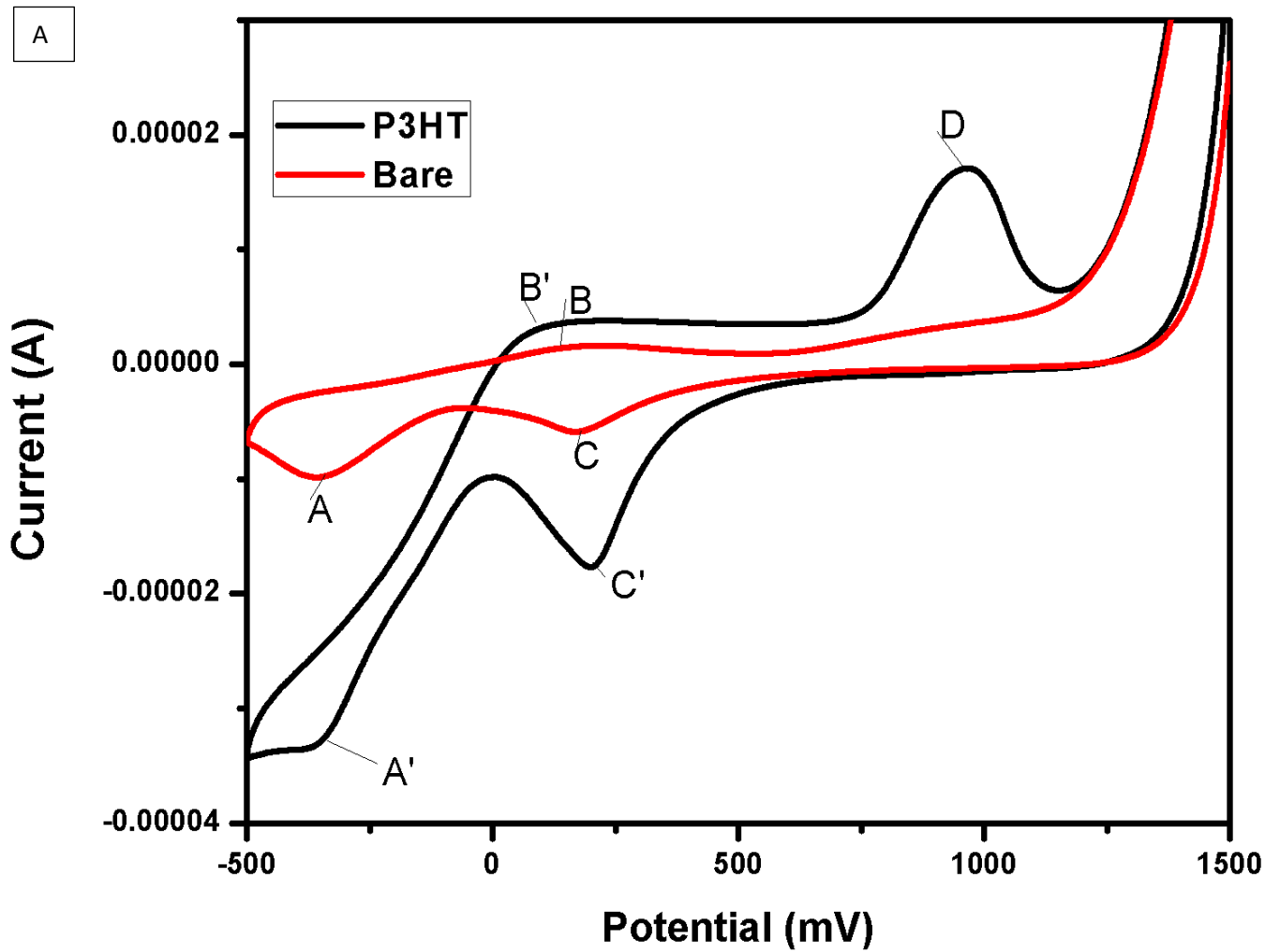
Figure 4.9.1: The CV for P3HT Film in 0. 2 M of LiClO$_4$ using platinum electrode.

The cyclic voltammogram (CV) at figure 4.9.1 shows the characterization of the donor material, P3HT film, on platinum electrode in 0.1 M LiClO$_4$ electrolyte which was carried out at different scan rates with an electrochemical potential window of -500 mV/s to 1500 mV/s. In Figure 4.9.1 (A) above the bare and the P3HT at 100 mV are presented. By comparing the bare platinum electrode and P3HT film, two oxidation and two reduction peaks were observed and labelled A, B, C and D these results proves that during oxidation two species were generated then later were stabilized by anodic potential similar results were reported by Cervantes *et al.*[7]. During this it was notice that the current on the electrode increased when the material was on the surface of the

electrode. The oxidation peaks observed are around +101.6 mV and 971.7 mV, and the reduction peaks are at -363.9 mV and 198.90 mV. The oxidation peak of P3HT was reported by Goncalves and the colleagues[8] to be at 900 mV which is almost the same as the one observed but a small shift that might be due to the supporting electrolyte or solvent used. The voltammogram in figure 4.9.1 B shows the average formal potential $E^{\circ\prime}$ of P3HT to be 576.71 mV and the average ratio of the anodic to cathodic peak current, I_{pa}/I_{pc} as 1.124, the results indicate that the reaction is reversible. However, the peak separation ($\Delta Ep = Ep,_A - Ep,_C$) values varied with scan rate and were all more than 65 mV expected for the electrochemistry of a surface-bound species undergoing fast reversible electron transfer reaction.

E (ox) (mV)	E (ox) Onset (mV)	HOMO (eV)	E (red) (mV)	E (red) Onset (mV)	LUMO (eV)	Eg (eV)
931.99	781.6	5.533	220.94	339.4	4.022	1.51

Table 1: CV data, HOMO, LUMO and band gap of P3HT**.**

In table 1 above the calculated HOMO and LUMO are presented, which were calculated using the formula $E_{LUMO}= [(E_{red}-E_{1/2(ferrocene)})) +4.8]$ eV or $E_{HOMO}= [(E_{ox}- E_{1/2(ferrocene)})) +4.8]$ eV. Ferrocene was used as external standard. Where HOMO was found to be 5.533 eV and LUMO was 4.022, the electrochemical band gap was also calculated using the formula of Eg= HOMO – LUMO and it was 1.51 eV. In the literature the electrochemical band was reported by Al-Ibrahim and colleagues was 1.67 eV [9] which was closer.

68

4.9.2 Cyclic Voltammetry (CV) for Poly Di(thien-2-yl)dimethylsilane
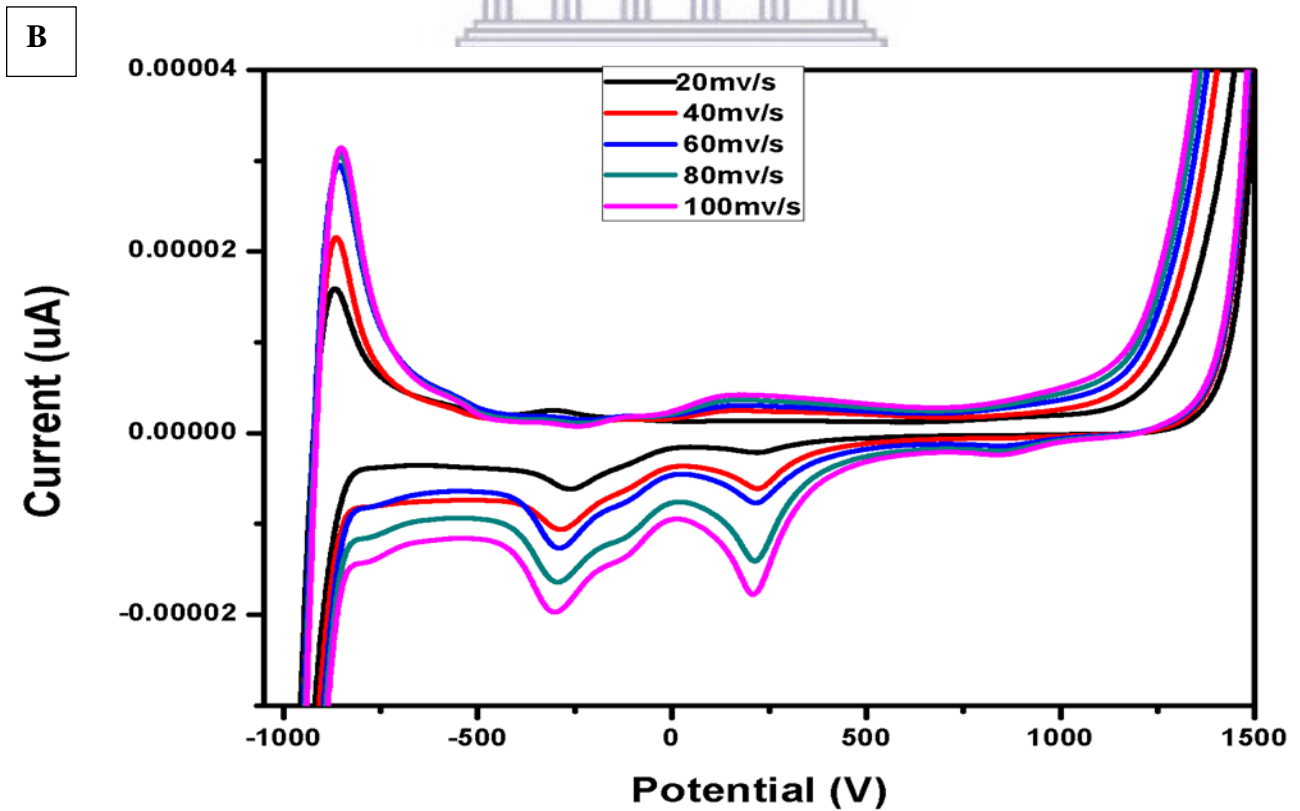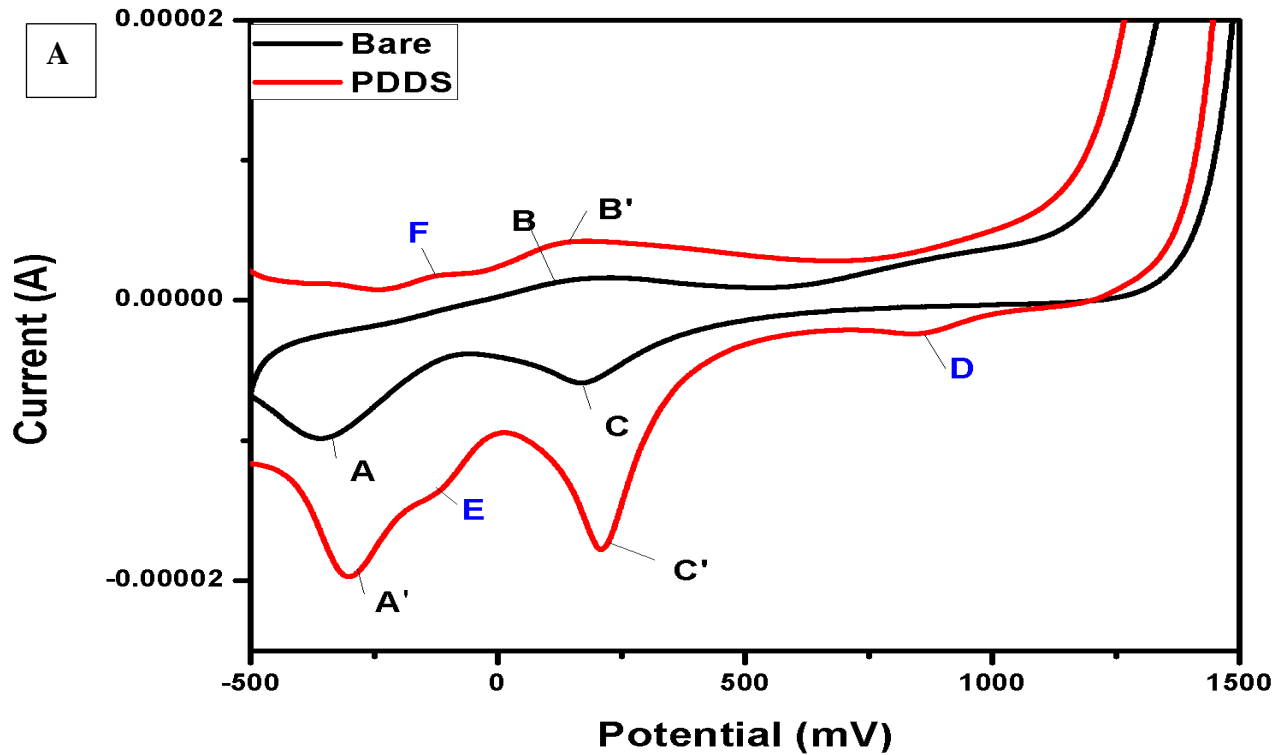
Figure 4.9.2: The CV for PDDS film in 0.1 M of LiClO₄ using platinum electrode

The cyclic voltammetry shown in figure 4.9.2 above is used as electrochemical characterization technique for polydi(thien-2-yl)dimethylsilane which is a donor material for hybrid solar cells. The voltammogram of the bare electrode with PDDS film is shown in figure 4.9.2 (a) above, where peaks labeled A, C, D and E are found to be cathodic while B and F are anodic, the results proves that during oxidation four species were generated but not all of them are stabilized by anodic potential . In figure 4.9.2 (b) it was shown that as the scan rate on the film increases the current also increases. The oxidation peaks observed are around -296.17 mV and 184.97mV labelled as F and B respectively, and the reduction peaks labelled A, C, D and E are at -296.17 mV, 217.1 mV, 848.75 mV and -117.92 mV respectively. The voltammogram also shows that the average formal potential $E^{\circ'}$ of PDDS to be 542.4 mV and the average ratio of the anodic to cathodic peak current, I_{pa}/I_{pc} as 0.682, the results indicate that the reaction is irreversible. However, the peak separation ($\Delta Ep = Ep,_A - Ep,_C$) values varied with scan rate and were all more than 65 mV expected for the electrochemistry of a surface-bound species undergoing fast irreversible electron transfer reaction.

E (ox) (mV)	E (ox) Onset	HOMO (eV)	E (red) (mV)	E (red) Onset	LUMO (eV)	Eg (eV)
1487.4	1078.82	6.29	-849.4	-717.45	4.493	1.8

Table 2: CV data, HOMO, LUMO and Band gap of PDDS.

In table 2 above the calculated HOMO and LUMO are presented, which were calculated using the formula $E_{LUMO}= [(E_{red}-E_{1/2(ferrocene)})) +4.8]$ eV or $E_{HOMO}= [(E_{ox}- E_{1/2(ferrocene)})) +4.8]$ eV.

70

Ferrocene was used as external standard. Where HOMO was found to be 6.29 eV and LUMO was 4.493 eV, the electrochemical band gap was also calculated using the formula of Eg= HOMO – LUMO and it was 1.8 eV.

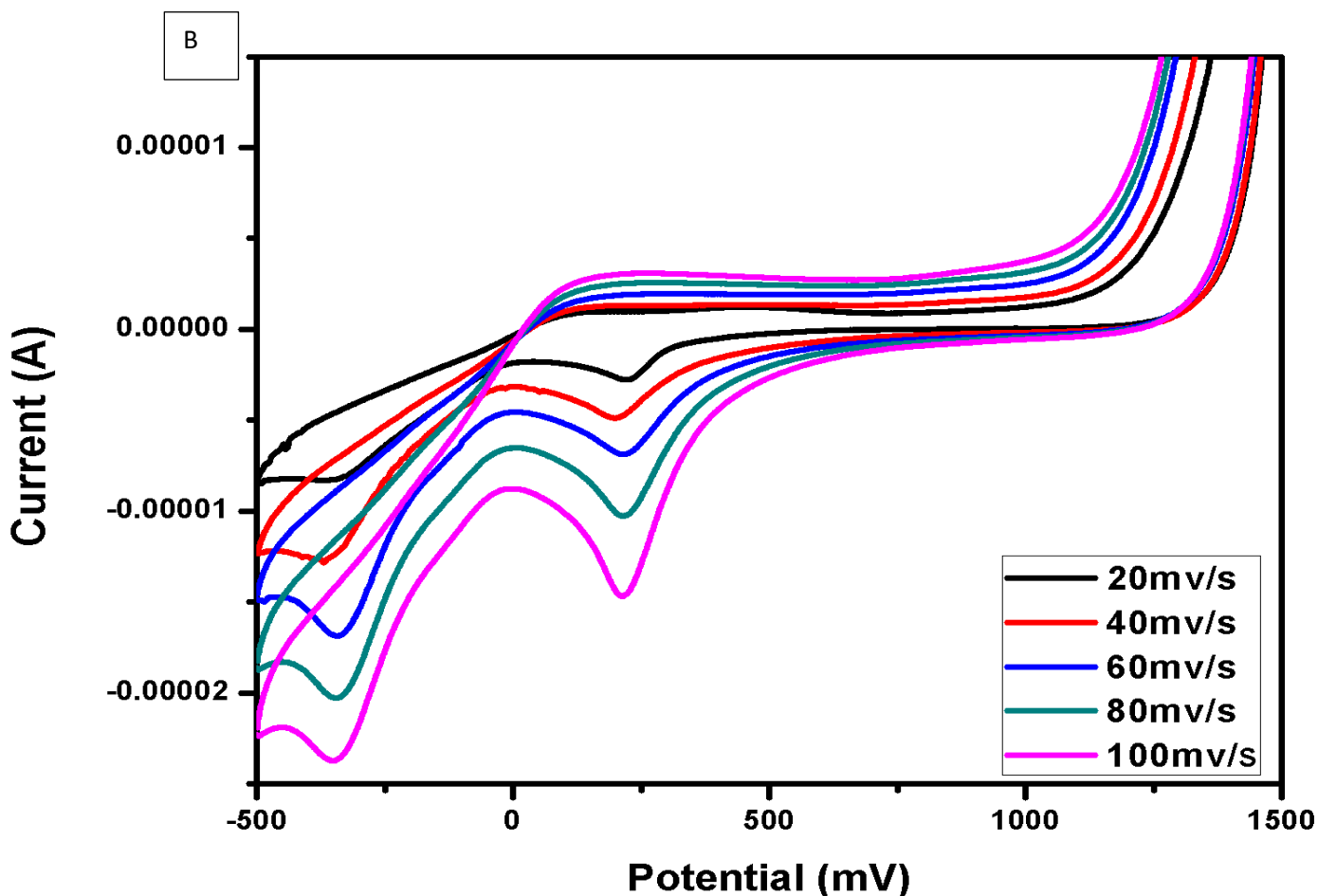**4.9.3 Cyclic Voltammetry (CV) for Poly(3-Hexyl-[2,2'] bithiophen-5-yl)-dimethyl-thiophenyl-2-yl-silane**
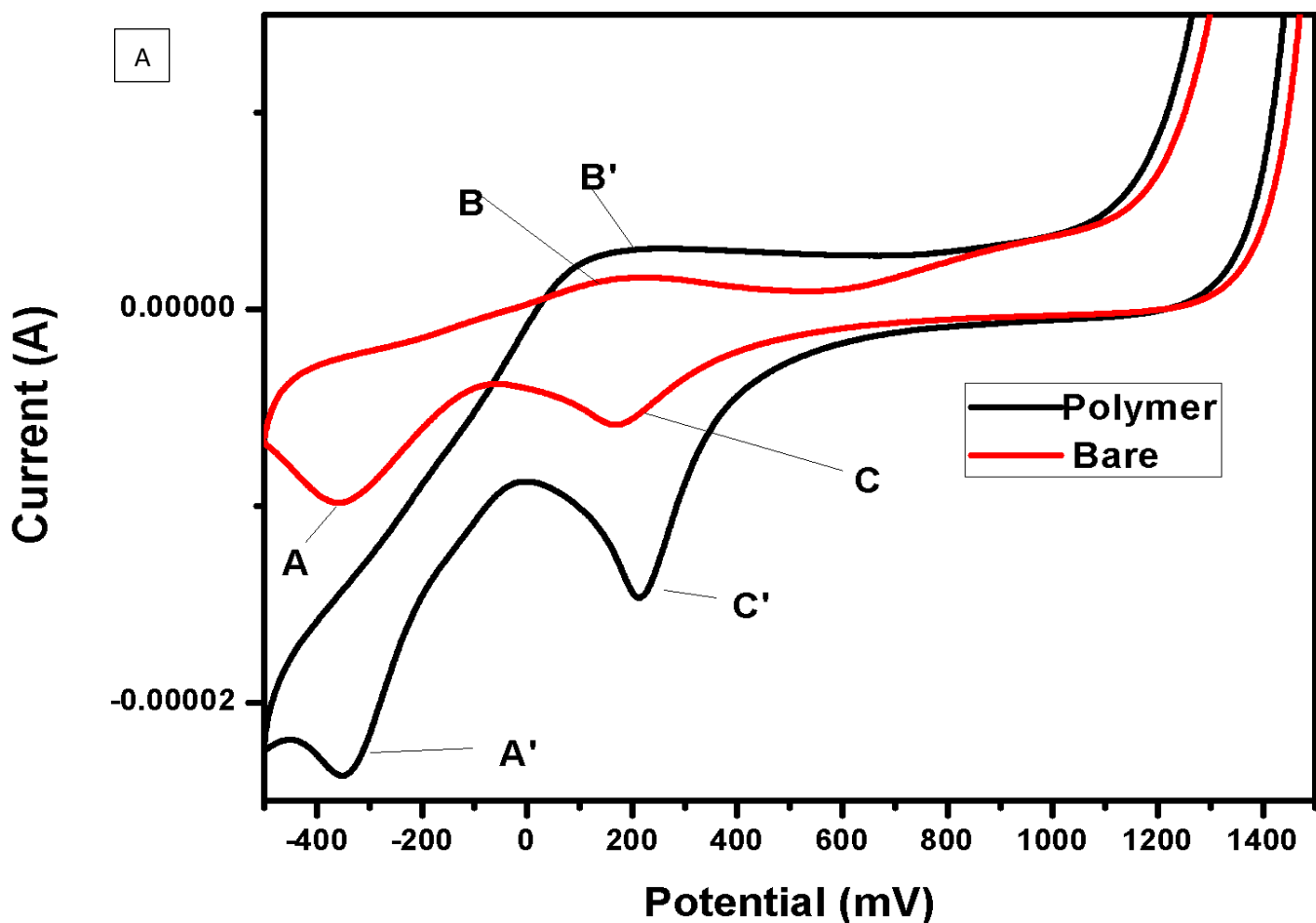
Figure 4.9.3: The CV for P3HDS Film in 0.1 M of LiClO$_4$ using platinum electrode.

The cyclic voltammetry of poly (3'-hexyl-[2,2']bithiophenyl-5-yl)-dimethyl-thiophen-2-yl-silane film in lithium perchlorate were measured and shown in figure 4.9.3 above. In the voltammogram shown by figure 4.9.3 (a), two reduction and oxidation peaks labelled A, B and C these observations proves that during oxidation two species were generated then later only one was stabilized by anodic potential. By plotting a bare electrode with P3HDS film it was shown that the current increased and the oxidation peak was around 151.09 mV while the reduction peaks were around -357.04 mV and 216.61 mV. Figure 4.9.3(b) represent the different scan rates of P3HDS voltammogram, where current increases with increase in the scan rate. The

72

voltammogram also shows that the average formal potential E°' of P3HDS to be 189.95 mV and the average ratio of the anodic to cathodic peak current, Ipa/Ipc as 0.96 which is close to one, the results indicate that the reaction is quasi-reversible. However, the peak separation ($\Delta E_p = E_{p,A}$ - $E_{p,C}$) values varied with scan rate and were all less than 65 mV a slow electron transfer is expected during this reaction.

E (ox) (mV)	E (ox) Onset (mV)	HOMO (eV)	E (red) (mV)	E (red) Onset (mV)	LUMO (eV)	E_g (eV)
153.5	1080.1	6.29	-349.7	232.3	4.62	1.7

Table 3: CV data, HOMO, LUMO and Band gap of P3HDS.

In table 3 above the calculated HOMO and LUMO are presented, which were calculated using the formula $E_{LUMO} = [(E_{red}-E_{1/2(ferrocene)}) +4.8]$ eV or $E_{HOMO}= [(E_{ox} - E_{1/2(ferrocene)}) +4.8]$ eV. Ferrocene was used as external standard. Where HOMO was found to be 6.29 eV and LUMO was 4.62 eV, the electrochemical band gap was also calculated using the formula of E_g = HOMO – LUMO and it was 1.7 eV.

CHAPTER 5

RESULTS AND DISCUSSION

In this chapter we discuss the results of zinc oxide nanorods that were annealed at different temperatures.

5.1 MICROSCOPIC ANALYSIS

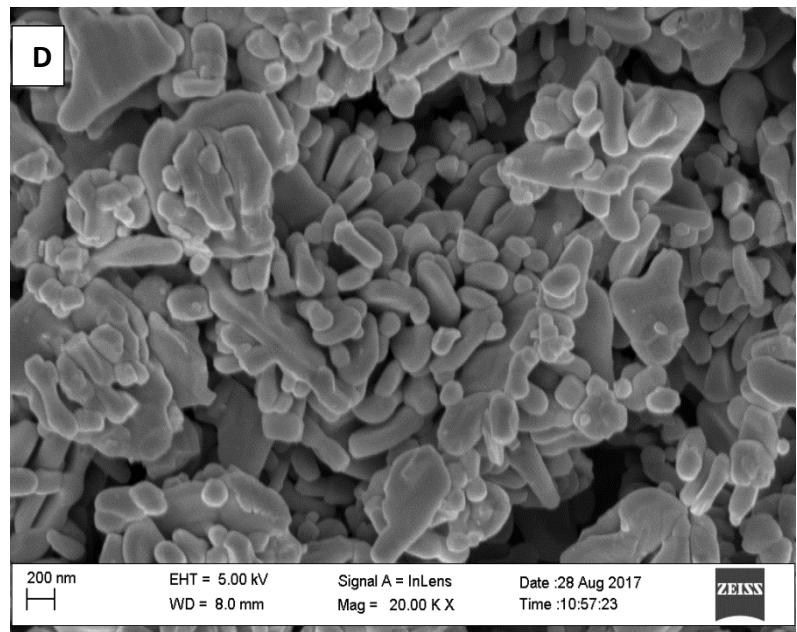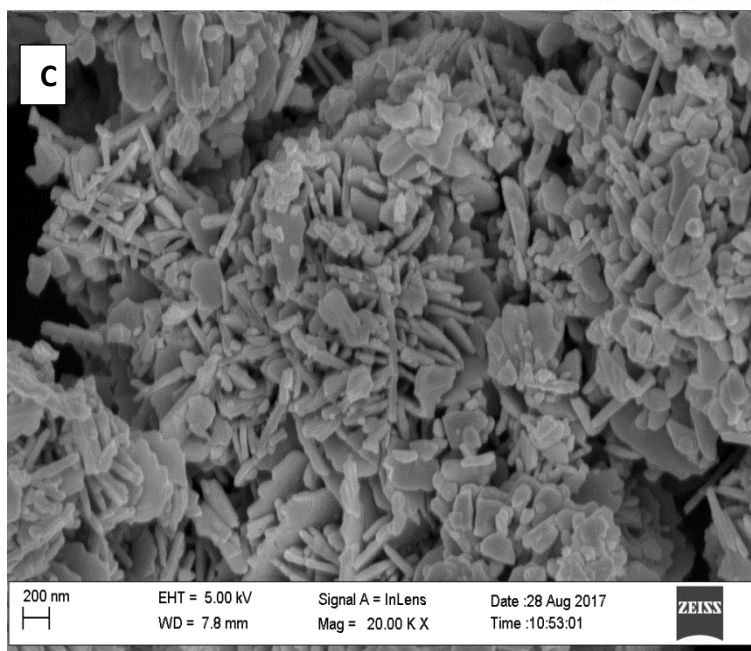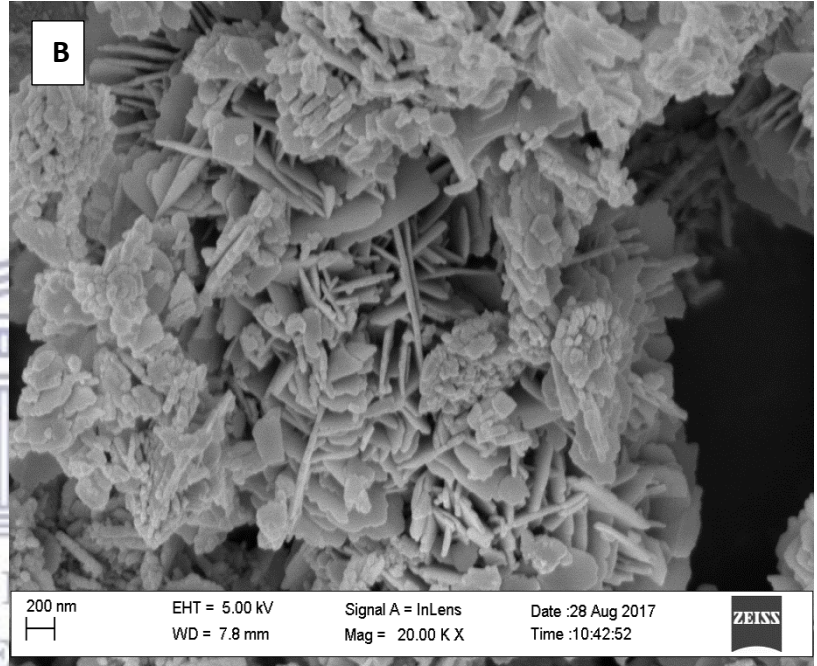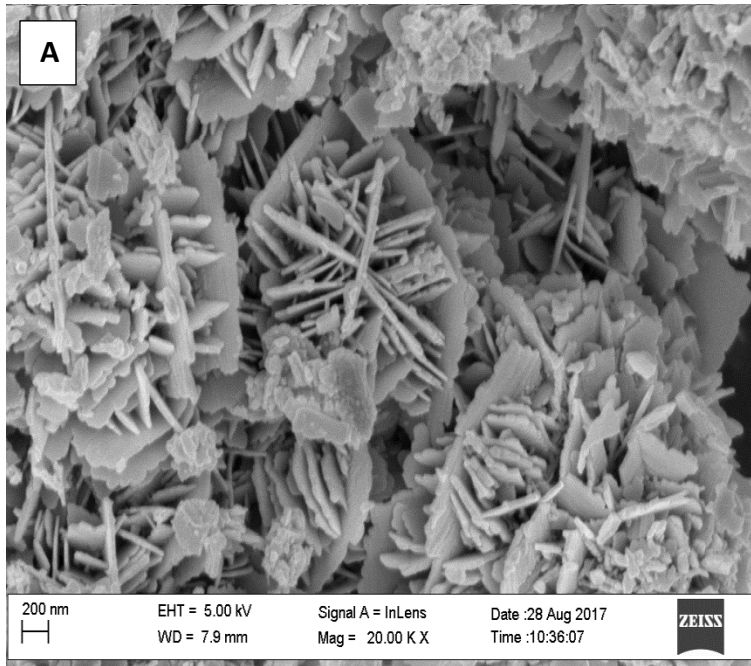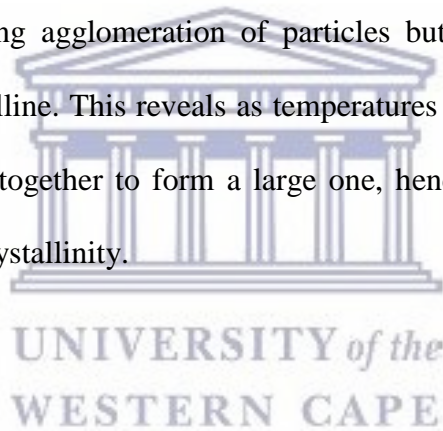### 5.1.1 High Resolution Scanning Electron Microscopy

Figure 5.1.1: The SEM images for ZnO nanorods at (A) 25 °C, (B) 100 °C, (C) 400 °C and (D) 800 °C

The surface morphology of the zinc oxide nanorods was studied using the high resolution scanning microscopy, All the ZnO nanorods represented in the data shown above are at a magnification of 100 000X. The SEM micrographs shown by figure 5.1.1 present the surface morphology of ZnO nanorods where size and distribution were investigated. The figure reveals that when nanorods are annealed at different temperature they have different geometrical structure. It was noticed that as temperatures increases the rods and plates that are shown at room temperatures which is figure 5.1.1(A) are becoming round and broader. At first the SEM images of ZnO nanorods were showing agglomeration of particles but as temperatures changes the particles were becoming crystalline. This reveals as temperatures increases during the annealing the small crystallites combine together to form a large one, hence the material becomes more clear and broader with better crystallinity.

75

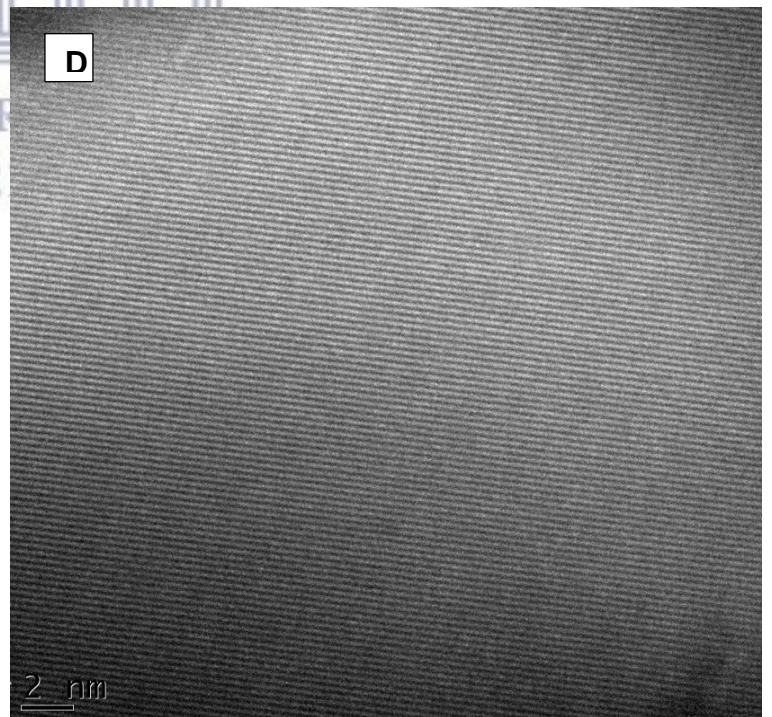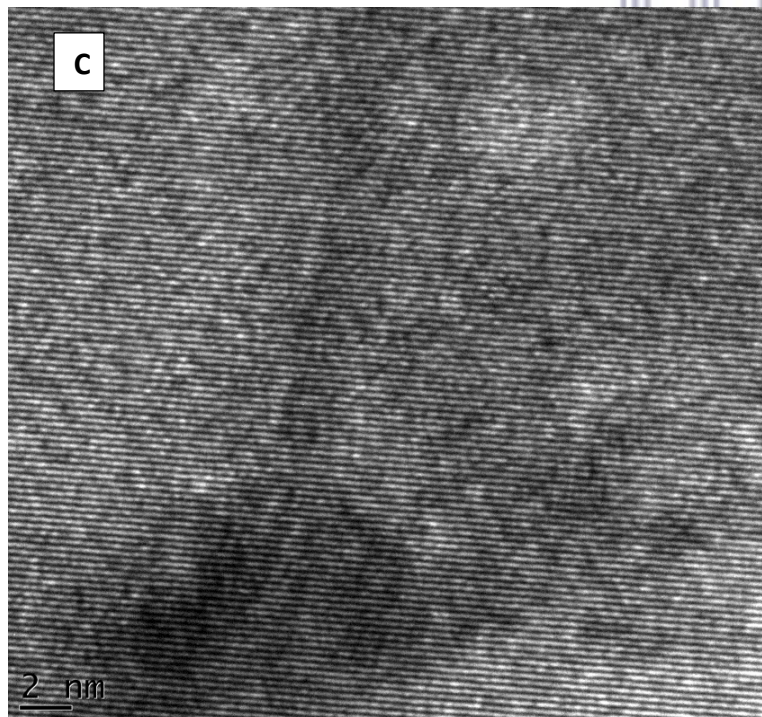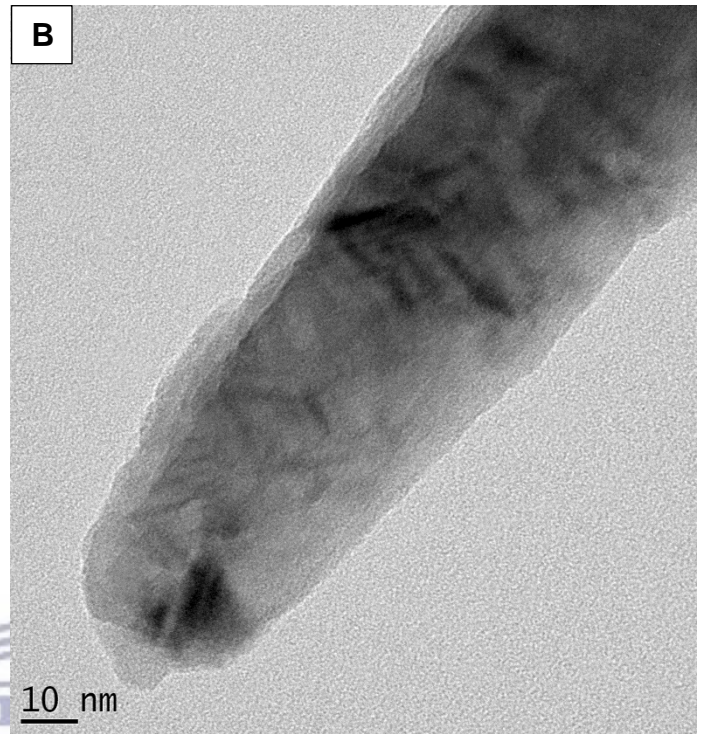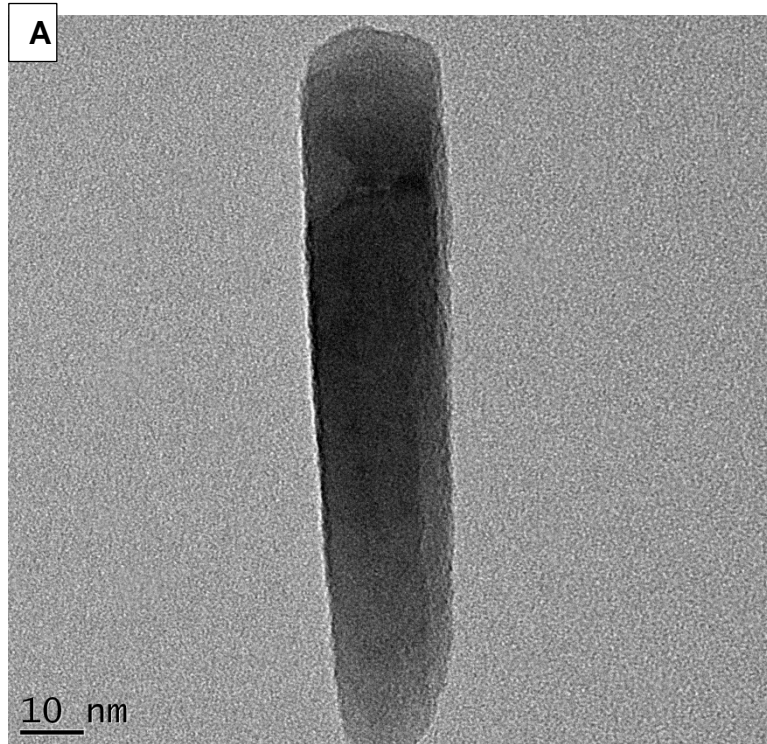## 5.1.2 High Resolution Transmission Electron Microscopy

Figure 5.1.2: The TEM image of the ZnO nanorods annealed at (a) 25 °C and (b) 400 °C and the lattice fringes (c) 25 °C and (d) 400 °C.

The HR-TEM was used to obtain the internal structure, crystallinity observed from lattice fringes, and confirm the element composition. The TEM images of the zinc oxide nanorods annealed at room temperature and 400 °C are shown in figure 5.1.2 a,b. The rod-like shape is represented where it was revealed that the room temperature has less size than 400 °C, which also confirms the SEM results. The lattice fringes are represented in figure 5.1.2 c,d, and give clear information on the crystallinity of the zinc oxide nanorods . The lattice fringes are able to reveal that both ZnO nanorods material are crystalline but at high temperature they are more crystalline compared to room temperature. The interplanar distance d_x for ZnO powders was calculated, for the powder at room temperature it was found to be 3.08 Ǎ while at 400 °C it was 3.3 Ǎ this confirms that as temperature increases the greater the crystallinity.

77
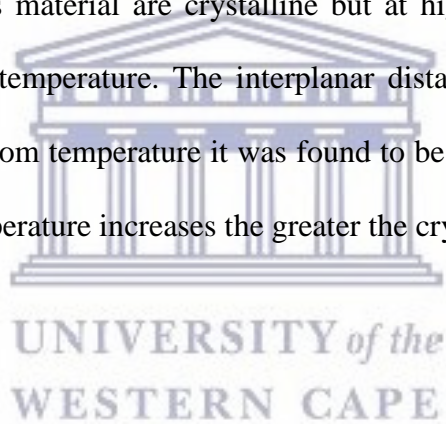
5.1.3 Energy dispersive x-ray spectroscopy (EDS)
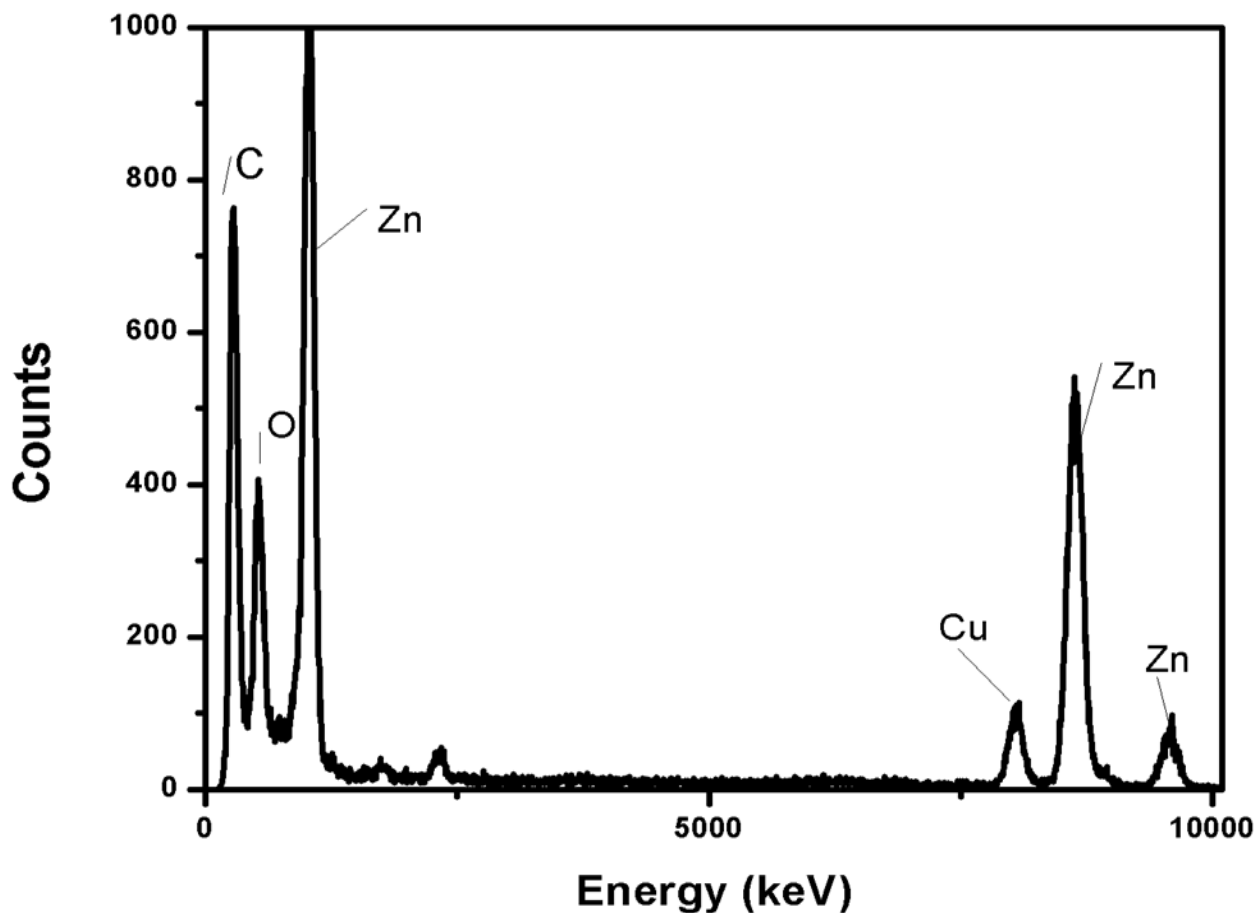
Figure 5.1.3: The EDS spectra of the ZnO nanorods

The Energy Dispersive X-ray Spectra of the zinc oxide nanorods was obtained from HR-TEM, during the analysis the carbon cupper grid was used. In figure 5.1.3 it shows all the elements expected from ZnO are shown in the EDS spectra such as zinc and oxygen. Such that there were no contaminants or impurities were revealed except the cupper and carbon that were used as a grid.
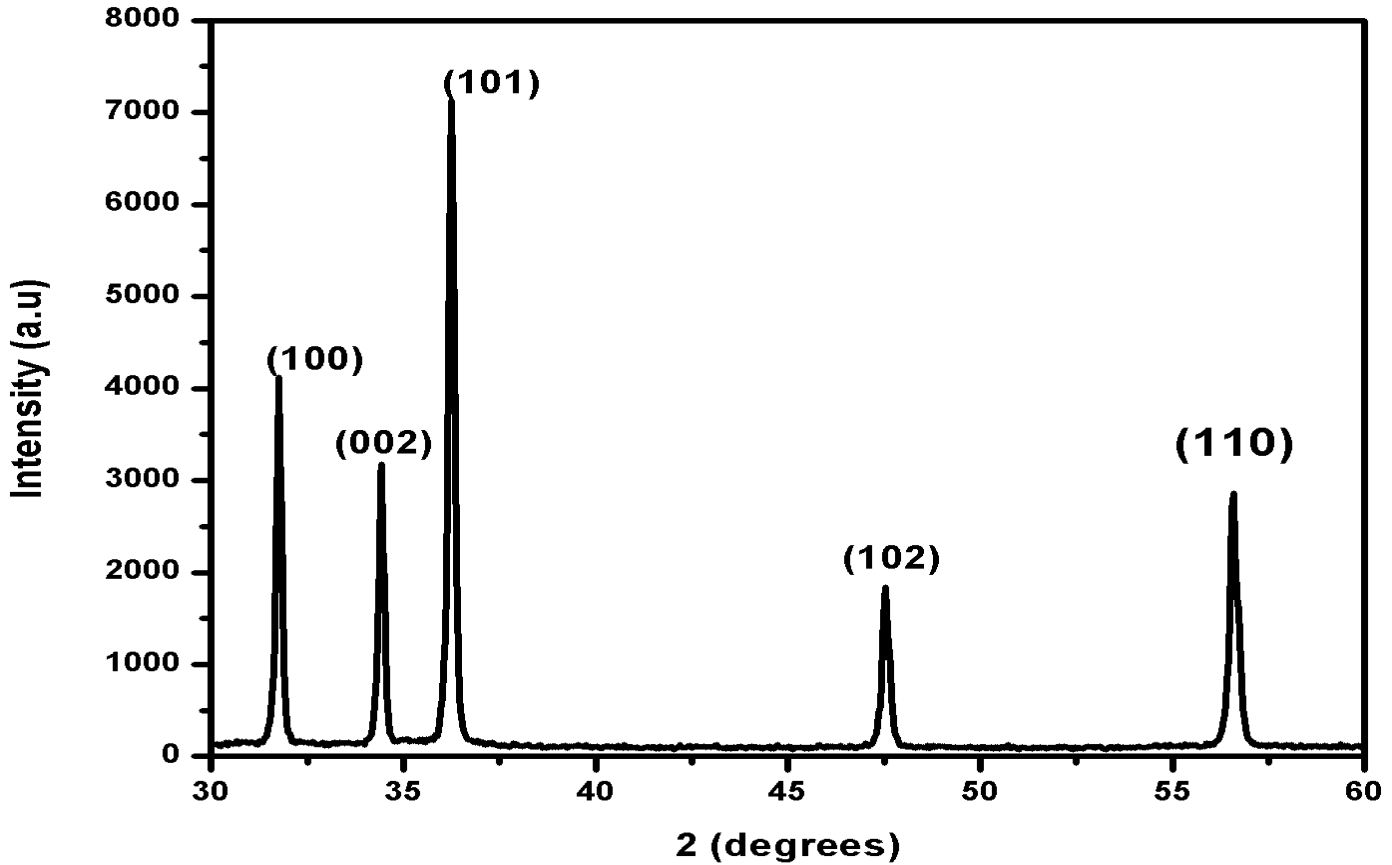
5.2 X-ray Diffraction

Figure 5.2: The XRD pattern of ZnO nanorods

X-ray powder diffraction (XRD) is the analytical technique that is mostly used for identification of crystalline materials where it provides information on unit cell dimension of zinc oxide nanorods. The diffraction peaks are well indexed to the hexagonal ZnO structure that corresponds with JCPDS no. 36–1451. No diffraction peaks corresponding determined that were due to impurities, this confirms the high purity of the synthesized products. The unit cells that were found on the hexagonal were (100), (002), (101), (102) and (110) which are the same as reported by Li and colleagues; Ramachandran and colleagues [10; 11]. The crystallite size was calculated using Scherer formula $D = \frac{0.89\,\lambda}{\beta\,cos\theta}$ .The crystallite size was found to be 43 nm and highly pure.

79

5.3 Small-Angle X-ray Scattering (SAXS)
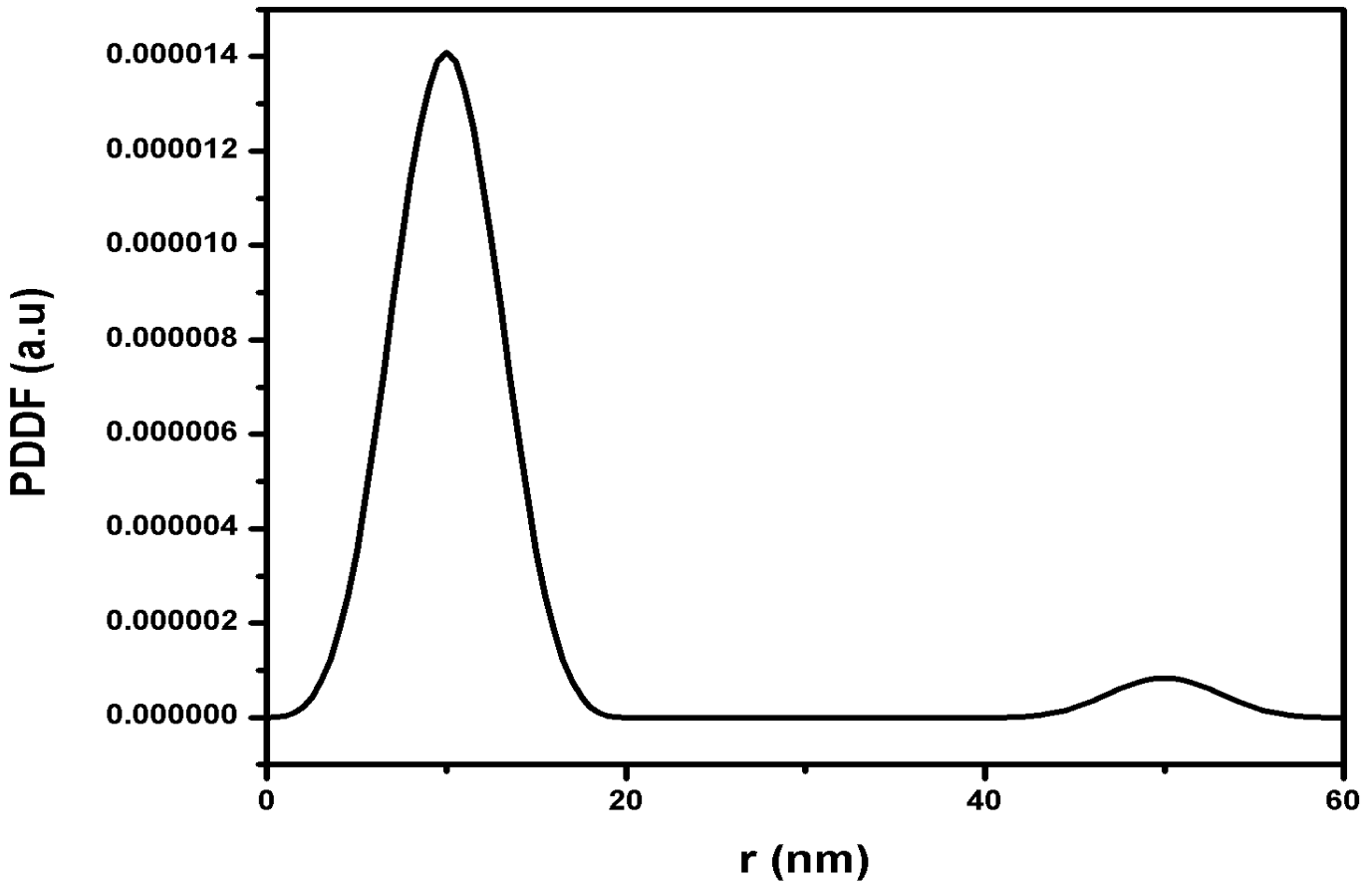
Figure 5.3: The PDDF of ZnO nanorods indicating the particle size and shape

The PDDF shown by figure 5.3 indicates the shape of zinc oxide nanorods that was found to be cylindrical and some are globular. This ZnO was found to have different particles, where the particles were found not to have the same shape and also different size and that was concluded to be polydispersity. The size of the particles was found to be roughly 12 nm and some particles were around 46 nm which is close to that of XRD, which was 43 nm.

5.4 Fourier Transform Infrared (FTIR)

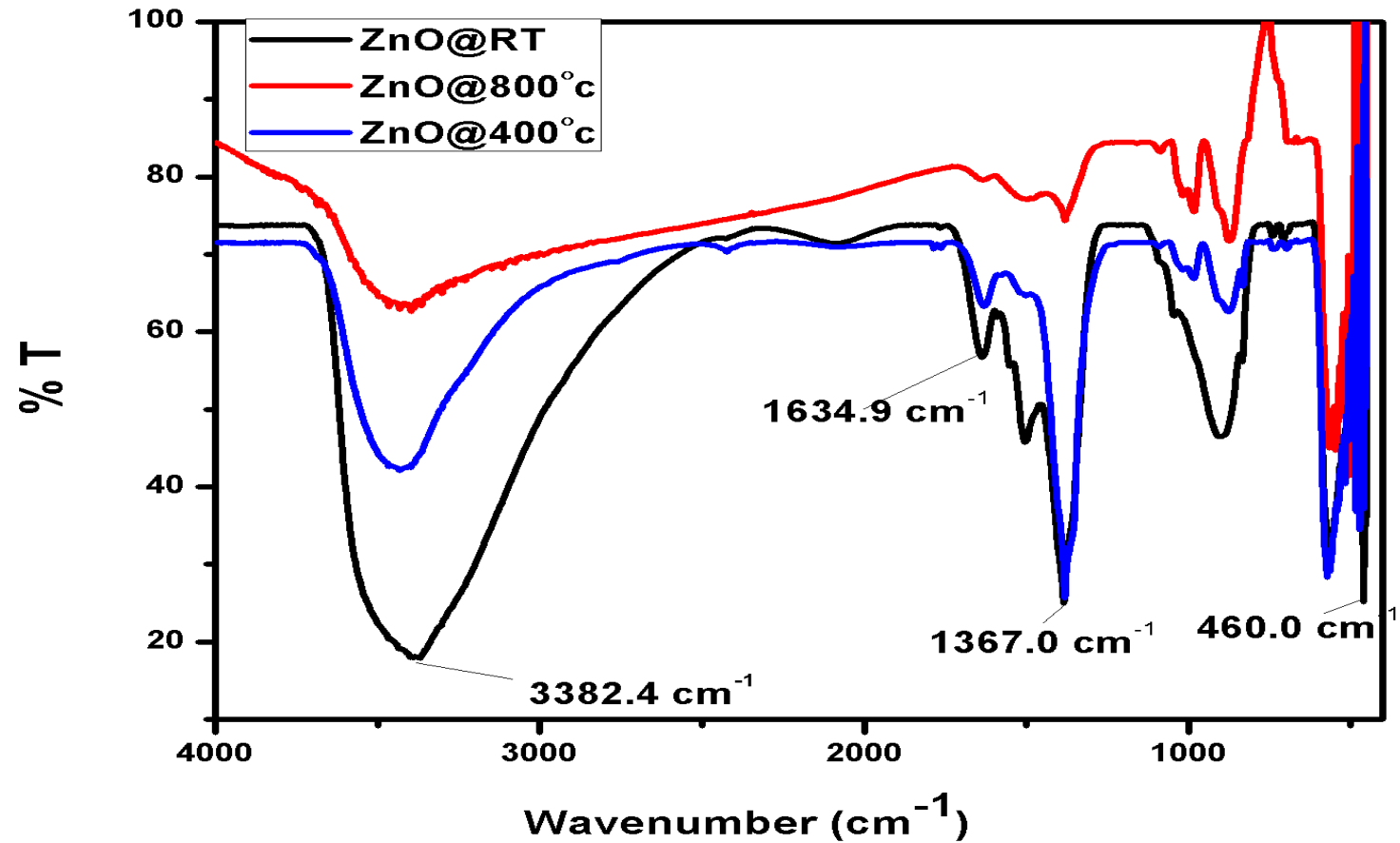**Figure 5.4:** The FTIR absorption of zinc oxide nanorods powder annealed at room temperature, 400 °C and 800 °C in KBr.

The figure 5.4 shows the FTIR spectrum of zinc oxide nanorods at room temperature, 400 °C and 800 °C. Bands were observed, there is a strong band at 460 cm^{-1} which was due to Zn-O stretching band that was reported by Samanta to be ~500 cm^{-1} [12]. The peak at 1634.9 cm^{-1} observed was also due to O-H bending of water as well as vibration mode of OH that appeared at 3382.4 cm^{-1}. By comparing the spectrums we can observe the OH bands are disappearing as the temperatures increases of which that might be due to the removal of water from the material.

81

There is also a strong band at 1367.0 cm^{-1} that appeared due to symmetric stretching of N=O that was due to the unreacted zinc nitrate.

5.5 Ultraviolet Visible Spectral Analysis (Uv-vis)
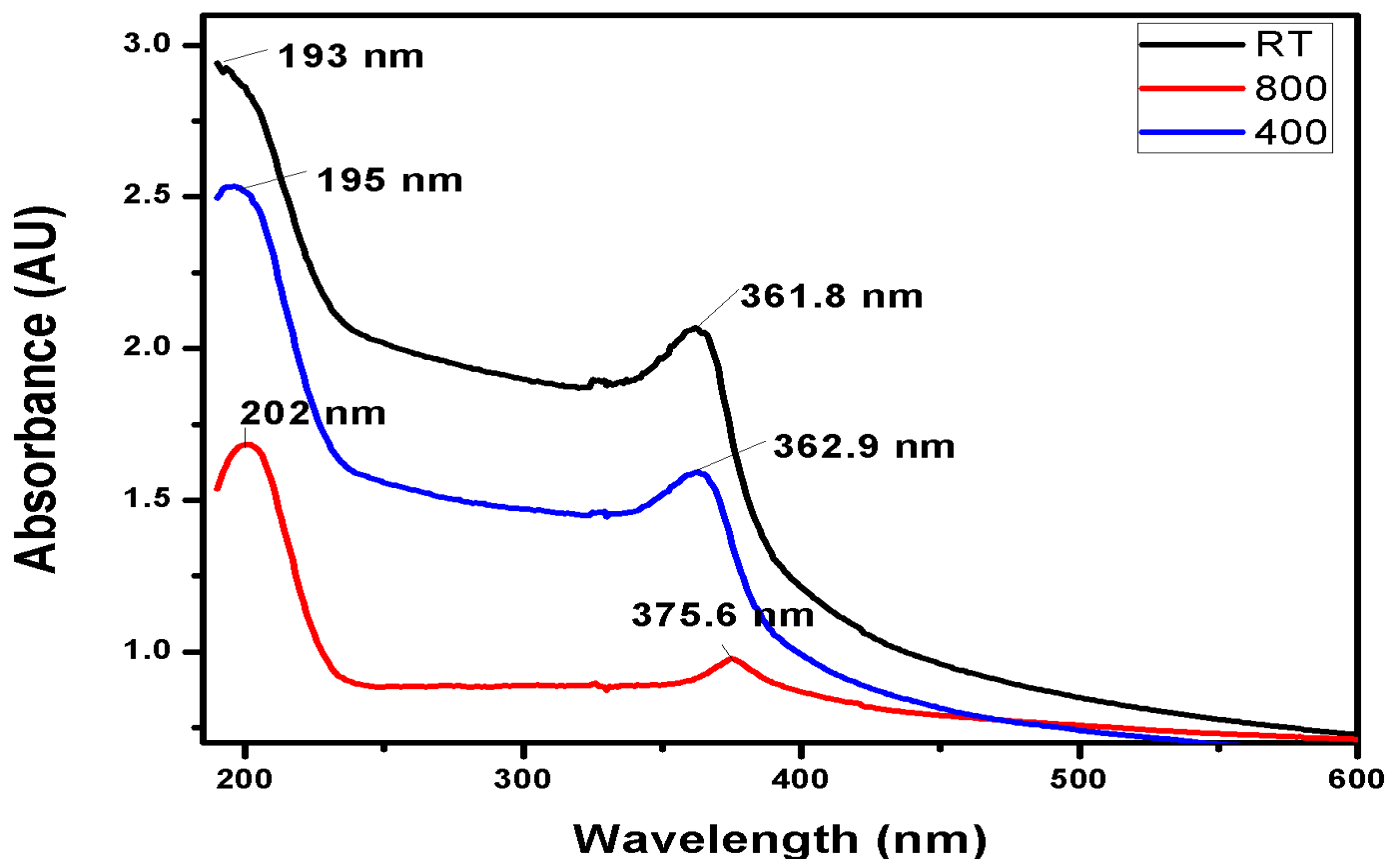
Figure 5.5: The UV-vis spectrum of zinc oxide nanorods annealed at different temperature.

Ultra-violet spectroscopy was used to determine the transition that took place during absorption of zinc oxide nanorods and also able to calculate the optical band gap. Figure 5.5 shows the UV-vis spectrum of zinc oxide nanorods at different temperatures. It was observed that the absorption maximum has shifted to higher wavelength as the temperatures increases, this red shift appeared were reported by Kumar and colleagues to be attributed to the agglomeration in the ZnO powders [13]. The optical bandgap of the zinc oxide nanorods was calculated at room

temperature it was 3.0 eV, at 400 °C and 800 °C it was found to be 2.98 eV and 2.83 eV respectively. It was noticed that the band gap of ZnO nanorods at different temperatures decreases with an increase in the temperature and this is due to increase in particle size as observed by SEM and TEM [13]. The optical bandgap for ZnO nanorods at room temperature was reported by Singh and colleague to be 3.23 eV [14] but it was a film hence it is different from the solution reported in this study.
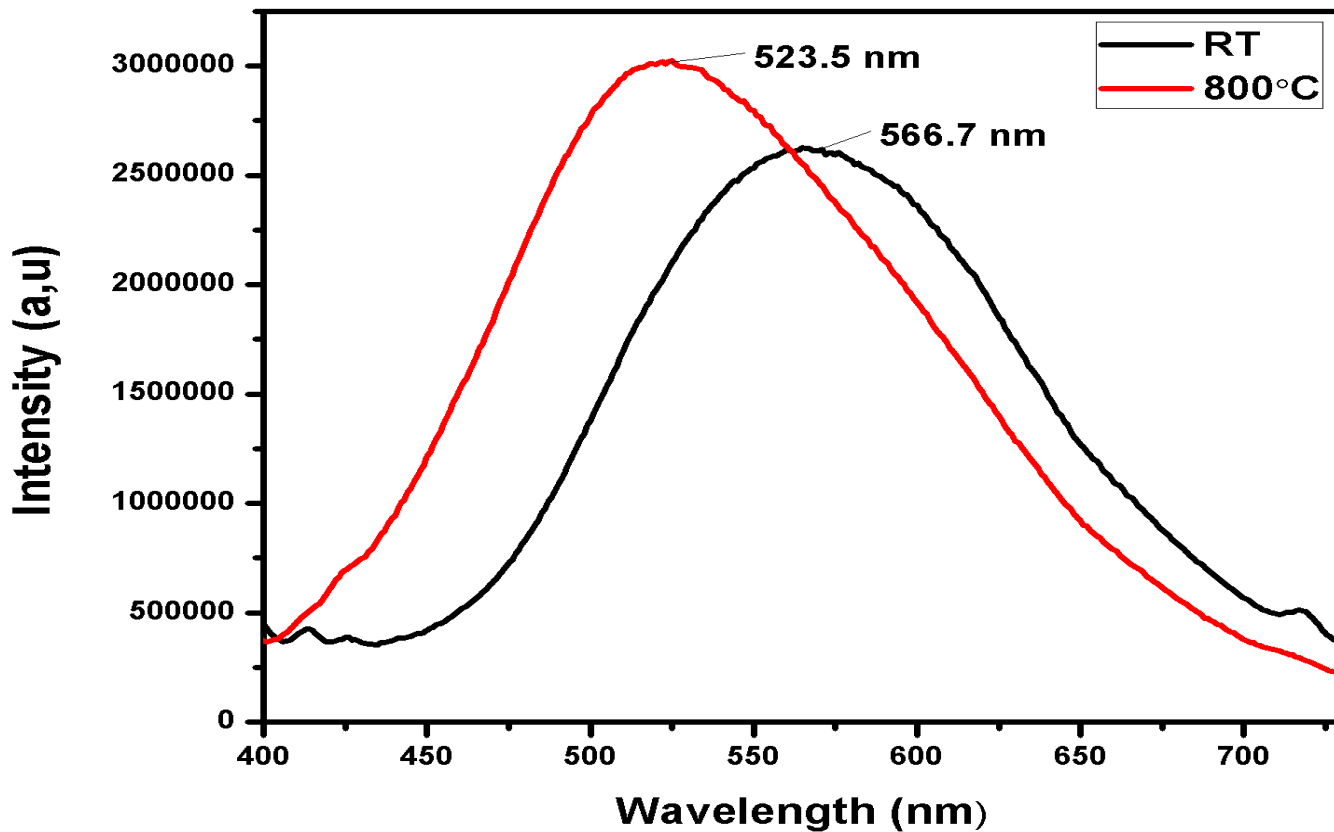
5.6 Photoluminescence (PL)

Figure 5.6: The PL spectra of zinc oxide nanorods at 25 °C and 800 °C in solution.

The figure 5.6 above shows the photoluminescence spectra of zinc oxide nanorods under excitation wavelength of 375 nm, in the range of 400-725 nm. During the preparation of

83

photoluminescence the compounds were dissolved using Chloroform and 1.2-Dichlorobenzene solvents. It was observed that the zinc oxide at room temperature it has a peak at 566.7 nm, while at 800 °C it was 523.5 nm. The blue shift that was observed was due to the removal or breaking of the O-H bond that was caused by water at room temperature. Also a shoulder was observed in at room temperature around 715 nm. As temperatures increases it was concluded that the intensity decreases this was also revealed on the spectrum on figure 5.6.

84

CHAPTER 6

RESULTS AND DISCUSSION

In this Chapter we discuss the results of P3HT, PDDS and P3HDS blended with Zinc Oxide nanorods.

6.1 Ultraviolet Visible Spectral Analysis (Uv-vis)

Figure 6.1.1: The UV-Vis spectrum of P3HT/ZnO nanorods in different ratios.

Ultra-violet spectroscopy was used to determine the transition that took place during absorption of P3HT/ ZnO nanorods blend and the optical band gap. The absorption spectrum in figure 6.1.1 shows absorption peaks of P3HT/ZnO solution. It was revealed that as the concentration of P3HT increases, while the concentration of ZnO nanorods is constant there is a redshift. When

85

the concentration of ZnO nanorods in the blend increases the blue shift is observed. The

transition bands can be attributed to the $\pi \to \pi^*$ transition due to the stacking of P3HT.

P3HT: ZnO	3:1	2:1	1:1	1:2	1:3
Absorption band (nm)	459	447	443	439	430
Absorption band edge (nm)	539.08	537.62	536.6	541.07	535.06
Band gap (eV)	2.299	2.310	2.311	2.291	2.317

Table 4: The UV-Vis table of absorption band and optical band gap.

The optical bandgap that was calculated from the absorption band edge, in the chapters above for

P3HT was discovered to be 2.42 eV and for ZnO it was 3.0 eV. In the table 4 above the band gap

is calculated from different ratio of the blend P3HT/ZnO and they are all less than that of P3HT

and ZnO before blending them
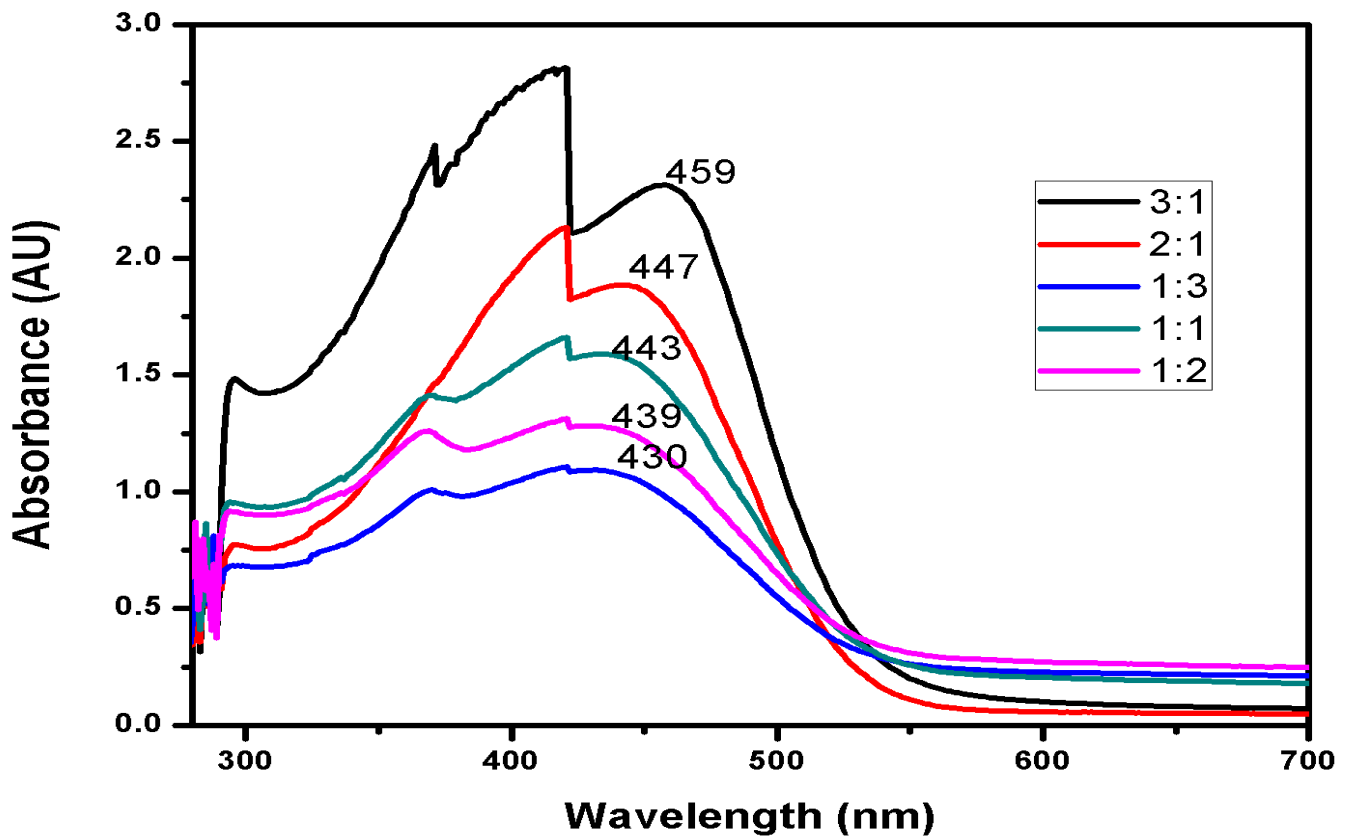
UNIVERSITY of the

WESTERN CAPE

Figure 6.1.2: The UV-Vis spectrum of P3HT/ZnO nanorods in different ratios.
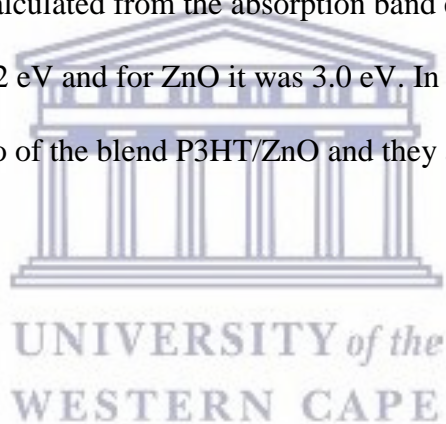
Ultra-violet spectroscopy was used to determine the transition that took place during absorption of PDDS/ ZnO nanorods blend and the optical band gap. The absorption spectrum in figure 6.1.2 shows absorption peaks of PDDS/ZnO solution. It was revealed that when the concentration of PDDS increases, while the concentration of ZnO nanorods is kept constant the absorption band decreases which cause a blue shift. While when the ZnO concentration increases the absorption band also increases of which the red shift is observed during this analysis.

87

PDDS: ZnO	1:1	1:2	1:3	2:1	3:1
Absorption band (nm)	363.4	366.5	367.9	297.9	293.3
Absorption band edge (nm)	418.3	441.2	445.7	511.3	403.1
Optical band gap	2.964	2.810	2.782	3.08	2.42

Table 5: The UV-vis table of absorption band and optical band gap

The optical band gap was calculated from the absorption band edge and is shown on the Table 5 above. The band gap of PDDS was calculated as 2.54 eV and the blend of PDDS and ZnO values were in between that of polymer and ZnO as shown in the table above.
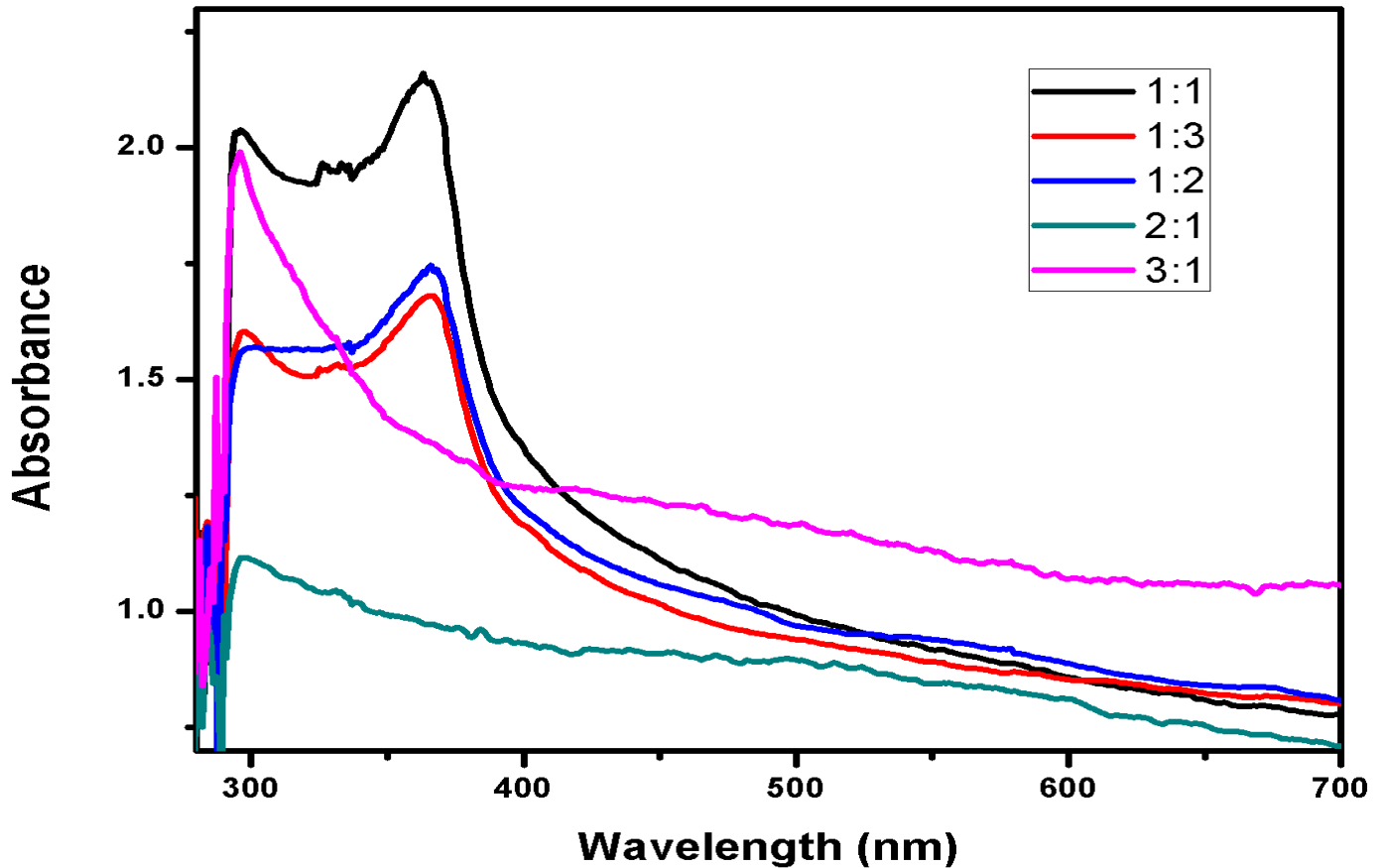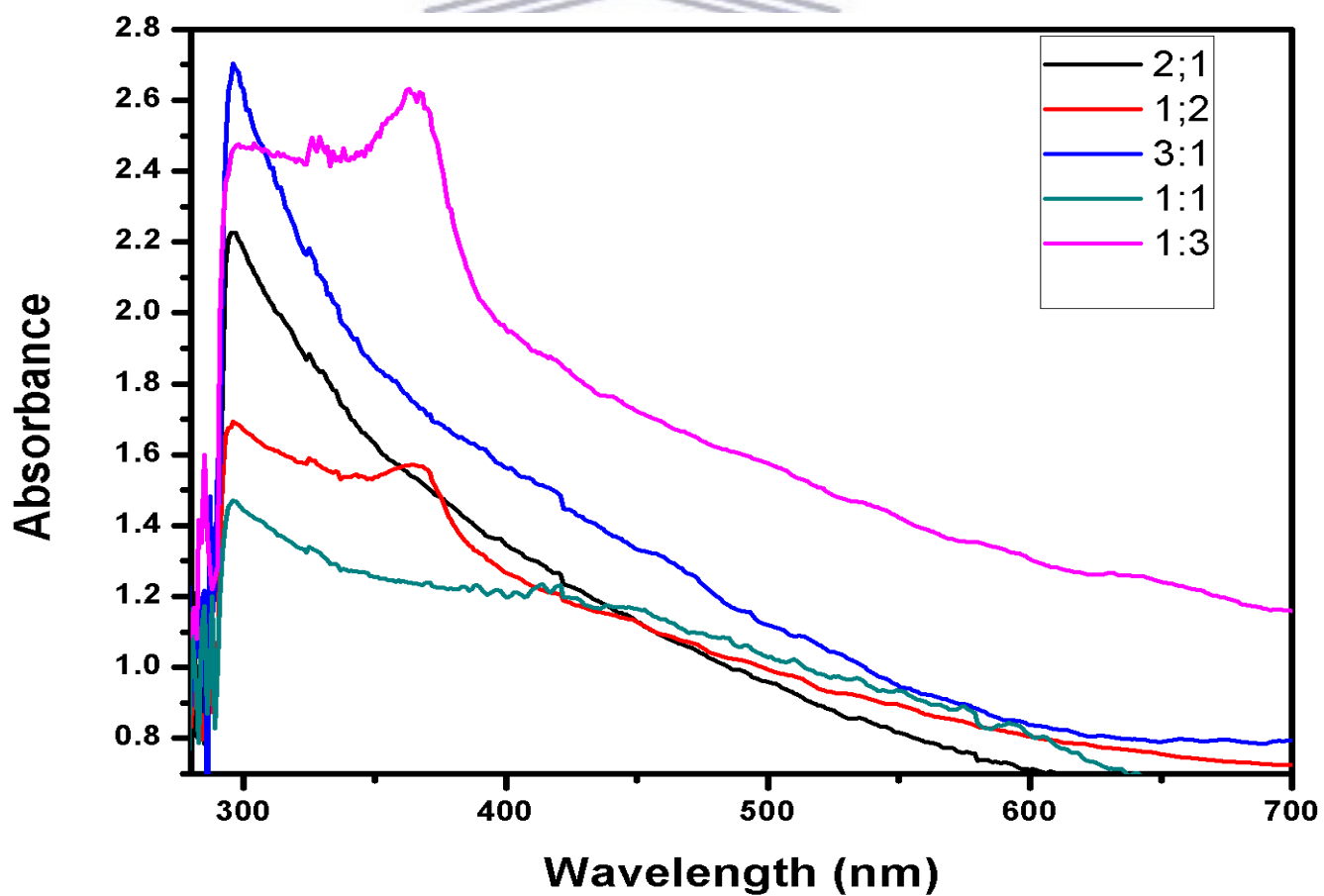

Figure 6.1.3: The UV-vis spectrum of P3HDS/ZnO nanorods in different ratios.

88

Ultra-violet spectroscopy was used to determine the transition that took place during absorption of P3HDS/ ZnO nanorods blend and the optical band gap. The absorption spectrum in figure 6.1.3 shows absorption peaks of P3HDS/ZnO solution. It was revealed that when the concentration of P3HDS increases, while the concentration of ZnO nanorods is kept constant the absorption band decreases which cause a blue shift. While when the ZnO concentration increases the absorption band decreases of which the blue shift is observed as well during this analysis.

| P3HDS: ZnO	1:1	1:2	1:3	2:1	3:1
Absorption band (nm)	419.8	366.5	367.9	296.4	297.9
Absorption band edge (nm)	633.2	608.8	532.6	596.7	572.2
Band gap (eV)	1.96	2.04	2.33	2.08	2.17

Table 6: The UV-vis table of absorption band and optical band gap

The optical band gap was calculated from the absorption band edge and is shown on the Table 6 above. The band gap of P3HDS before blending was calculated as 2.31 eV and after the blend of P3HDS and ZnO values were all found to be less than before the blending.

89

6.2 Photoluminescence (PL)
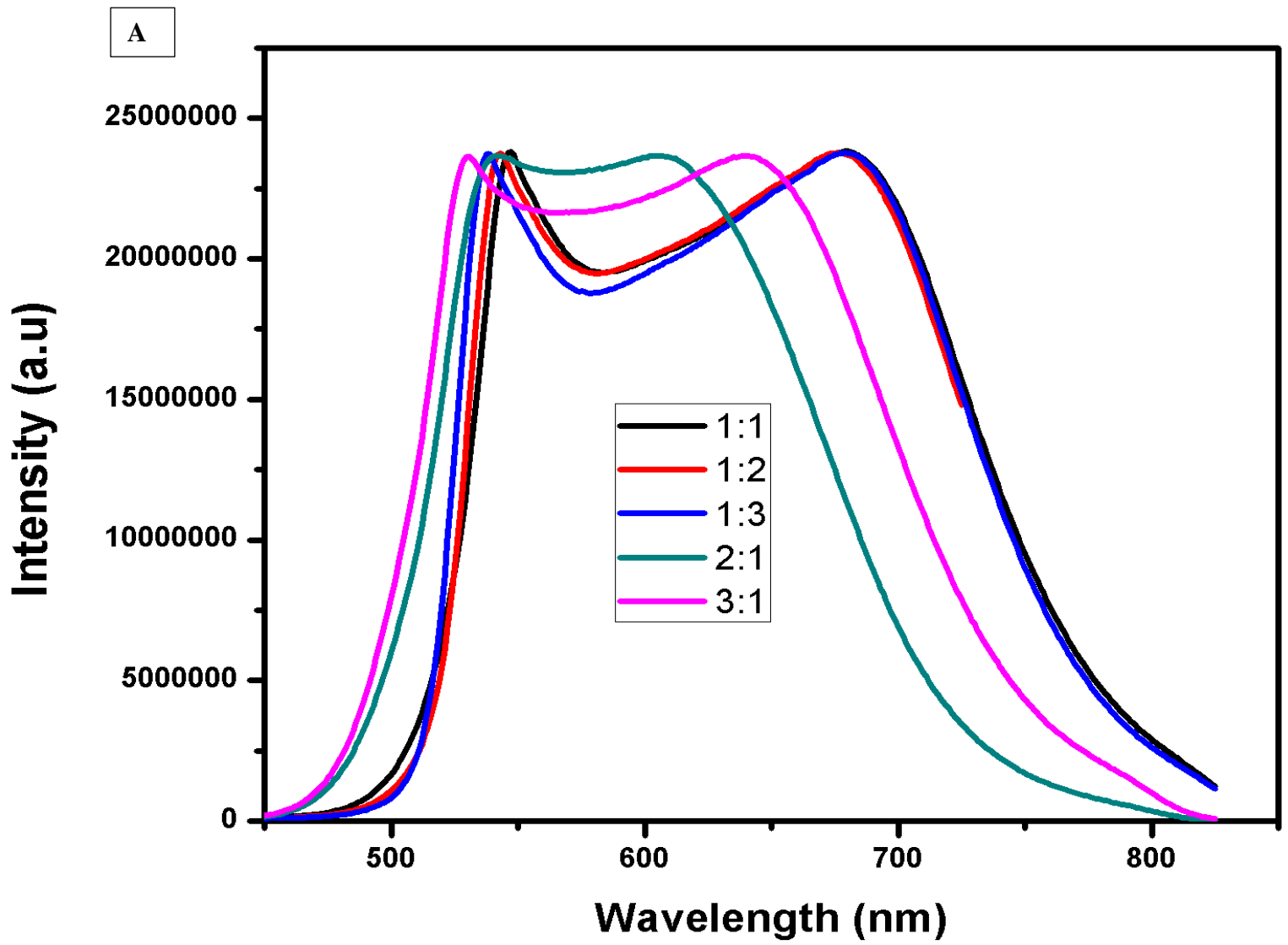
B
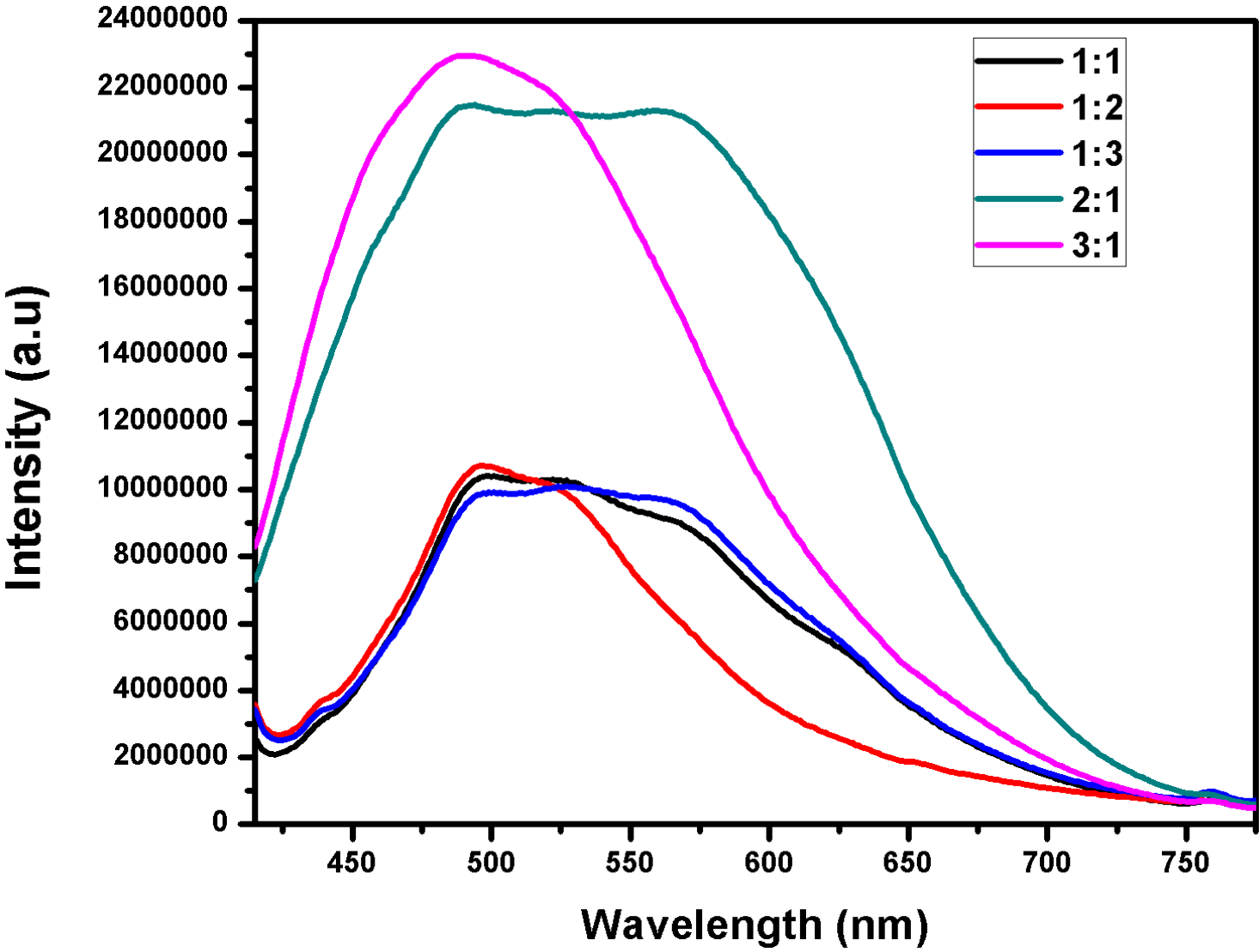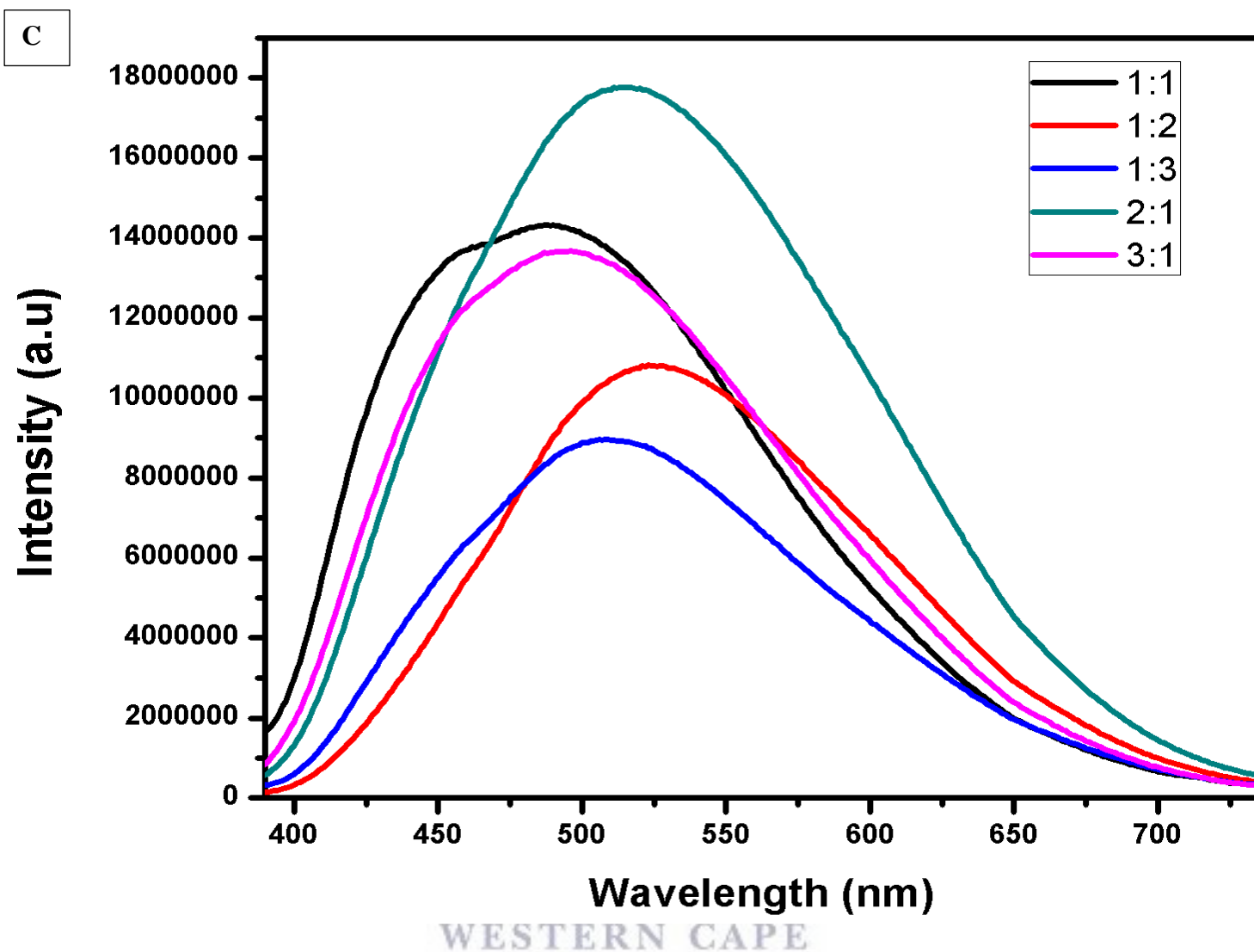
Figure 6.2: The PL spectra of (A) P3HT, (B) PDDS, (C) P3HDS polymers blended with ZnO nanorods in different ratio in a solution.

The figure 6.2 above shows the photoluminescence spectra of (A) P3HT, (B) PDDS, (C) P3HDS all blended with zinc oxide nanorods for 24 hour in room temperature. The photoluminescence of the compounds were dissolved using chloroform and 1.2-dichlorobenzene solvents. The P3HT: ZnO in figure 6.2 (a) was measured under excitation wavelength of 400 nm, in the range of 400-820 nm. It was observed that during these measurements, the concentration of ZnO nanorods had no influence but when the concentration of P3HT was increased while ZnO

92

concentration is kept constant the red shift was observed. The blend of PDDS:ZnO nanorods shown by figure 6.2 (b) it was observed that the concentration of ZnO nanorods had no effect but the particle distribution was all over which might be due by polydispersity. The concentration of PDDS caused the increase in the intensity and small shift on the wavelength. In the figure 6.2 (c) above, it was observed that when the concentration of P3HDS was kept constant while the concentration of ZnO nanorods was increased, the decrease in the intensity and the redshift were observed. When P3HDS concentration was increased while ZnO nanorods concentration was kept constant the redshift and an increase in the intensity were observed.

93

References

1. Tamanai, A., Beck, S. and Pucci, A., 2013. Mid-infrared characterization of thiophene-based thin polymer films. Displays, 34(5), pp.399-405.

2. Andriot, M., Chao, S.H., Colas, A.R., Cray, S.E., DeBuyl, F., DeGroot, J.V., Dupont, A., Easton, T., Garaud, J.L., Gerlach, E. and Gubbels, F., 2007. Silicones in industrial applications. Inorganic polymers, pp.61-161.

3. Baleg, A.A.A.A., 2011. Synthesis and electrochemistry of novel conducting dendrimeric star copolymers on poly (propylene imine) dendrimer.

4. Hussein, A.A., Sultan, A.A., Obeid, M.T., Abdulnabi, A.T. and Ali, M.T., 2015. Synthesis and Characterization of poly (3-hexylthiophene). International Journal of Scientific Engineering and Applied Science (IJSEAS)-Volume-1, Issue-7.

5. Angiolini, L., Salatelli, E., Bolognesi, A. and Botta, C., 2002. Photoluminescence and electroluminescence of mono-and dialkyl-substituted soluble polythiophenes. e-Polymers, 2(1), pp.572-578.

6. Schnablegger, H. and Singh, Y., 2011. The SAXS guide: getting acquainted with the principles. Austria: Anton Paar GmbH.

7. Cervantes, T.N.M., Bento, D.C., Maia, E.C.R., Zaia, D.A.M., Laureto, E., da Silva, M.A., Moore, G.J. and de Santana, H., 2012. In situ and ex situ spectroscopic study of poly (3-hexylthiophene) electrochemically synthesized. Journal of Materials Science: Materials in Electronics, 23(10), pp.1916-1921.

94

8. Gonçalves, R., Pereira, E.C. and Marchesi, L.F., 2017. The Overoxidation of poly (3-hexylthiophene)(P3HT) Thin Film: CV and EIS measurements. INTERNATIONAL JOURNAL OF ELECTROCHEMICAL SCIENCE, 12(3), pp.1983-1991.

9. Al-Ibrahim, M., Roth, H.K., Zhokhavets, U., Gobsch, G. and Sensfuss, S., 2005. Flexible large area polymer solar cells based on poly (3-hexylthiophene)/fullerene. Solar energy materials and solar cells, 85(1), pp.13-20.

10. Li, J.Y., Chen, X.L., Li, H., He, M. and Qiao, Z.Y., 2001. Fabrication of zinc oxide nanorods. journal of crystal growth, 233(1), pp.5-7.

11. Ramachandran, D., Brijitta, J., Raj, N.N., Jayanthi, V. and Rabel, A.M., 2013, July. Synthesis and characterization of Zinc Oxide nanorods. In Advanced Nanomaterials and Emerging Engineering Technologies (ICANMEET), 2013 International Conference on (pp. 566-568). IEEE.

12. Samanta, P.K and Bandyopadhyay, A.K., 2012. Chemical growth of hexagonal zinc oxide nanorods and their optical properties. Applied Nanoscience, 2(2), pp.111-117.

13. Kumar, S.S., Venkateswarlu, P., Rao, V.R. and Rao, G.N., 2013. Synthesis, characterization and optical properties of zinc oxide nanoparticles. International Nano Letters, 3(1), p.30.

14. Singh S, and Chakrabarti P., 2013. Optical characterization of ZnO thin films grown by thermal oxidation of metallic zinc. Advanced science, Engineering and Medicine, 5(7), pp.677-682.

95

CHAPTER 7

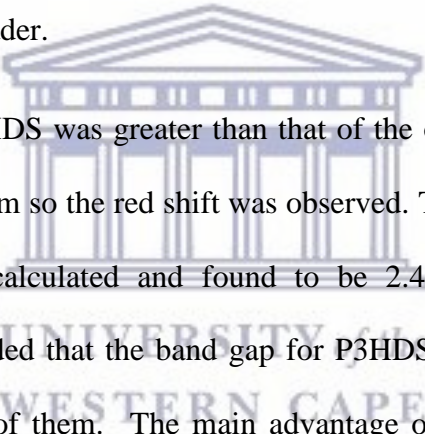## CONCLUSION AND RECOMMENDATIONS

7.1 Conclusion

The goal of the project was to synthesis a novel highly branched Organosilane polymers such as poly(3-hexythiophene) (P3HT), polydi(thien-2-yl)dimethylsilane (PDDS) and poly (3-hexyl-[2,2'] bithiophenyl-5-yl)-dimethyl-thiophen-2yl-silane) (P3HDS) as electron donors as well as zinc oxide nanorods as electron acceptors, that were able to bring the efficiency of the resultant photovoltaic cell close to that of Si solar cell as well as the band gap. The Novel thiopheno-organosilicon polymers P3HT, PDDS and P3HT were all found to be agglomerating and amorphous on the SEM images but the P3HT had some crystallinity with interpanar distance d_x of 3.6 Å that was observed on HR-TEM and XRD. The polymer were found to be electron active and they have a great thermal stability of which they were ready to be used as electron donors for hybrid solar cells.

Zinc oxide nanorods were used as electron acceptor for hybrid solar cell to improve the band gap of the polymers. It was noticed from FTIR that during the annealing as temperatures increases the water was being removed. The HR-SEM and the HR-TEM images revealed that the ZnO became more crystal as the temperatures increases with a change in geometrical structure. The interplanar distance for these ZnO was increasing with an increase in temperature. Both SAXs and XRD showed that the size of ZnO nanorods was roughly between 43-46 nm. The optical bandgap was also decreasing with an increase in temperature and the red shift was observed.

96

The XRD, HR-SEM and HR-TEM confirmed that the polymers were amorphous. The P3HDS was synthesized by combining the monomer of P3HT and PDDS; this was done to improve the structure and the backbone of the polymer there by improving the band gap as well. During the TGA analysis it was noticed that the P3HT was more thermally stable than the other polymers and it was concluded that the polymers are strong enough to be exposed on the sun for long period of time. The size by number of the polymers was confirmed by SAXS and they were all less than 80 nm and they had a core-shell which was caused by the Fe which was used as a catalyst during the synthesis this meant that the polymers synthesized were all nanomaterials.P3HT was further characterized by GPC and it was discovered that it had different polymer chains that made it broader.

The absorption band of the P3HDS was greater than that of the other polymers which means it was more optical active than them so the red shift was observed. The optical band gap for P3HT, PDDS and P3HDS were all calculated and found to be 2.41 eV, 2.54 eV and 2.31 eV respectively so this was concluded that the band gap for P3HDS was improved which was the main goal for synthesizing all of them. The main advantage of P3HDS than other polymers synthesized in the study was the fact that it consisted of Si and the alkyl substituent and this was confirmed through optical and electrochemical studies. The observations which were confirmed by electrochemistry were the bandgap where it was observed that the bandgap of P3HDS was in between that of P3HT and PDDS. As well as higher electronic conductivity supports faster charge transportation at high current rates, which means the polymers are good to be electron donors.

The polymers were all blended with Zinc Oxide nanorods by stirring at room temperature for 24hrs in different ratios. This was done to improve the band gap and efficiency of hybrid solar

97

cells. This was confirmed by optical studies where the band gap of P3HT was improved from 2.41 eV to 2.291 eV with the ratio of 1:2 (P3HT:ZnO). For PDDS it was 2.54 eV to 2.42 eV while the band gap of P3HDS was 2.31 to 1.96 eV. The overall conclusion was that, the P3HDS had a better and improved band gap when blended with ZnO nanorods compared to other polymers of which it is the first time that the composite of organosilicon/ ZnO nanorods will be produced this means that the efficiency of solar cells can be improved using these material which was the main aim of the study.

7 .2 Recommendations

The study and characterizations of the polymers and zinc oxide nanorods should be prepared on glass substrate through drop coating, which would make things easy for applications. For future work on the study, is to study the electrochemical properties and electrochemical performance of both donor and acceptor along with their blend, should further be probed by cyclic voltammetry, square wave and electrochemical impedance (EIS) to determine the conductivity of all the materials. Investigation of the power conversion efficiency should be studied by fabrication the hybrid solar cells using the materials and also study other photovoltaics parameters as well as the performance of the solar cell.